Vrije Universiteit Brussel

Faculteit Ingenieurswetenschappen
Vakgroep Werktuigkunde

Model-based control of a one-dimensional pendulum actuated with Pleated Pneumatic Artificial Muscles with adaptable stiffness

Bruno Meira y Duran

Proefschrift ingediend tot het behalen van de academische graad van
Burgerlijk Werktuigkundig-Elektrotechnisch Ingenieur

Academiejaar 2004-2005
Promoter: Prof. dr. ir. Dirk Lefeber
Co-Promotor: Prof. dr. ir. Patrick Kool

Abstract

Model-based control of a one-dimensional pendulum actuated with Pleated Pneumatic Artificial Muscles with adaptable stiffness

Due to the compressibility of air and the dropping force to contraction characteristic of the muscle, a joint actuated by two of these muscles set in antagonistically position, shows a compliant behaviour and can be adapted while controlling position. This compliance adaptation enhances the possibilities of exploitation of natural dynamics so that energy consumption and control activity is decreased.
The main purpose of the project is to investigate the exploitation of natural dynamics in combination with the joint trajectory control. The joint tracking controller tracks the desired trajectory while adapting the joint compliance, as such that the natural regime corresponds as much as possible to the reference trajectory.

Currently the pendulum is assembled and its hardware components have been tested. This thesis reports on the design and construction of the pendulum. The effect on valve control activity and energy consumption by changing the compliance characteristics are shown by means of a simulation and experiments on the physical pendulum. A technique to change the stiffness online has been evaluated.

The next steps in the study are a correct estimation of the system's parameters and the extension of the system to a three dimensional pendulum, in that way that it can be used for implementation on the walking biped "Lucy", from the Vrije Universiteit Brussel.

Samenvatting

Studie van een modelgebaseerde controle van een slinger aangedreven door balgactuatoren met regelbare stijfheid.

Een scharniergewricht, aangedreven door een stel antagonistisch opgestelde spieren, vertoont een soepel en elastisch gedrag te wijten aan de samendrukbaarheid van lucht en de dalende kracht - contractie karakteristiek van de spier. Bovendien kan deze soepelheid ingesteld worden, onafhankelijk van de positie van het gewricht. De variabele stijfheid, het omgekeerde van de soepelheid, beïnvloedt de eigenfrequentie van het systeem en biedt dus de mogelijkheid om de natuurlijke dynamica van de slinger uit te buiten om zo het energieverbruik en de controleactiviteit te verminderen.

Het hoofddoel van dit project is te komen tot een controle van de slinger waarbij de uitbuiting van de natuurlijke dynamica van het systeem gecombineerd wordt met een trajectsturing. De trajectsturing volgt een opgelegd traject, terwijl de stijfheid van de structuur zodanig wordt ingesteld dat de slingerbeweging volledig binnen de natuurlijke dynamica van het systeem valt.

De slinger is gebouwd en de bijhorende hardware componenten zijn getest. Deze thesis geeft een beschrijving van het ontwerp en de bouw van de slinger. De invloed van de variabele stijfheid op het energieverbruik en de kleppenacties wordt geïllustreerd aan de hand van simulaties en experimenten op de werkelijke slinger. Een techniek om de optimale stijfheid langsheen een opgelegd traject te bepalen en te variëren werd onderzocht.

De volgende stappen binnen dit onderzoeksgebied zijn de correcte bepaling van de parameters van het systeem en een uitbreiding naar een driedimensionale slinger, om de opgedane kennis te kunnen gebruiken voor verdere ontwikkeling van de tweepotige stappende robot ‘Lucy’.

Résumé

Contrôle basé sur un modèle, d'une pendule, actionnée par des muscles artificiels pneumatiques pliés avec une raideur adaptable.

Grâce à la compressibilité de l'air et de la caractéristique force-contraction décroissante du muscle, une jointure actionnée par deux muscles antagonistes, présente un comportement compliant, dont la souplesse peut être controlée indépendamment de la position. Cette souplesse adaptive permet de bénéficier du régime naturel du système pour ainsi diminuer la consommation d'énergie et l'effort de contrôle.
L'objectif de cette thèse est de combiner l'exploitation du mouvement naturel de la pendule avec un contrôle en position de type suivi de trajectoire. Une trajectoire spécifiée est suivie par un contrôle en position pendant que la souplesse de la jointure est adaptée de telle façon que le régime naturel correspond le plus possible à la trajectoire de référence.

La pendule est actuellement assemblée et les composant testés. Cette thèse donne une déscription de la construction de la pendule. L'influence de la souplesse de la jointure sur l'effort de contrôle et la consommation d'énergie est illustrée par des moyens de simulations et d'expérimentations sur la pendule réelle. Une technique qui permet de déterminer la souplesse optimale tout au long d'une trajectoire specifiée est étudiée.

La prochaine étape dans le domaine est d'estimer correctement les paramètres du système et d'étendre ce sytème vers une pendule tridimensionelle. De cette façon, l'incorporation de la technique pourra se faire sur le robot bipède 'Lucy'.

Acknowledgements

Na een jaar van pure fun in Barcelona, heeft het mij veel moeite gekost om me weer in het leven van een ingenieursstudent te storten. Tijdens de periode waar ik vorig jaar op één van de vele terrasjes aan het genieten was van het mooie weer, heb ik nu de meeste tijd doorgebracht in het labo, vloekend op de zoveelste klep die maar niet wilde werken. Na hard werk te hebben geleverd, ben ik dan toch gekomen tot een (zelf)bevredigend resultaat.Dit afstudeerwerk is uiteraard niet zonder de hulp en steun van anderen tot stand gekomen en daarom dit dankwoord.

Ten eerste wil ik mijn promotor Prof. Lefeber en co-promotor Prof. Kool bedanken om mij de mogelijkheid te geven tot deze eindverhandeling.
Bram Vanderborght en Björn Verrelst zou ik willen bedanken voor de begeleiding, de goede raad, de hulp bij praktische problemen en vooral voor het nalezen van de eindverhandeling.
Een groot deel van deze thesis werd verwezenlijkt in samenwerking met mijn klasgenoot Pieter Beyl. We hebben dan ook vele uren samen doorgebracht in het labo en zou hem willen bedanken voor de vlotte samenwerking.
Voor de technische hulp kon ik steeds terecht bij Ronald Van Ham, Jean-Paul Schepens, André Plasschaert, Thierry Lenoir en Gabriël Van den Nest en dank hen hiervoor.
Joris Naudet en Michael Vandamme wil ik bedanken voor hun hulp bij het programmeren.
Verder zou ik nog mijn vrienden willen bedanken voor hun aanwezigheid en het plezier dat we doorheen de jaren aan de VUB hebben beleefd. Thomas, ik ben je enorm dankbaar voor je hulp bij het maken van de User Interface. Nathalie, jou wil ik speciaal bedanken, niet alleen voor het nalezen van mijn proefschrift, maar ook voor je steun en de vele koffiepauzes die mij er steeds weer bovenop hielpen.

Papi y Mami, os quiero agradecer por vuestro interés, apoyo y amor durante toda mi carrera universitaria. Sin vosotros, no hubiera sido lo mismo. Os quiero mucho!

Tenslotte zou ik mijn ouders willen bedanken, voor het vertrouwen, de steun en de vrijheid die ze me door alle jaren heen gegeven hebben. Aan hen heb ik dan ook alles te danken.

Brussel Bruno
Juni 2005

Contents

List of Figures

List of Tables

Nomenclature

Acronyms

AICH	Analog Input Channel
DACOUT	Analog Channel Ouptut
DIO	Digital Input/Output
PPAM	Pleated Pneumatic Artificial Muscle
USB	Universal Serial Bus controller

Symbols

α	coefficient denoting centre of gravity of the pendulum link	
α_i	angular design parameters of the joint muscle setup	°
ε	muscle contraction	
ε_i^c	contraction of muscle i at chosen central position θ^c	
ρ_0	air density at standard conditions	kg/m³
ε_i	contraction of muscle i in a joint setup	
θ	angular joint position	rad(°)
θ^c	chosen central position in the joint setup	rad(°)
$\Delta\tilde{p}$	control variable of delta-p control unit	bar
τ	actuator torque	Nm
a	reaction level of bang-bang pressure controller	bar
b	reaction level of bang-bang pressure controller	bar
b_i	distance between origin O and points B_i	m
B_i	fixed base points of the joint muscle setup	
c	reaction level of bang-bang pressure controller	bar
C	pneumatic valve flow constant	Std.l/min/bar
$C(q,\dot{q})$	centrifugal/coriolis matrix	
d_i	distance between R and points D	m
D_i	moving points of a joint muscle setup	
$D(q)$	inertia matrix	
e	reaction level of bang-bang pressure controller	bar
f	reaction level of bang-bang pressure controller	bar
$f_i(\theta)$	dimensionless force function of muscle i in the joint setup	
$f\left(\varepsilon, \frac{l_0}{R}\right)$	dimensionless muscle force function	
f_i	coefficients of a polynomial force fitting	
F_t	muscle traction force	N
g	acceleration of gravity	m/s²

G_i	centre of gravity of part i of the pendulum	
$G(q)$	gravitational torque/force vector	
I_i	moment of inertia of part i	kgm²
$k_i(\theta)$	joint stiffness function for a joint setup	Nm/bar
K	joint stiffness	Nm
	kinetic energy	J
l_0	initial muscle length	m
l_b	base suspension bar length of the muscle joint setup	m
l_i	length from pivot to part i	m
l_{m_i}	actual length of muscle i in the joint setup	m
$\dot{m}_{air_i}$	air mass flow through valves of muscle i	kg/s
m_i	mass of part i	kg
n	number of fibres	
	polytropic exponent	
p	gauge pressure	bar
p_S	stiffness parameter of delta-p control unit	Nm
p_{i_0}	initial gauge pressure when muscle i was closed	bar
P_{i_0}	initial absolute pressure when muscle i was closed	bar
q_i	generalized coordinate	
Q_θ	generalized torque associated to q_i	
$r_i(\theta)$	leverage arm of muscle i in the joint setup	m
R	rotation point of the joint muscle setup	
t	time	s
$t_i(\theta)$	torque function of muscle i in a joint setup	Nm/bar
T	joint torque	Nm
	temperature	K
T_i	torque generated by muscle i in the joint setup	Nm
U	potential energy	J
$v\left(\varepsilon, \frac{l_0}{R}\right)$	dimensionless volume function	
v_i	coefficients of polynomial muscle volume fitting	
V_i	enclosed volume of muscle i	m³
V_{i_0}	initial volume when muscle i was closed	m³
W	work	J

Subscript

air	of compressed air
atm	atmospheric
d	derivative
i	muscle number

	part number
isotherm	at isothermal conditions
s	sample

Superscript

a	analog
d	digital
ex	of exhaust valve
in	of inlet valve
supply	of compressed air supply
~	required value
^	calculated with estimated parameter values
•	derivative with respect to time

Chapter 1

Introduction

1.1 Motivation and goal

Nowadays, robots are widely used in all kinds of production and assembly chains to assist in very hard, repetitive and labour intensive tasks with optimum performance. Most of the robots built, use heavy electrical drives, making these machines heavy and power demanding and not safe for humans. Robots in assembly halls are completely isolated and can not be accessed when working. As the field of robotic solutions is still expanding and more robots will be used in the immediate surroundings of people, there is a need for safety against all possible accidents. Therefore, soft actuators are being developed. Such soft actuators offer a natural compliance, making them human friendly. At the University of Pisa, an electromechanical Variable Stiffness Actuation [10] motor has been developed, and specifically designed for machines and robots physically interacting with humans. Another example of such an actuator is the AMASC (Actuator with Mechanically Adjustable Series Compliance)[4], which uses two motors, one for controlling the position and the other for controlling the stiffness, the inverse of compliance.

Figure 1.1: Industrial robot with heavy electrical drives and the soft actuator AMASC

For the last ten years the Robotics and Multibody Mechanics Research Group of the Vrije Universiteit Brussel is conducting research in the domain of legged bipedal robots. Bipeds can be divided into 2 main categories: on the one hand the full actuated robots, which don't use natural or passive dynamics at all, like Asimo [17] and QRIO [18], on the other hand the "Passive walkers" who don't require actuation at all to walk down a sloped surface or only use a little actuation just enough to overcome energy losses, due to friction and impact effects, when walking over level ground. An example of such a robot is the Dutch robot Denise.

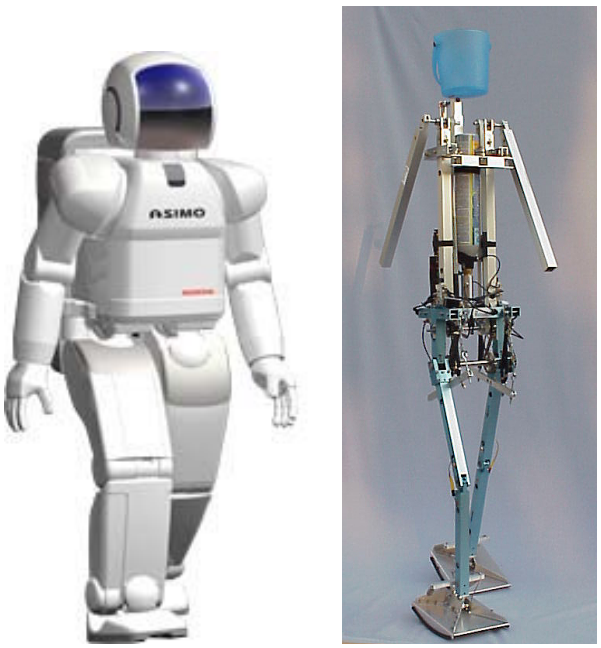

Figure 1.2: The active walker 'Asimo' and the passive walker 'Denise'

The main advantage of "passive walkers" is that they are highly energy efficient but unfortunately they are of little practical use. They have difficulties to start, can't change their speed and cannot stop in the same way a completely actuated robot can. But on the other hand, a completely actuated robot consumes a lot of energy. As energy consumption is an important issue for bipeds, it remains important to exploit the natural dynamics by trying to incorporate the unforced motion of a system instead of ignoring or avoiding it.

The goal of the Robotics and Multibody Mechanics Research Group is to develop a robot which combines these two categories. This robot should be able to adapt the natural dynamics as a function of the imposed walking motion. For

this research a joint with controllable compliance is needed in order to influence the natural dynamics. But the variable stiffness actuators mentioned previously are too complex and too heavy for an application such as an autonomous bipedal robot. Therefore, an interesting alternative is the pleated pneumatic artificial muscle (PPAM), developed at the Robotics and Multibody Mechanics Research Group.

It is believed that these pneumatic actuators have interesting characteristics, which can be used in the field of legged robotics. In this context, the development of a planar walking robot actuated with pleated pneumatic artificial muscles (PPAM) was started. The robot has been given the name "Lucy" (figure 1.3). It weighs 30 kg and is 150 cm tall. It uses 12 muscles to actuate 6 pin joints, as such Lucy is only able to walk in the sagittal plane. A sliding mechanism prevents the robot from falling side-wards. The goal of this project is to create a lightweight biped, which is able to walk in a dynamical stable way while exploiting the adaptable passive behaviour of the pleated pneumatic artificial muscles in order to reduce energy consumption and control efforts. The robot is currently able to move in a quasi-static way, but stiffness in the joints is still set constant [11],[14].

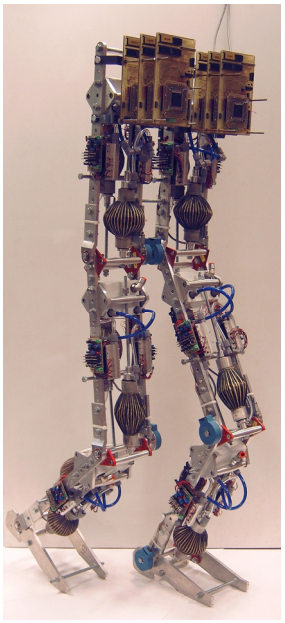

Figure 1.3: The bipedal walking robot 'Lucy'

The main purpose of this master thesis is to investigate the adaptable passive behavior of the Pleated Pneumatic Artificial Muscle, which allows the stiffness

of a joint, actuated by two antagonistically coupled muscles, to be varied online. Because the research on this topic will be used for further implementation on 'Lucy', the investigation is done on one modular part of 'Lucy'. With such a modular part a single pendulum set-up, shown in figure 1.4, was created in order to investigate energy consumption reduction with imposed swinging motion of the pendulum while the stiffness of the joint is changed. The idea in this work is to change the natural frequency in combination with pure trajectory control in such a way that control efforts are minimized. This strategy is tested on both a physical and mathematical computer simulation model.

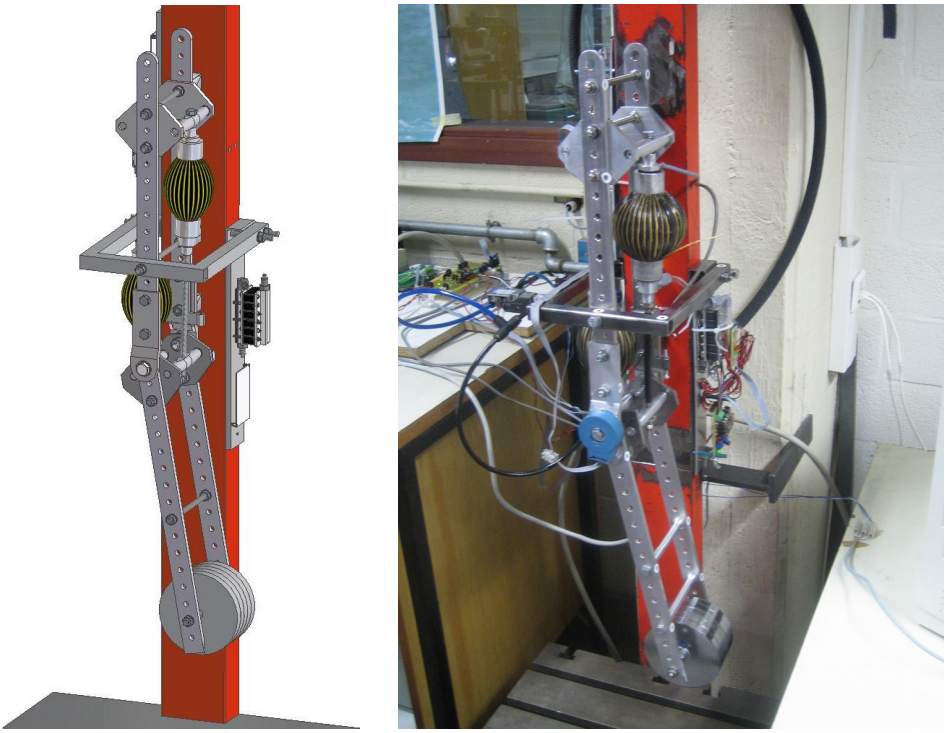

Figure 1.4: CAD drawing and photograph of the physical pendulum

1.2 Background information

The first official recordings of passively walking toys goes back till 1888 (e.g. Fallis patent). Inspired by the observation of human data, in which the muscles of the swing leg are activated only at the beginning and the end of the swing phase, Morawski & Wojcieszak were the first to give a mathematical formulation

for these toys. They concluded that in human locomotion the motion of the swing leg is merely a result of gravity acting on an unactuated double pendulum.
Inspired by this calculations, it was McGeer [5] who introduced the concept of Passive Dynamic Walking. McGeer showed that a simple planar mechanism with two legs could be made to walk in a stable way down a slight slope with no other energy input or control. This system acts like two coupled pendula. The stance leg acts like an inverted pendulum, and the swing leg acts like a free pendulum attached to the stance leg at the hip. Given sufficient mass at the hip, the system will have a stable trajectory that repeats itself and will return to this trajectory even if perturbed slightly. McGeer also constructed a physical example. His research was continued by the group of Andy Ruina [3]. They studied the models of McGeer in more detail and extended the two dimensional model to three dimensions while building several "Passive Walkers".
Using natural frequencies of the robot is a useful concept for energy efficient walking. However, the natural frequency of a system is defined by inherent system properties like: dimensions, mass distribution, collision behavior and joint compliance. As a result, the eigenfrequency of these models is set during construction, which limits the different passive walking patterns and walking speeds. In order to change the natural frequency of the system, passive elements with variable compliance were implemented. In this context the group of Takanishi developed the two-legged walker WL-14, where a complex non-linear spring mechanism makes changes in stiffness possible. A more elegant way to implement variable compliance is to use pneumatic artificial muscles. Stiffness can easily be changed by changing the applied pressures. Research on this topic was done by van der Linde [12] and Wisse [15] through implementation of McKibben's type of pneumatic artificial muscles.

1.3 Approach

Pneumatic artificial muscles have the possibility to adapt the stiffness while controlling position. Exploitation of the natural dynamics of a walking robot by varying the compliance characteristics can be approached in two ways: a more biological inspired approach and an analytical approach. The first option is to

design the robot, taking into account all the inertial and compliance parameters, in such a way that the system performs a motion close to walking without actuation, by making the system oscillate at its natural frequency. By controlling the joint compliance, the motion characteristics are then adapted and as such adapt the walking pattern. Concerning dynamic robot stability, this is however a complex task and will probably result in a small range of feasible motion patterns. A second approach is to design joint trajectories for a specific robot configuration, so that dynamic stability is ensured if these trajectories are tracked by a trajectory tracking controller. In order to reduce valve control activity, the joint trajectory tracking unit then adapts the compliance of the different joints, so that the natural motion "best" fits the given trajectories. As a result the global stability is ensured due to the calculated trajectories, while energy consumption is lowered by adapting the joint compliances. But of course, setting the ranges in which the natural motion corresponds to the calculated trajectories required for dynamic stability, asks for a proper design of all inertial and joint design parameters. So that in the end, a combination of these two different approaches will give interesting results.

In this context, two master theses were proposed by the Robotics and Multibody Mechanics Research Group of the Vrije Universiteit Brussel. In this report the model based approach will be discussed. My colleague, Pieter Beyl, will carry out a more biological approach, by using Fuzzy Logic controllers, artificial neural networks (ANN), central pattern generators (CPG), Look Up Tables or combinations of all strategies mentioned above.

As we both needed an experimental set-up to check our simulation results, the first part of our thesis consisted of designing and constructing the pendulum. Therefore, the following steps were executed:

- Determination of the dimensions of the leverage mechanism and consequently the joint torque characteristics.
- Building, testing and debugging the electronic components.
- Building a program library, used to send and receive data by use of a data acquisition board.

- Assembling the pendulum
- Implementation of the joint trajectory controller
- Writing a user interface to communicate with the pendulum and extract the data information.
- Implementation of a controller for setting the joint stiffness in order to incorporate natural dynamics.
- Measuring and analyzing the results.

The first five tasks were done together with my colleague Pieter Beyl. The remaining tasks were carried out by myself, since a completely different approach was chosen.

1.4 Outline

This thesis proceeds as follow:
Chapter 2 (*Design)* gives an extensive description of the mechanical design, with the joint torque characteristics as an important discussion. The electronic design, needed to control the valves which set the pressures in the muscles is also given. Those pressures define the joint stiffness and position. A manual guide of the user interface is given, in order that further research on this topic can be done by other people.
Chapter 3 (*Control*) reports on the controller used for tracking a desired trajectory in combination with exploitation of the natural dynamics. The tracking control strategy consists of a multilevel construction of several essential blocks, trying to cope with the nonlinear structure by using model-based feedforward techniques. The method used to take into account the natural dynamics will be formulated. In order to evaluate this control architecture a computer simulation model was built. A description of the modelling of the robot dynamics and the thermodynamics of the muscle/valve system is given, followed by an overview of the complete simulator. Some energy consideration will be given, so that the method proposed for incorporating the natural dynamics can be evaluated.

Results and discussions on both the simulation model and the physical pendulum are given in chapter 4. For both cases, the performances of the joint trajectory tracking controller will be discussed. In the context of the exploitation of the natural dynamics, simulation and experimental results will be given. Finally, a comparison between simulation and experiments on the real pendulum will be discussed, in order to conclude whether or not an online changing stiffness can be used for further implementation on 'Lucy'.

*General conclusion*s are drawn in chapter 7, followed by the planning of *future research* in the domain of exploitation of natural dynamics.

Chapter 2

Design

2.1 Introduction

The main goal of the pendulum is to investigate whether the PPAM can be an interesting actuator for exploitation of natural dynamics in combination with trajectory tracking. The pendulum set-up has been designed for that purpose and should be suitable for experiment on the following main items:

- Evaluation of a trajectory tracking control strategy with the specific pneumatic system.
- Evaluation of the adaptable passive behaviour of the PPAM and the influence on the natural dynamics of the system.

This chapter starts with a description of the *mechanical design* of the pendulum. The PPAM and its characteristics will be discussed. The kinematics of a one-dimensional joint setup controlled by two antagonistically positioned muscles, are reported. Special attention is devoted to the design of the actuator connection. The electronics needed to control the pressures in the muscles will be explained in the second paragraph, *electronic design*.
In the third paragraph, *software*, a user manual of the guided user interface will be given, so that the experimental set-up can be easily used by other persons.

Constructing the pendulum by just one person would have taken too much time in the context of a master thesis. Therefore, my colleague Pieter Beyl and I worked as a team. As a consequence, all the work, except from the GUI, referred to in this chapter has been carried out together.

2.2 Mechanical Design

2.2.1. Pleated Pneumatic Artificial Muscle

The PPAM consist of a membrane made of an aromatic polyamide such as Kevlar to which a thin liner of polypropylene is attached in order to make the membrane airtight. The membrane of this muscle is arranged into radially laid out folds that can unfurl free of radial stress when inflated. Reinforcing high tensile Kevlar fibers are positioned in each crease. The high tensile longitudinal fibres of the membrane transfer tension, while the folded structure allows the muscle to expand radially, which avoid energy losses and hysteresis. The folded membrane is positioned into two end fittings, which close the muscle and provide tubing to inflate and deflate the enclosed volume. An epoxy resin fixes the membrane and the Kevlar fibres to the end fittings.

Figure 2.1: The Pleated Pneumatic Artificial Muscle

Daerden [2] extensively discusses several characteristics concerning the PPAM, for inelastic as well as elastic membranes. In this work mainly two characteristics are important: generated traction and enclosed volume for each contraction. The first is used for joint torque dimensioning and control purposes, while the latter is used to predict joint compliance with closed muscles. Furthermore, the maximum

diameter when the muscle is fully bulged should be taken into account when designing the different joints of the robot in order to provide enough space for the muscle to bulge.

When inflated with pressurised air, the muscle generates a unidirectional pulling force along the longitudinal axis. Generally, if the number of fibres is large enough, the generated muscle force depends on the applied gauge pressure (p), the contraction (ε) and the two parameters, initial muscle length (l_0) and slenderness ($\frac{l_0}{R}$) [14]

The traction characteristic is given by :

$$F_t = p l_0^2 f(\varepsilon, \frac{l_0}{R}) \tag{2.1}$$

with $f(\varepsilon, \frac{l_0}{R})$ the dimensionless force function as defined by Daerden [2].

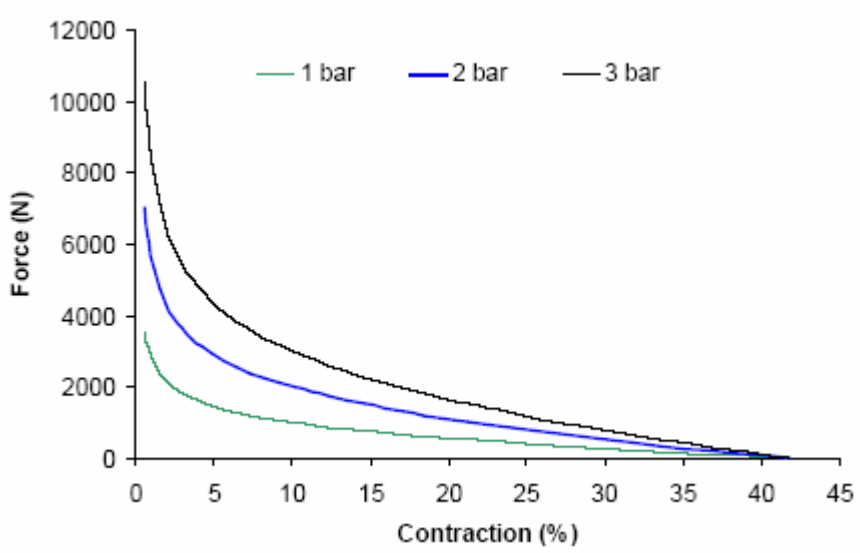

Figure 2.2: Theoretical forces at pressure levels 1,2 and 3 bar as a function of the contraction

Using l_0 = 110 mm, R = 11.5 mm and n = 40, results in the theoretical force characteristics depicted in figure 2.2, [14]. The traction as a function of contraction is drawn for different applied gauge pressures: 1, 2 and 3 bar. The graph shows the non-linear character of the generated muscle force. For small

contractions, the forces are extremely high, while for large contractions, the forces drop to zero. For the pendulum, contractions will be bounded somewhere between 5 and 35 %. The first limit is set to bound the stresses on the fibres and consequently extends the lifetime of the muscle. And beyond 35 % contraction, forces drop too low to be of practical use.

Figure 2.3 depicts the theoretical maximum diameter to contraction for the considered muscle [2]. This approximated maximum diameter should be taken into account during the design of the joints of the pendulum in order to provide enough space for the muscle to bulge.

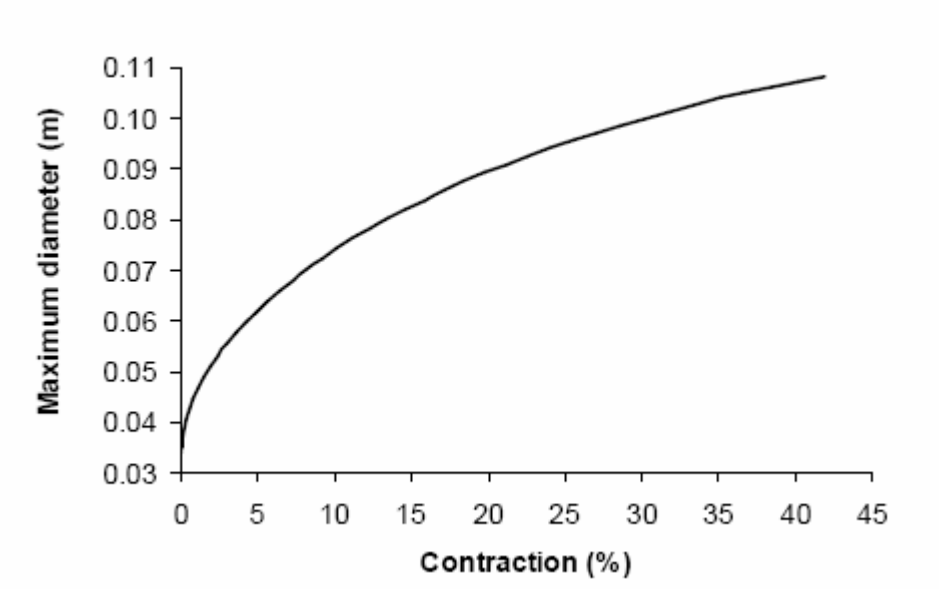

Figure 2.3: Theoretical maximum muscle diameter as function of contraction

To compare the theoretical characteristics with those of the physical PPAM, static load tests were carried out by Verrelst. A brief discussion on the results will be given. For more information we refer to [14].

A deviation between measured data and theoretical model of the force was observed. For dimensioning purpose, the theoretical model can be used. However, for the trajectory tracking control, an accurate estimation of the real force function is required. Since the force functions of different muscles are very similar, a 4th order polynomial function fit on the pressure scaled measured data was performed in order to achieve a better force estimation. The force function can be expressed as:

$$F_t = pl_0^2 f(\varepsilon) = pl_0^2 (f_4\varepsilon^3 + f_3\varepsilon^2 + f_2\varepsilon + f_1 + f_0\varepsilon^{-1}) \qquad (2.2)$$

Finally, for reason of programming convenience, a polynomial fitting was performed on the theoretical data for the enclosed muscle volume:

$$V(\varepsilon) = l_0^3 v(\varepsilon) = l_0^3 (v_5 \varepsilon^5 + v_4 \varepsilon^4 + v_3 \varepsilon^3 + v_2 \varepsilon^2 + v_1 \varepsilon + v_0) \qquad (2.3)$$

Those equations are much easier to handle than the numerical solution derived from the mathematical model as derived by Daerden and Verrelst. In table 2.1 and table 2.2, the coefficients of respectively the force and volume fitting are given. The values are valid when the generated force F_t is expressed in N, the initial muscle length l_0 in m, the pressure expressed in bar, the volume given in ml and the contraction ε expressed in %. Both polynomial fittings are shown in Figure 2.4

f_0	f_1	f_2	f_3	f_4
146099	128611.6	− 7178.93	171.623	− 2.0413

Table 2.1: Coefficients of the polynomial force function approximation

v_0	v_1	v_2	v_3	v_4	v_5
71728	30080	− 2386.3	113.82	− 2.6296	0.02254

Table 2.2: Coefficients of the polynomial volume fitting approximation

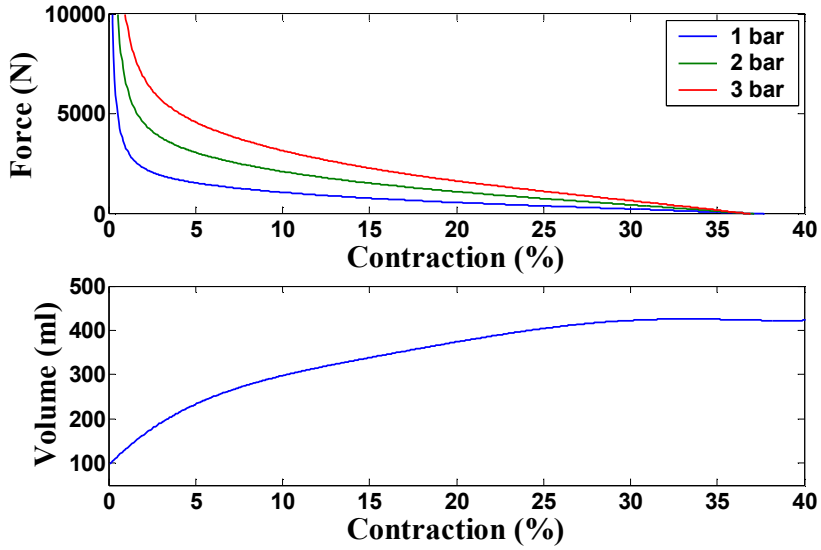

Figure 2.4: Forces at pressure levels 1,2 and 3 bar and volume resulting from the polynomial fitting as a function of the contraction

2.2.2. The one-dimensional joint set-up

2.2.2.1. Introduction

Pneumatic artificial muscles can only exert a pulling force. In order to have a bi-directional working revolute joint, two muscles are coupled antagonistically. The antagonistic coupling of the two muscles is achieved with a pull rod and leverage mechanism, as is depicted in figure 2.5. The lever arm can be varied in such a way that the highly non-linear force-length characteristic of the PPAM is transformed to a more flattened torque-angle relation. While one muscle contracts and rotates the joint in its direction, the other muscle will elongate.

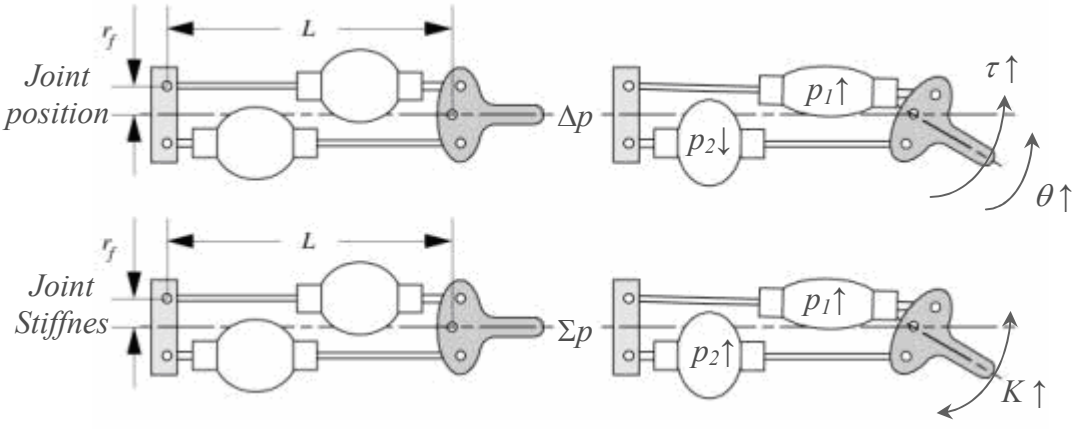

Figure 2.5: The antagonistic muscle setup and the possibility to adapt both position and compliance independently.

The gauge pressure difference between the two muscles determines the generated torque (T), and consequently also angular position (θ). Furthermore, both pressures can be increased (decreased) in such a way that joint stiffness (K) raises (lowers) without affecting angular position. Thus both position and compliance can be controlled independently.

2.2.2.2. Kinematics of the one-dimensional pendulum

The kinematics of the pendulum have the same structure as one modular part of 'Lucy'. For the sake of convenience, the same discussion will be given as in [14]

The basic configuration of the pull rod and leverage mechanism is depicted in figure 2.6

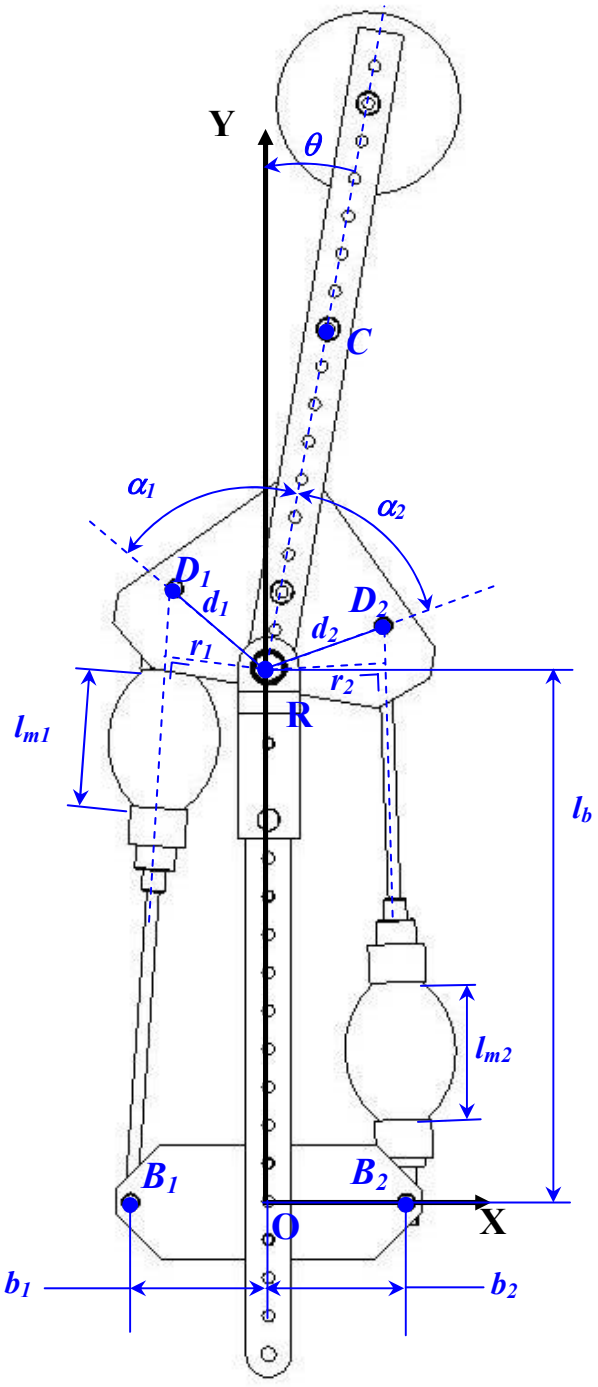

Figure 2.6: Basic configuration of the pull rod and leverage system

The two muscles are connected at one side of the system to a fixed base in the points B1 and B2 respectively. The other ends of the muscles are attached to a

pivoting part at the points D1 and D2, of which the rotation axis passes through a point R. The rods are assumed to be rigid.

An orthogonal X, Y - coordinate system is defined. The X -axis is aligned with the base points B_1 and B_2, while the vertical Y -axis intersects the physical pivoting point R and lies along the base suspension bar of the pull rod mechanism.

The essential parameters to be determined during the design process of the joint are the following:

- b_i is the distance between the origin O and the point B_i .
- d_i is the distance between the pivoting point R and the point D_i .
- α_i is the angle between the vector $\overline{RD_i}$ and $\overline{RC_i}$ point on the rotating part. (α_i is not oriented and always positive)
- l_{mi} is the actual length of muscle i
- l_b is the length of the base suspension bar, measured between the origin O and the pivot point R.
- θ represents the rotation angle, measured between $\overline{RC}$ and the Y -axis. (θ is oriented, counter-clockwise is positive)

The generated torque can be found by combining the traction force generated by the muscles and the orthogonal leverage arms r_1 and r_2 :

$$\begin{aligned} T(\theta) = T_1(\theta) - T_2(\theta) &= F_{t1}(\theta) r_1(\theta) - F_{t2}(\theta) r_2(\theta) \\ &= p_1 l_{0_1}^2 f_1(\theta) r_1(\theta) - p_2 l_{0_2}^2 f_2(\theta) r_2(\theta) \qquad (2.4) \\ &= p_1 t_1(\theta) - p_2 t_2(\theta) \qquad (2.5) \end{aligned}$$

with $t_1(\theta)$ and $t_2(\theta)$ the torque functions depending on the angular position of the joint. To calculate the force functions, we will use the polynomial function fitted on the measured force data as described in the first paragraph.

The vectors $\overline{B_iD_i}$ and $\overline{RD_i}$ are being calculated with following equations:

$$\overline{B_1D_1} = \left[b_1 - d_1 \sin(\alpha_1 - \theta), l_b + d_1 \cos(\alpha_1 - \theta)\right] \tag{2.6}$$

$$\overline{B_2D_2} = \left[d_2 \sin(\alpha_2 + \theta) - b_2, l_b + d_2 \cos(\alpha_2 + \theta)\right] \tag{2.7}$$

$$\overline{RD_1} = \left[-d_1 \sin(\alpha_1 - \theta), d_1 \cos(\alpha_1 - \theta)\right] \tag{2.8}$$

$$\overline{RD_2} = \left[d_2 \sin(\alpha_2 + \theta), d_2 \cos(\alpha_2 + \theta)\right] \tag{2.9}$$

The expression for $r_i(\theta)$ can then be found as:

$$r_i(\theta) = \frac{\left|\overline{B_iD_i} \times \overline{RD_i}\right|}{\left|\overline{B_iD_i}\right|} \tag{2.10}$$

The muscle contraction ε_i as function of the rotation angle θ is given by:

$$\varepsilon_i(\theta) = 1 - \frac{l_{mi}}{l_{0i}} = \varepsilon_i^c + \frac{l_{mi}^c - l_{mi}}{l_{0i}} = \varepsilon_i^c + \frac{\left|\overline{B_iD_i}^c\right| + \left|\overline{B_iD_i}\right|}{l_{0i}} \tag{2.11}$$

The contraction $\varepsilon_i(\theta)$ is defined with respect to ε_i^c, which is the contraction of muscle i at a chosen central position θ_c. In our case $\theta_c = 0$. The parameters are fixed during the joint design process.

2.2.2.3. Adaptable passive behaviour of a revolute joint

A PPAM has two sources of compliance, being gas compressibility, and the dropping force to contraction characteristic [2]. The latter effect is typical for pneumatic artificial muscles while the first is similar to standard pneumatic cylinders. Joint stiffness, the inverse of compliance, for the considered revolute joint, can be obtained by the angular derivative of the torque characteristic:

$$K = \frac{dT}{d\theta} = \frac{dT_1 - dT_2}{d\theta} = \frac{dp_1}{d\theta} t_1 + p_1 \frac{dt_1}{d\theta} - \frac{dp_2}{d\theta} t_2 - p_2 \frac{dt_2}{d\theta} \tag{2.12}$$

The terms $\frac{dp_i}{d\theta}$ represent the share in stiffness of changing pressure with contraction, which is determined by the action of the valves controlling the joint and by the thermodynamic processes taking place. If the valves are closed and if we assume polytropic compression/expansion, the pressure changes inside a muscle are a function of volume changes [9]:

$$P_i V_i^n = P_{io} V_{io}^n \tag{2.13}$$

with:

$$P_i = P_{atm} + p_i \tag{2.14}$$

leading to:

$$\frac{dp_i}{d\theta} = -n(P_{atm} + p_{io}) \frac{V_{io}^n}{V_i^{n+1}} \frac{dV_i}{d\theta} \tag{2.15}$$

With P_i, V_i the absolute pressure and volume of muscle i, P_{io} the absolute initial pressure, V_{io} the initial volume when the valves of muscle i were closed, p_i and p_{io} the gauge pressure and initial gauge pressure respectively, P_{atm} the atmospheric pressure and n a polytropic exponent. The polytropic exponent is introduced to describe deviations from the isentropic expansion/compression. An isentropic process assumes reversible adiabatic thermodynamic conditions and the exponent becomes in this case $n = \gamma = c_p / c_v = 1.4$ for dry air [9].

During the joint design process, it is ensured that the torque to angle and the volume to angle characteristics of a joint are monotonous functions. Meaning that the derivatives $dt_i / d\theta$ and $dV_i / d\theta$ keep the same sign within the range of

motion for which the joint was designed. Thus, referring to figure 2.6, increasing the joint angle θ will increase the torque function $t_1(\theta)$, while the volume of the respective muscle will decrease. Indeed the larger θ, the lesser muscle 1 is contracted. Consequently, the generated force is bigger. On the contrary, less contraction means that the muscle gets thinner and that volume decreases. Thus $dt_1/d\theta > 0$ and $dV_1/d\theta < 0$. For the other muscle 2 in the antagonistic setup, the actions are opposite: $dt_2/d\theta < 0$ and $dV_2/d\theta > 0$. Combining (2.12), (2.13) and (2.15) with this information gives:

$$K = k_1(\theta)p_{1o} + k_2(\theta)p_{2o} + k_{atm}(\theta)P_{atm} \tag{2.16}$$

with

$$\begin{aligned} k_1(\theta) &= t_1(\theta)n\frac{V_{1o}^n}{V_1^{n+1}}\left|\frac{dV_1}{d\theta}\right| + \frac{V_{1o}^n}{V_1^n}\left|\frac{dt_1}{d\theta}\right| > 0 \\ k_2(\theta) &= t_2(\theta)n\frac{V_{2o}^n}{V_2^{n+1}}\left|\frac{dV_2}{d\theta}\right| + \frac{V_{2o}^n}{V_2^n}\left|\frac{dt_2}{d\theta}\right| > 0 \\ k_{atm}(\theta) &= k_1(\theta) + k_2(\theta) - \left|\frac{dt_1}{d\theta}\right| - \left|\frac{dt_2}{d\theta}\right| \end{aligned}$$

The coefficients $k_1(\theta), k_2(\theta), k_{atm}(\theta)$ are determined by the geometry of the joint and its muscles.

From equation (2.16), we can conclude that when muscles in an antagonistic joint setup are closed, a passive spring element with an adaptable stiffness is created. The stiffness is controlled by a weighted sum of both initial gauge pressures. Since stiffness depends on a sum of gauge pressures while position is determined by differences in gauge pressure, the angular position can be controlled while setting stiffness. How to use this interesting property and how to incorporate it into the control of the pendulum in order to reduce energy consumption and valve control, will be discussed in detail in the next chapter.

2.2.2.4. Design of the one-dimensional pendulum

All the equations described above, in combination with the muscle force function, are used to design the characteristics. A description on how the design parameters of the former paragraph are chosen is now given.
As mentioned before, the pendulum consists of one modular part of the biped 'Lucy'. Therefore, some of the parameters are already fixed, namely:

$$b_i = 40\,mm$$
$$l_{mi} = 110\,mm$$
$$l_b = 350\,mm$$

The central position of the pendulum was set to $\theta_c = 0°$

For designing the remaining parameters, some requirements should be met:

- We want an angle range between -20° and 20°, or larger.
- Within the angle range, the contraction has to be limited between 5% and 35%. A smaller contraction leads to stresses that are too high for the muscle fibres. At higher contraction, the forces drop too low for practical use.
- Enough torque should be provided by the antagonistic setup to hold a mass of 10 kg at the maximum of the angle range. Therefore static torque characteristics of the joint should be compared with the torque needed to hold a mass of 10 kg.
- Stability has to be insured. The torque characteristic of the joint with closed muscles is important here. As the stiffness of the joint is given by $K = \frac{dT}{d\theta}$, this characteristic has to be increasing ($K = \frac{dT}{d\theta} > 0$). In that case, the joint stiffness is positive. If that is not the case, the swing motion will be amplified and instability will occur. Besides this, within the angle range, we want this torque characteristic to be as linear as possible. The joint stiffness will then be almost constant within our working domain.

- The diameter of the muscles should be taken into account during the design, in order to provide enough space for the muscle to bulge.

The joint range is determined via the minimum and maximum angles at the minimum and maximum contraction of the muscles. Angle range and torque characteristics are determined as a function of the joint application. The design of all these functionalities is complex and is linked to the specific motion of the pendulum.

A small Matlab program has been written to investigate the influence on the joint characteristics by changing the design parameters. The characteristics are shown in Figure 2.7 and 2.8. Figure 2.7 shows the contraction of one muscle in function of the joint angle. Maximum and minimum limits of the contraction are also plotted. In the left plot d_i is changed. In the right plot, the contractions for different values of α_i are given.

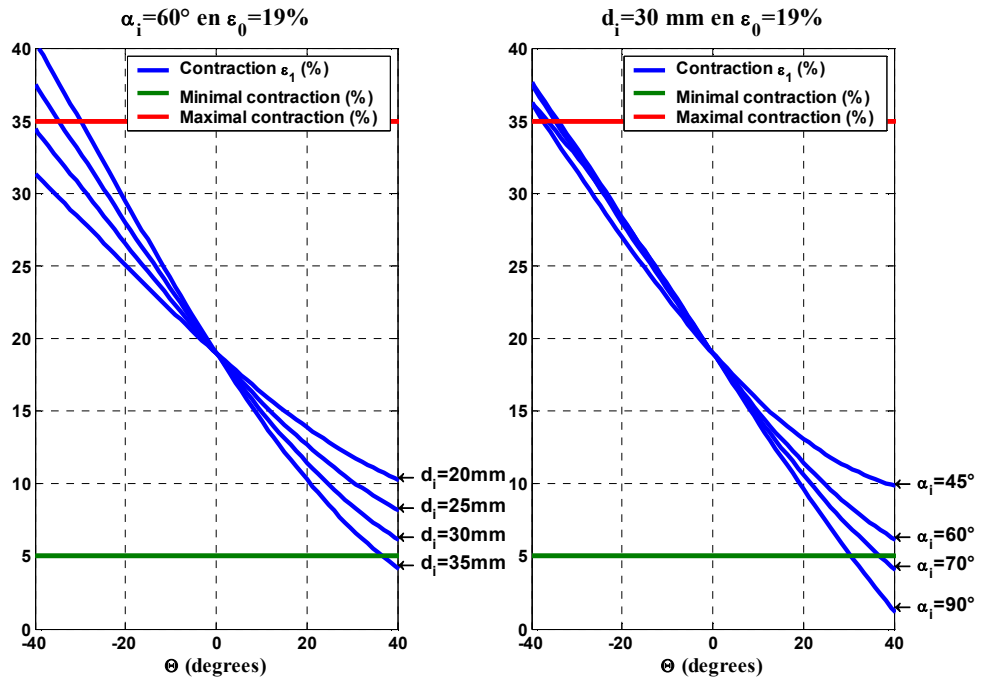

Figure 2.7: Influence on muscle contraction by changing d_i and α_i

Figure 2.8 shows two different torque characteristics. On the left side, the static torque of the joint is plotted for a maximum pressure of 3 bar in both muscle 1 and 2. The influence on the static torque characteristic by changing d_i is also

shown. On the right side, the torque characteristic of the joint with closed muscles is plotted to analyze the joint stiffness when muscles are closed. This characteristic is found by setting 3 bar into the muscle and closing the muscle at zero degrees. By moving the pendulum out of is equilibrium, a repelling torque is generated. This torque characteristic is plotted on the right.

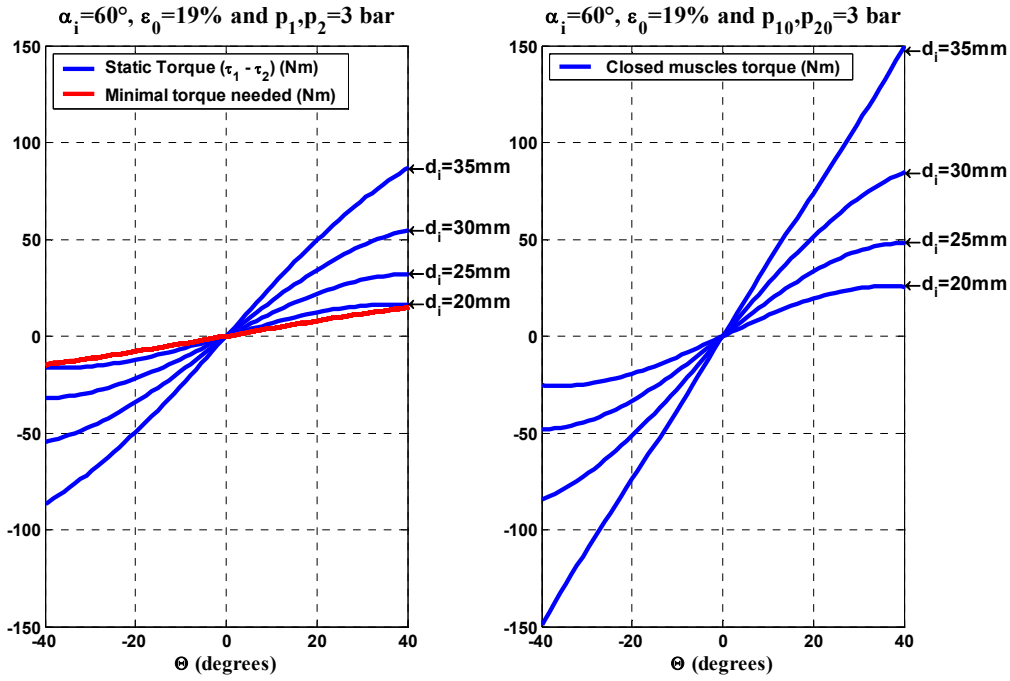

Figure 2.8: Static and closed muscle torque characteristics

Based on these plots the design parameters were set to the following values:

$$d_i = 30\,mm$$
$$\alpha_i = 60°$$
$$\varepsilon_0 = 19\,\%$$

As we can see on figure 2.7, for these values the contraction stays between the limits of 5% and 35% for an angle range between -35 degrees and 35 degrees.
In figure 2.9, the static torque characteristics and torque characteristics with closed muscle were redrawn with the chosen design parameter values. This was done for different pressure levels

Within the angle range, Figure 2.9 shows that enough torque can be provided to lift the mass. If we now look at the torque characteristics of the pendulum with closed muscles, we see that there is an almost linear evolution of the torque between -20 degrees and 20 degrees. The angle range is now fixed and all requirements are met.

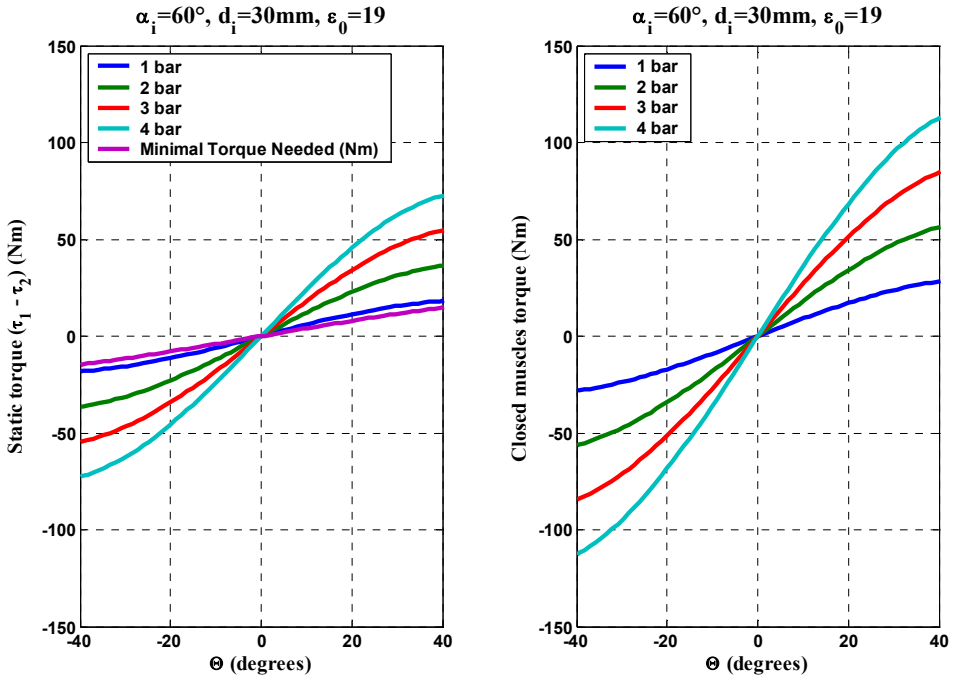

Figure 2.9: Static and closed muscle torque characteristics at different pressure levels, with the design parameters set to the one used in the experimental set-up.

2.2.3. Constructing the experimental set-up

2.2.3.1. The frame

As was argued previously, a pull rod and leverage mechanism was selected to position two muscles in an antagonistic setup. The basic frame in which this system is incorporated, is depicted in figure 2.10. The modular unit is made of two slats at the side, which are connected parallel to each other by two linking bars. A joint rotary part, provided with roller bearings, is foreseen for the

connection with an other modular unit. The fixed base for the pull rods mechanism includes two rotary axes at which the muscles are attached. The small rotations of these axes are guided by sliding bearings positioned in the frame. All the parts of the basic frame are made of a high-grade aluminium alloy, AlSiMg1, apart from the bolts and nuts, required to assemble the frame.

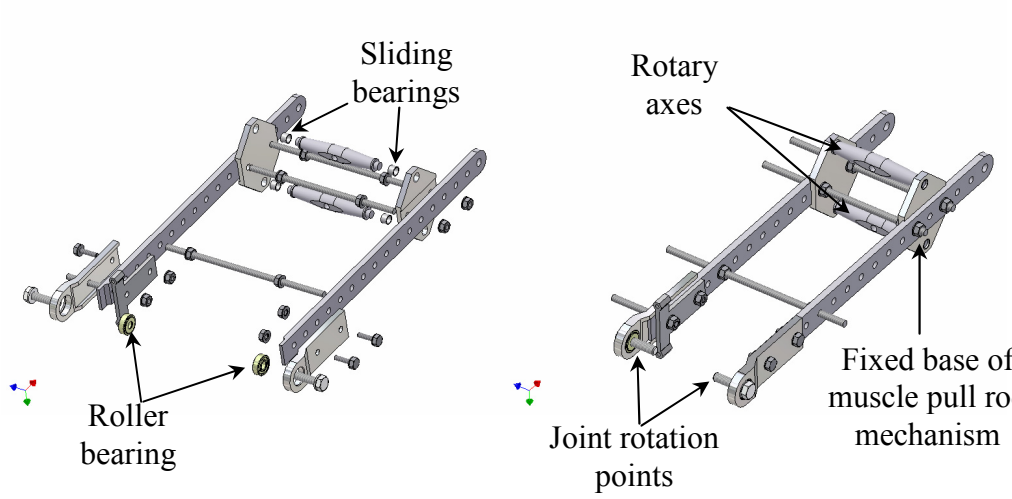

Figure 2.10: Exploded and assembled view of the basic frame

Two more linking bars are connected to the joint rotary part of the basic frame. This is the swinging part of the pendulum. The mass is attached to the screw thread connecting the two linking bars. The mass consists of simple discs, recuperated from dumbbells. In order to attach the discs and because the diameters of the discs' centre holes are different to the diameter of the screw thread, centering rings were fabricated. The discs are colour marked, so that the mass of each disc is known. They can be easily changed to alter the load.

The muscles are positioned crosswise to allow complete bulging. At one side they are attached to the frame via the fixed rotary base and at the other side the interface to the next modular unit is provided via the leverage mechanism. Two connection plates showed in figure 2.11, are fixed to the next modular unit and incorporate the leverage mechanism. Again sliding bearings are used to guide the rotations of both rotary axes. The position of the rotation points determines the dimensions of the leverage mechanism and consequently joint torque characteristics. The mathematical formulation of the torque as a function of force relation was given in section 2.2.2.2. The connection plates incorporate the parameters α_1, α_2, d_1 and d_2 of the leverage mechanism for both muscles. Since

these parameters have a large influence, the connection plate system is the one which can be changed easily, besides muscle dimensions, to alter joint torque characteristics. Therefore the two plates have to be replaced with only different positioned holes for the sliding bearings.

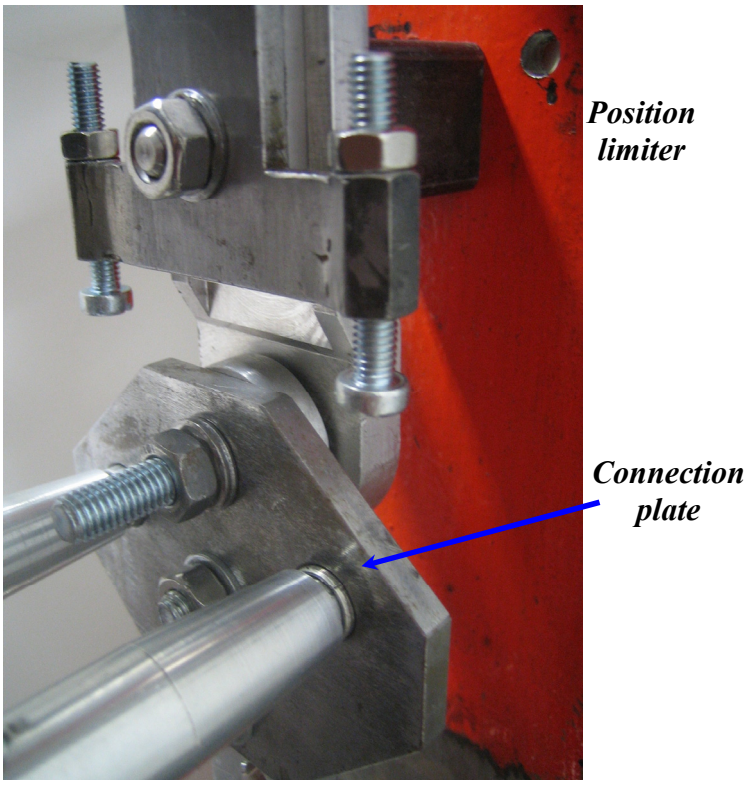

Figure 2.11: View of the connection plate and the position limiter

At the joint rotation side, an angular position limiter is provided. This device is equipped with two screws, which can be regulated separately in order to set the joint rotation range. The limiter is used for the two following reasons:

- Avoid singular joint configurations in the pull rod and leverage mechanism. This happens when the axis of the muscle is aligned with the joint rotation point and the muscle attachment point in the leverage mechanism. In this situation the muscle can seriously damage the leverage mechanism when increasing pressures would by required by the controller.
- Limit the contraction between 5 and 35 %.

2.2.3.2. The valve system

The force developed by the muscles is proportional to the pressure into the muscle. Therefore, a rapid and accurate pressure control is needed to set stiffness and position. Fast switching on/off valves are used. The pneumatic solenoid valve 821 2/2 NC made by Matrix, weighs only 25 g. They have a reported switching time of about 1 ms and flow rate of 180 Std.l/ min. The permitted pressure difference over the valve ranges, for each type, between 0 . . . 6 bar and 2 . . . 8 bar respectively.

To pressurise and depressurise the muscle, which has a varying volume up to 400 ml, it is best to place a number of these small on/off valves in parallel. Obviously the more valves used, the higher the electric power consumption, price and weight will be. Simulations of the pressure control on a constant volume were done by Van Ham et al. in the context of the development of 'Lucy' and this led to the compromise of 2 inlet and 4 outlet valves. The different number between inlet and outlet comes from the asymmetric pressure conditions between inlet and outlet and the aim to create equal muscle's inflation and deflation flows. For detailed information on the simulations is referred to [13].

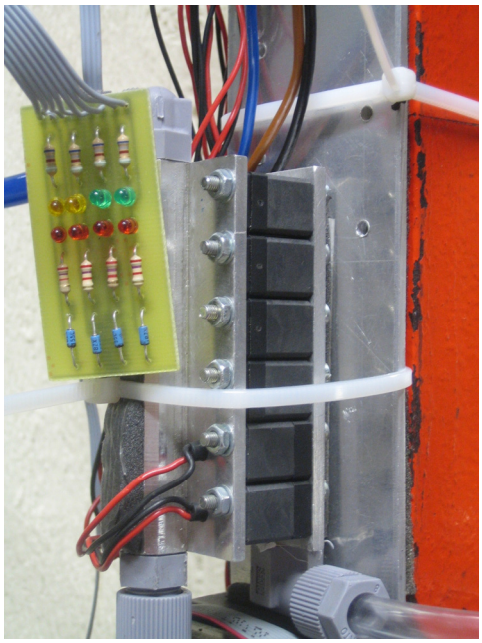

Figure 2.12: View of the valve island

The 6 valves are brought together in a valve island with special designed inlet and outlet collectors after removing parts of the original housing material. A photograph of the valve island is given in figure 2.12. The total weight of this device is less than 150 g. [14]

Particles of epoxy present in the muscles and other dirtiness can affect the good working of the valves. To protect the valves, a filter gauze is placed at the supply connection of the valve island and between the muscle and the valve island.

Leaks were detected there where the electric wiring is passing through the valve island. To prevent the air to escape through these holes, a supplementary rubber joint is placed between valve and valve island.

2.2.3.3. The pneumatic circuit

Figure 2.13 gives an overview of the pneumatic circuit, which is used to regulate the supply pressure of the different muscles of the pendulum. The pneumatic scheme shows the 2 identical pneumatic circuits of which each drives one antagonistic muscle. The valve island is depicted with separately inlet and exhaust, which each of them is represented by two "2/2 electrically actuated" valve symbols. These two symbols represent the 2 reaction levels of the valve system. The number of actual valves, which are included in each configuration are depicted as well. The right and left muscle are connected to the supply pressure regulating unit by separate tubes. The

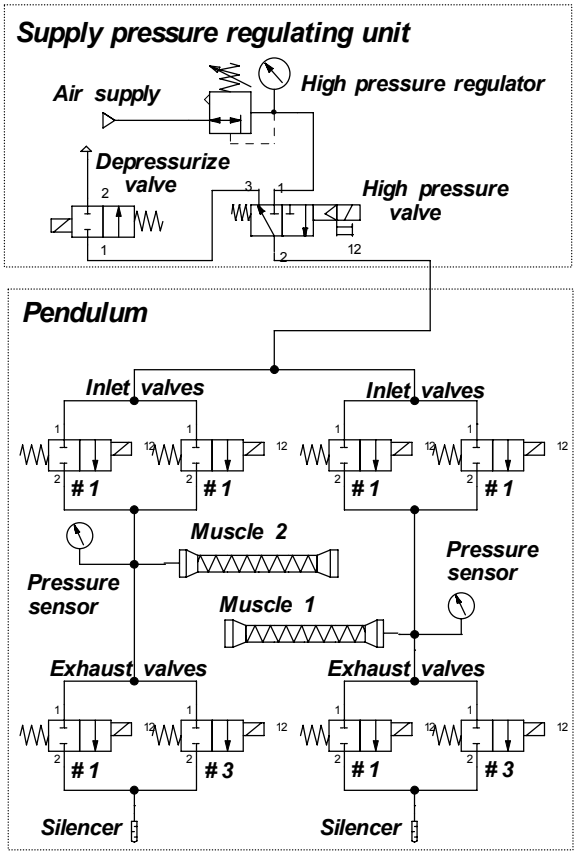

Figure 2.13: Schematic overview of the pneumatic circuit

pressure regulating unit consists of a mechanical unit that determines the pressure in the circuit. The circuit is interrupted with an electrically actuated 3/2 valve. The exhaust of this valve is connected to an electrically actuated 2/2 depressurizing valve in order to deflate the complete pendulum.

2.2.3.4. The exhaust silencer

Additionally, a silencer is added at the exhaust of each valve island. Without a silencer, the immediate expansion to atmospheric conditions of the compressed air at the exhaust creates a lot of noise. A silencer consists of a closed permeable tube which makes the pressurised air leave the volume slowly, resulting in a strongly reduced noise generation. But generally, a silencer also obstructs the dynamic performance of muscle deflation, since a pressure rise in the silencer lowers the exhaust airflow. It is therefore important to use large silencers with good permeable material [14]. As the basic frame of the pendulum is not moving and the valves very large exhaust silencers. For implementation on 'Lucy' it should be taken into account, that the valves island are connected to the moving robot, so smaller exhaust silencers are used.

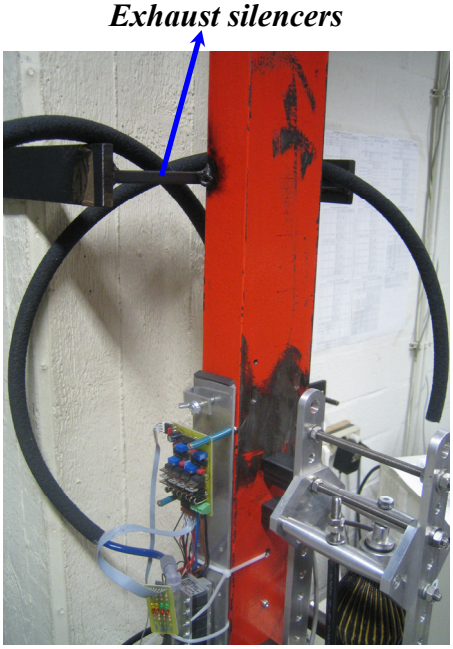

Figure 2.14: View of the exhaust silencers

2.2.3.5. The support

As pneumatic muscles can easily exert forces up to 5000 N and the pendulum is swinging at frequencies where dynamic forces are being important, a strong supporting structure has to be provided to hang up the pendulum. Besides this,

the supporting structure has to be as such that the pendulum can be easily dismounted and inverted. Several configurations can be used for this purpose. Figure 2.15 shows a picture of the used supporting structure. It has been decided to use a rectangular pole that is clamped to the wall. One side of the slats of the basic frame is pressed against the pole with screw thread and rectangular tubes used as washers. Holes were made into the pole in order to fix both inverted and non- inverted pendulum. To avoid oscillations of the basic frame due to dynamical forces generated by the swing motion, the other slat is attached to a rectangular frame. The pendulum is now resting in a kind of symmetrical cage, and can easily be disassembled and inverted. In the future a second rectangular frame should be used, because oscillations were still observed at higher frequencies of the swing motion.

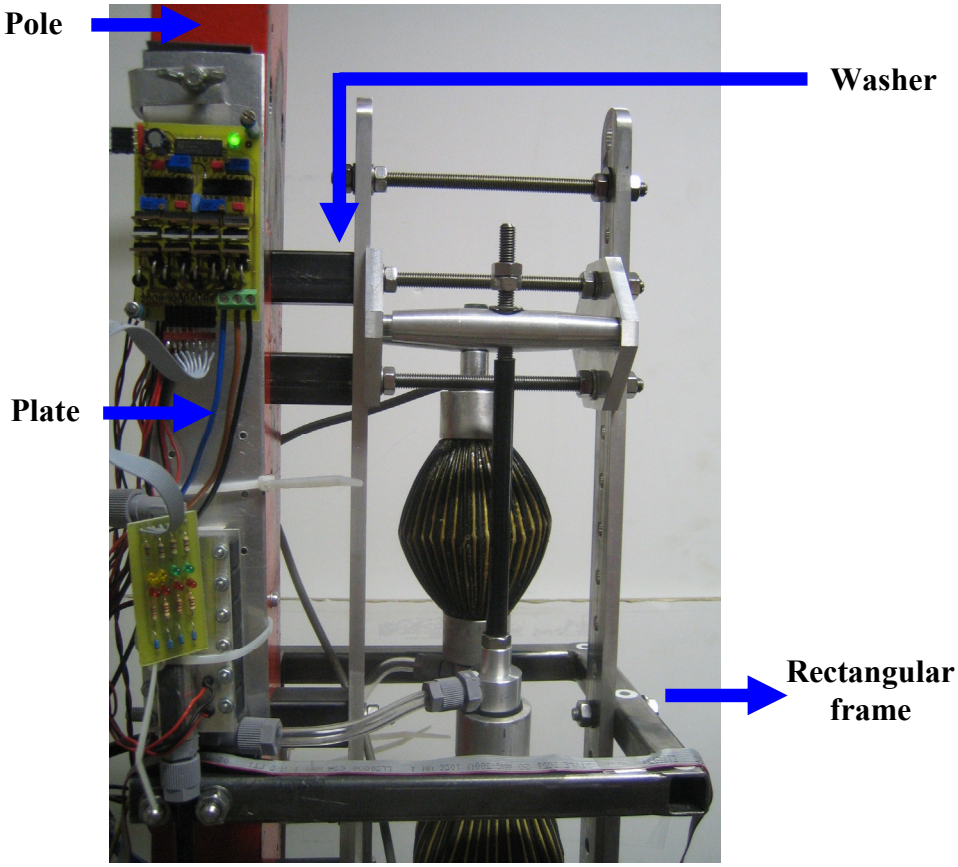

Figure 2.15: View of the supporting structure of the pendulum

Each valve island, together with its electronic circuit, is mounted on a plate. Each plate is clamped at one side of to the pole. It can be easily positioned where desired.

2.3 Electronic design

In figure 2.16 an overview of the control hardware used to control joint position and stiffness, is given. A multifunction I/O data acquisition card from NI-DAQ is used to exchange data with a central PC, used to control the whole pendulum.

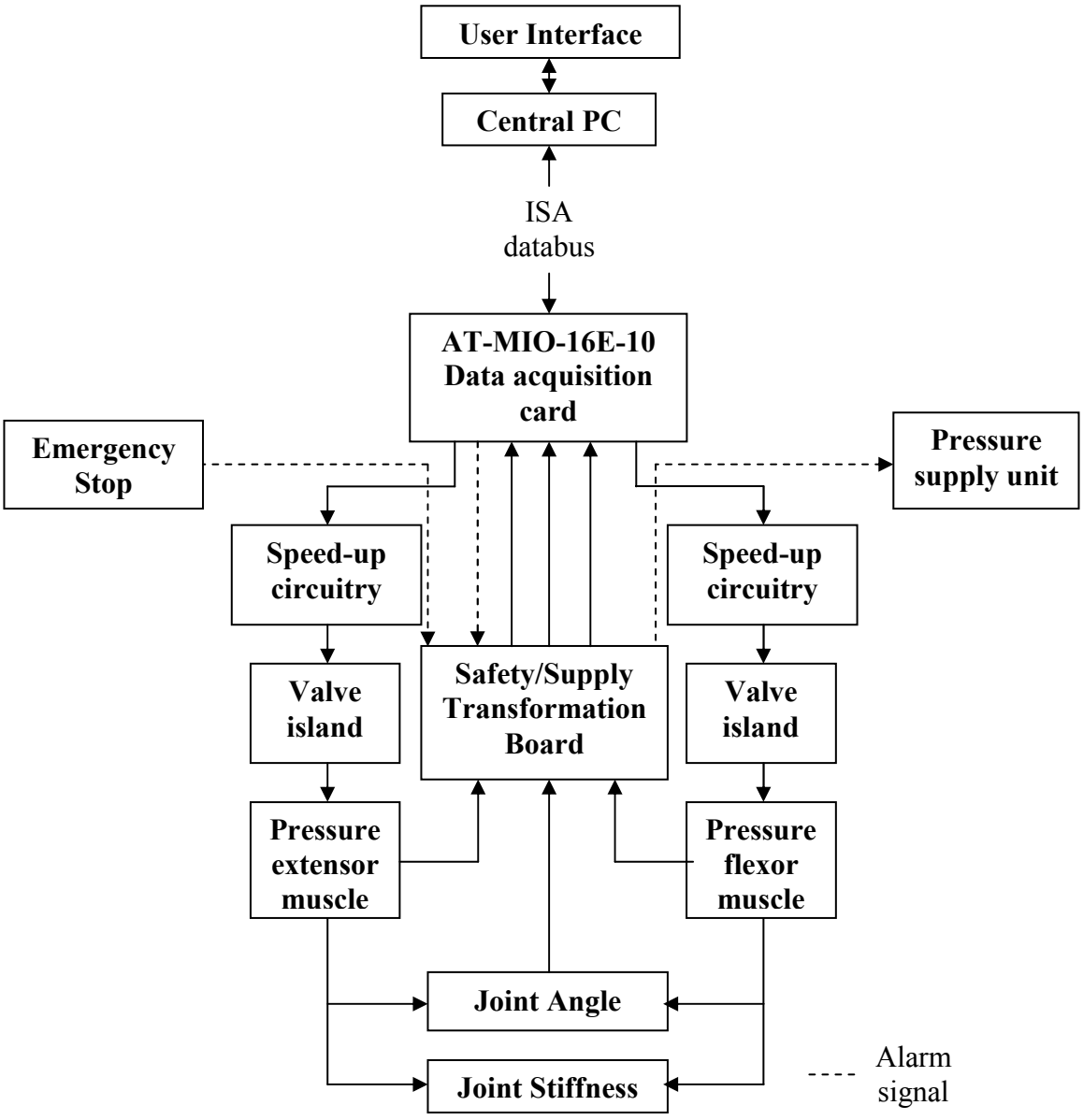

Figure 2.16: Schematic overview of the control hardware

Pressures are measured with absolute pressure sensors and the angular position is captured with an incremental encoder. The valves of the two islands are

controlled by digital micro-controller signals after being transformed by the speed-up circuitry in order to enhance switching speed of the valves. In the next sections detailed information is given about the different elements of the control hardware.

2.3.1. Valve system speed-up circuitry

To have a rapid and accurate pressure control, switching time of the valves should be as little as possible. In order to enhance the opening time of the Matrix valves, the manufacturer proposes a speed-up in tension circuitry, shown in photograph 2.17. Several practical tests, for which is referred to [13], have resulted in an opening and closing times of about 1 ms. An opening voltage of 32 V is being applied during 1 ms.

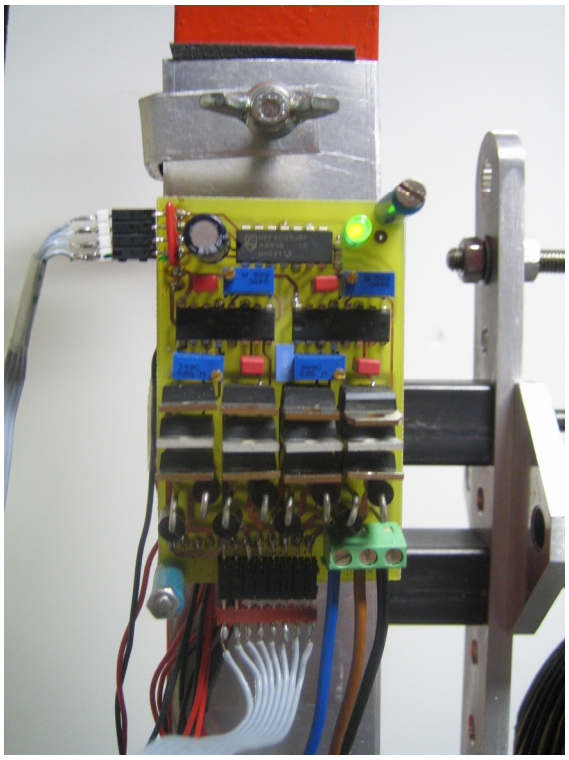

Figure 2.17: View of the speed-up circuitry

The data acquisition card commands the valves via discrete 5 V on/off signals. Two circuits control separately the two inlet valves and another two control the

exhaust valves. Hereby three valves are controlled simultaneously by one circuit. For the electronic scheme of the speed-up circuitry we refer to [14, D.2]

2.3.2. Pressure Sensor

To have a good dynamic pressure measurement, the pressure sensor, shown in figure 2.18, is positioned inside the muscle. The pressure sensor and its electronics are the same as used for 'Lucy', except from the AD-converter. Since this sensor is inside the muscle volume, an absolute pressure sensor is provided. In order to pass through the entrance of a muscle, the size of the sensor and its electronics has to be small (12 mm). An absolute pressure sensor, CPC100AFC, from Honeywell has been selected for this purpose. The sensor measures absolute pressure values up to 100 psi (6.9 bar) and has an accuracy of about 20 mbar. The output of the pressure sensor is amplified by a differential amplifier. As the pressure sensor outputs an analogue signal, special attention should be given to possible noise interferences. High precision and accuracy is required, so a cable consisting of three-wire signal leads is used. The third signal lead, or shield, is necessary and is grounded at the signal source to reduce common-mode noise. In section 2.2.4., more information on how this noise was reduced, is given.

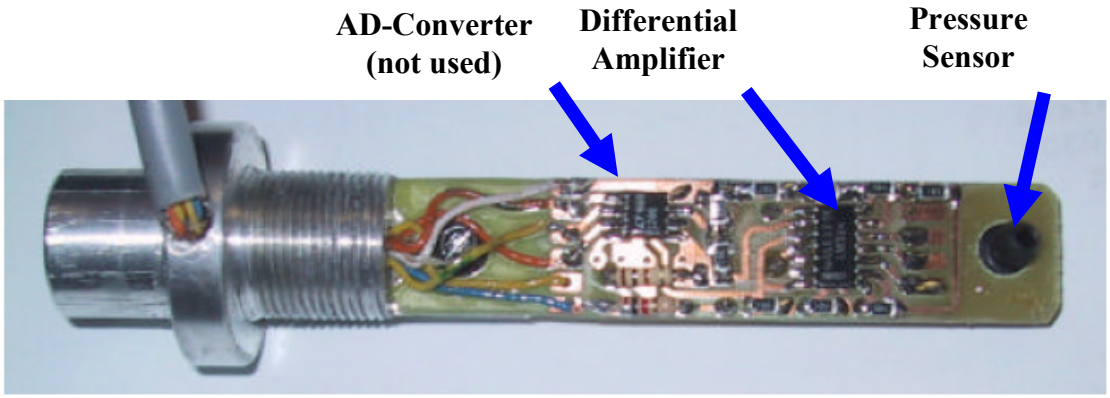

Figure 2.18: View of the pressure sensor

Because the electronics of the pressure sensors are handmade, they differ from each other. That's why a calibration has to be done. By doing this, offset and sensitivity of each pressure sensor are determined, so that at the same pressure

level, the same voltage is output for both sensors. For several pressure levels, the output voltage of the left and right pressure sensors has been acquired. This output voltage is proportional to the applied pressure in the muscle, so by means of simple linear fitting of the measured data, voltage offset and sensitivity can be found.

2.3.3. Incremental encoder

The angular position is measured with an incremental encoder (HEDM6540, Agilent). Such a device converts rotary displacements into digital pulse signals. This type is an optical encoder, which consist of a rotating disk, a light source and a photodetector (light sensor). The disk, which is mounted on the rotating shaft, has pattern of opaque and transparent sectors coded into the disk. As the disk rotates, these patterns interrupt the light emitted onto the photodetector, generating a digital or pulse signal output. The encoder is incremental, which means that the encoder does not output absolute position. To determine direction and reference position, 3 channels are used. Using two code tracks (A and B) with sectors positioned 90°, if A leads B, for example, the disk is rotating in a clockwise direction. If B leads A, then the disk is rotating in a counter-clockwise direction. The third output channel is used as a zero or reference signal, which supplies a single pulse per revolution. In our case, only channel A and B are used. We assume that the position where no muscle is inflated, corresponds with zero degrees and is therefore taken as reference position.

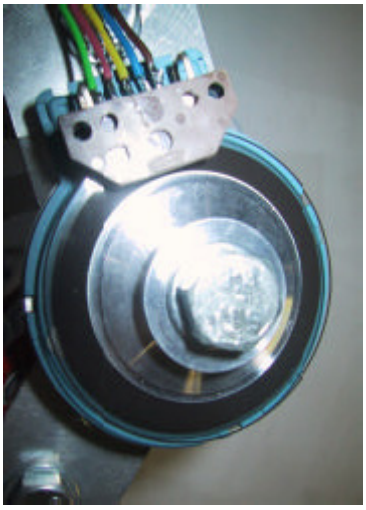

Figure 2.19: View of the incremental encoder

When using a quadrature encoder with the data acquisition card, there are two options. For simple applications, you can connect the encoder directly to the counter/timer of the data acquisition card, without any extra logic or signal conditioning. In this configuration, the counter will increment on state transitions on channel A. Depending on the state of B at those transitions, the counter will count up or down. While this method is very

simple to implement, it has a couple of potentially serious drawbacks. If the encoder disk is not rotating, but is vibrating enough back and forth to cause active transitions on channel A, without changing the state of channel B, then each movement will be incorrectly counted. Another problem results when encoder outputs include noise or jitter that is large enough to be erroneously counted as a valid state transition. Therefore a clock converter device (LS7084, LSI Computer systems) is used. This device converts the A and B signals into a clock and up/down signal that can be connected directly to the data acquisition card. The UP/DN output indicates the direction of rotation. When in X4 mode, resolution is increased four times as the CLK output will now pulse once on every transition of either the A or B signals. The LS7084 includes low-pass filters to prevent miscounts due to noise and jitter. In addition, the LS7804 uses dual one-shots to prevent the miscounting produced by vibration, or dither, as described previously.

2.3.4. Data acquisition card

The AT-MIO-16E-10 data acquisition card has 16 single-ended or 8 differential analog inputs with a sampling rate of 100 kSamples/s, 2 analog output channels and 8 digital I/O channels built in. A Data Acquisition System Timing Controller (DAQ-STC) is available. The DAQ-STC includes 10 counter/timer devices, eight of which are designed to control the timing of analog input and analog output operations. The remaining two counter/timers are 24-bit up/down counter/timers available for a wide variety of timing and counting applications and will be used for retrieving information on the joint angle and also used as an internal clock. Each of the two 24-bit counter/timers of the DAQ-STC includes three input signals (SOURCE, GATE, and UP_DOWN) and two output signals (OUT and INTERRUPT). The DAQ card is installed in a Pentium 500 Mhz computer.

When programming the DAQ hardware, any application development environment (ADE) can be used but in either case a NI-DAQ driver must be installed. This driver has an extensive library of functions that can be called

from the ADE. Those functions can be found in [20]. The driver also carries out many of the complex interactions, such as programming interrupts, between DAQ and computer. In the beginning Matlab was used to program the DAQ card, but complicated programming and low sampling rate made us change our mind and we finally decided to use Visual C++. The minimum control period during which all control calculations are done is 2 ms. Therefore a controller sampling time of 2 ms is used.

A cable connector is used to connect the data acquisition card with the sensors and valves islands. The pressure sensor outputs a non-referenced single-ended (NRSE) analog signal. The left muscle pressure sensor is connected to analog input 6 (PIN 15), the right muscle pressure sensor to analog input 7 (PIN 17). As we mentioned before, analog signals can be disturbed by noise. A proper wiring system and correct grounding of the signal circuit can strongly reduce this problem. To measure a grounded signal source with a single-ended configuration, the DAQ card was configured in the NRSE input configuration. The signal is then connected to the desired analog input (ACH6 for left pressure sensor and ACH7 for right pressure sensor) of the DAQ card, and the signal local ground reference is connected to AIGND. The ground point of the signal should now be connected to the AISENSE pin. Any potential difference between the DAQ card ground and the signal ground appears as a common-mode signal at both the analog input (ACH6/ACH7) and AIGND and this difference is rejected by the internal electronics of the DAQ card. If this method is not used, a difference in ground potentials would appear as an error in the measured voltage.
As mentioned before, the incremental encoder has 3 output channels, but only 2 will be used. The clock converter transforms these two signals into CLK and UP/DOWN. The pulse signal, CLK, is connected to Programmable Function Input (PFI) GPCTR0_SOURCE and the direction signal, UP/DOWN, is connected to the UP_DOWN (DIO6) input. The DAQ-card is configured for a simple event count with hardware up/down control. In this configuration, the DAQ card will control the counter, in such a way that it will count up/down on every transition of either A or B.
Each valve island has 6 valves to be controlled, so 8 digital signals are needed. Because one of the digital channels is already occupied by one of the signals of

the encoder, an analog signal is used. The valves are connected through DIO1…DIO8, except from DIO6. The remaining valve is connected to DAC0OUT

DAC1OUT is used to determine the control time of the whole set-up, by means of a scope.

The remaining 24-bit counter/timer is configured in such a way that an internal base clock of 100 kHz is used as timer.

The time, the encoder counter and sensors values are read at the beginning of every control loop and valve states are changed if necessary.

2.3.5. Safety, supply and transformation board

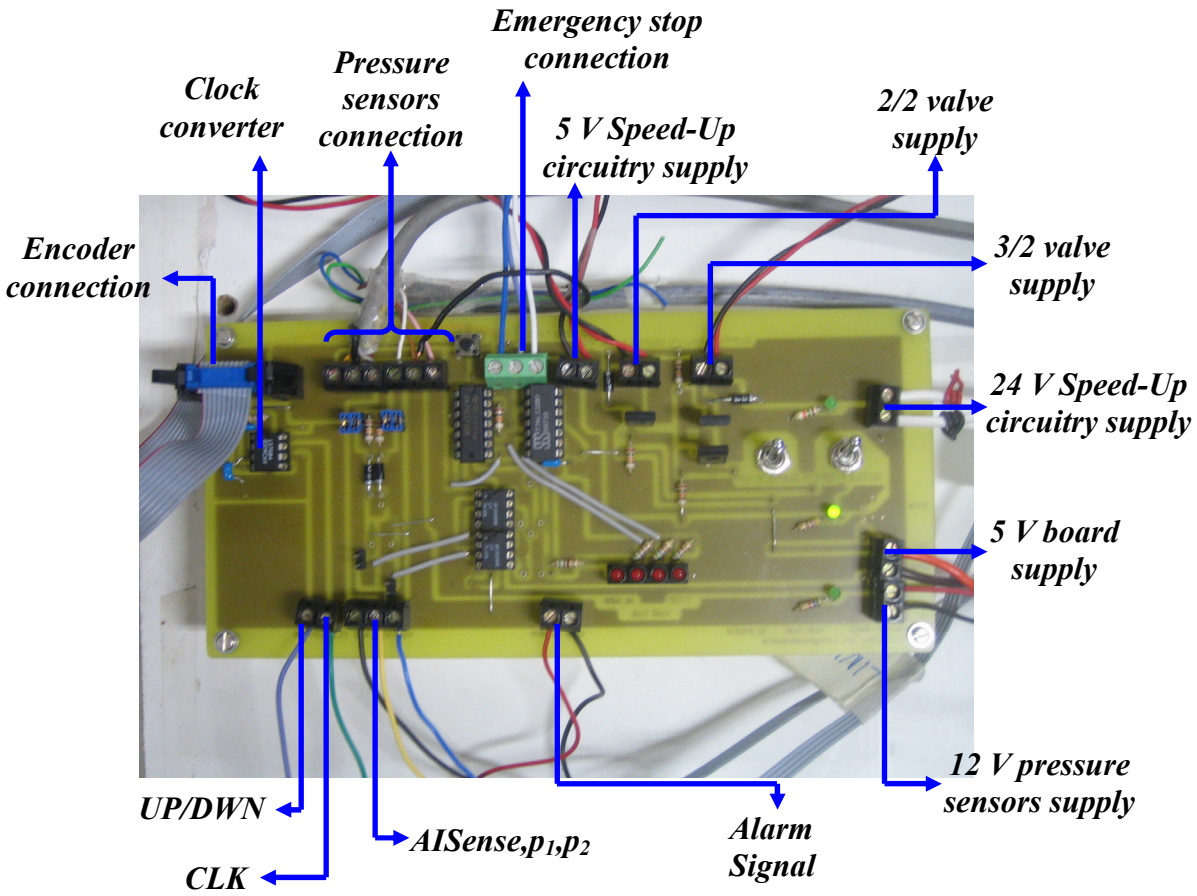

Figure 2.20: View of the safety, supply and transformation board

The maximum absolute pressure in the muscles, without damaging them, is about 4,5 bar. The supply pressure, however, is 7 bar. If working properly, the pressure is limited to 4 bar by the controller. If a problem occurs with the controller, the pressure can exceed this limit, and the muscles will be damaged. To avoid such a situation and to protect the muscles against high pressure, we implemented a safety circuit, which handles all the alarm signals, originating from the pressure sensor inside the muscle and an emergency stop. Whenever an alarm signal is activated, the 3/2 supply valve of the two pressure regulating pneumatic circuits is closed, while the depressurising valve is opened in order to deflate all the muscles.
The safety, supply and transformation board showed in figure 2.20, consists of the safety circuit, the connection to all voltage supply sources and to the signals from the pressure sensors and encoder. On this board, the encoder signals are also transformed by the clock converter.

2.4 Software

As mentioned before, Visual C++ is used to program the DAQ card. To make experiments and testing more user friendly, a graphical user interface (GUI) was developed. A brief explanation on how to use the GUI will now be given.
The GUI consists of different tabs. Each tab has some parameters, to be filled in by the user.

The first tab to appear is the *Control* tab and is shown in figure 2.21 . In this tab, parameters like sampling rate, acquisition time and PID gains used by trajectory tracking controller are set. These values can be varied online. A special attention is given to the compliance calculation. More information on the definition of p_S is given in chapter 3
In the second tab shown in figure 2.22 , the *Model* parameters are set. As explained in the mechanical design, we can alter the load of the pendulum by removing or adding discs. By clicking on the check boxes, the user can enter the discs used during the experiments. Other masses, free oscillation period and

atmospheric pressure are also to be filled in, so that the pendulum can be modelated.

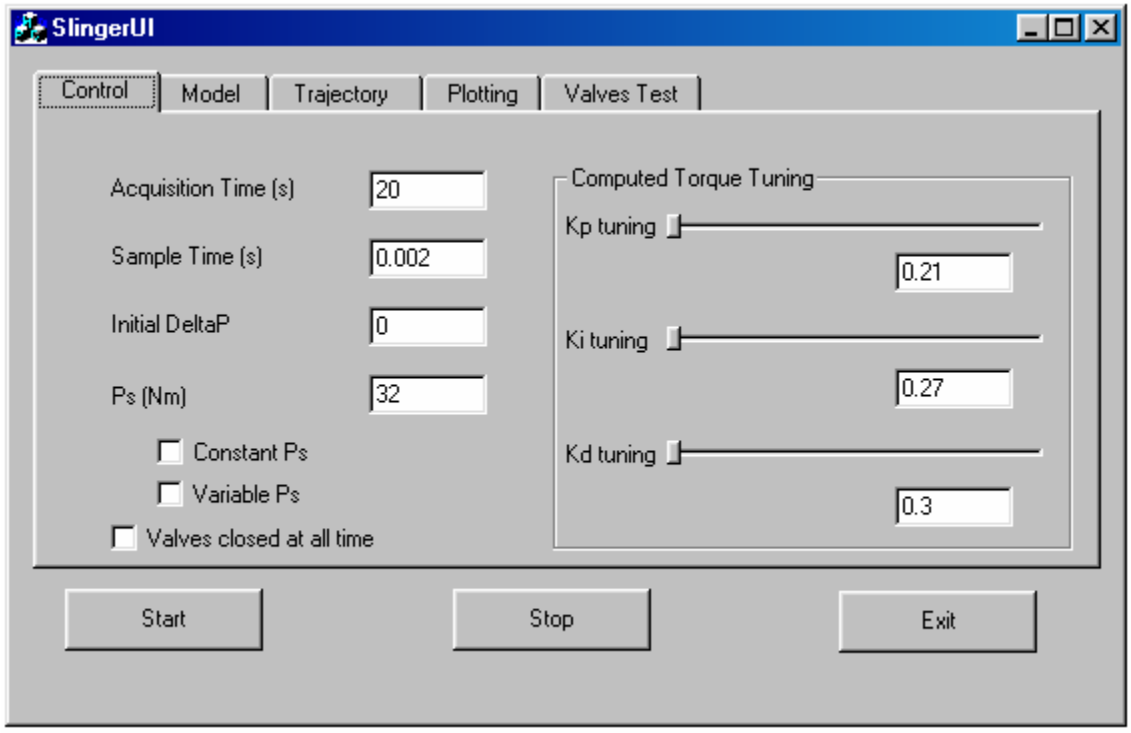

Figure 2.21: The Control tab of the GUI

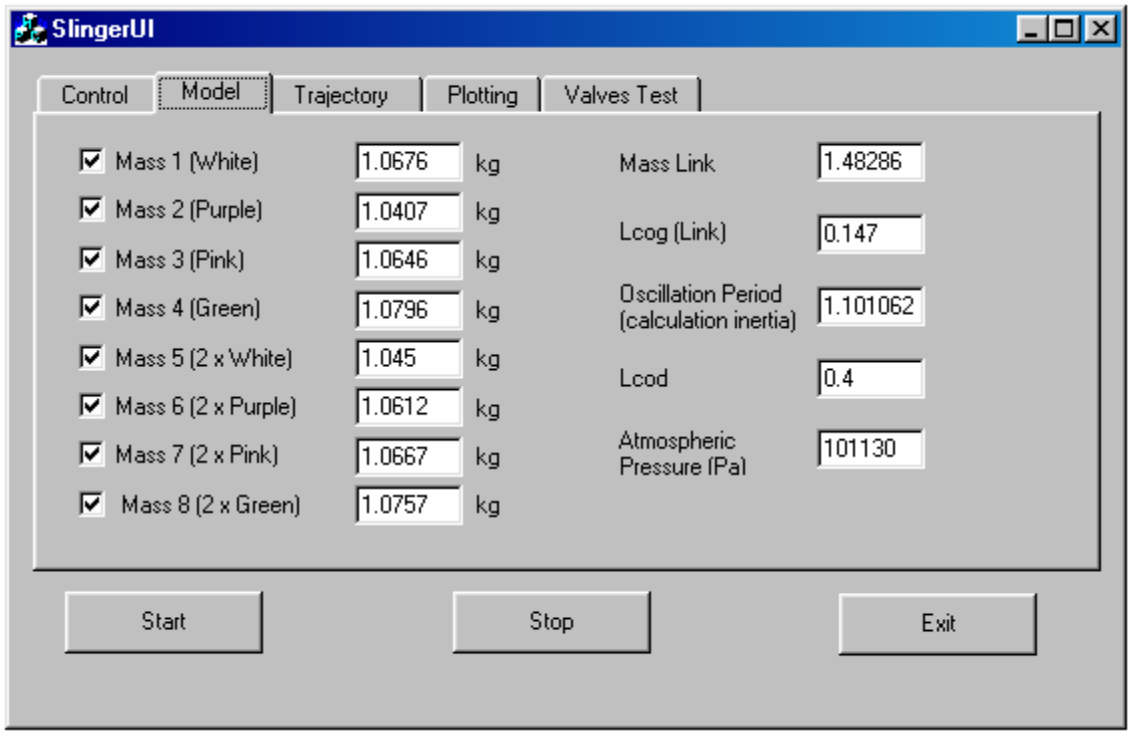

Figure 2.22: The Model tab of the GUI

The *Trajectory* tab, is used to specify the initial angle, the offset and the frequency of the desired trajectory we want to be tracked by the tracking controller.

In the *Plotting* tab, the user can specify the file where data has to be written to. Because plotting data in Visual C++ is too complicated, we rather use Matlab. Therefore, data acquired in Visual C++ has to be sent to Matlab. The Matlab engine is loaded in C++ to access Matlab's prebuilt graphics functions. By using this engine, we are able to send the data to the Matlab workspace and plot them directly from Visual C++. After each experiment the data is automatically sent to Matlab and plotted. The option to plot different type of data during the experiment or test, can also be enabled. Plotting the data during the experiment takes a lot of time, so it should only be done when no control action is needed.
Once the data is plotted, Matlab workspace will open, so that the data can be manipulated if necessary. To calculate the energy consumption during the experiment, a Matlab M-file is made. Typing "CalcEnergy" into the workspace will give the valve action and energy consumption. More information on how energy is being calculated will be given in the next chapter.

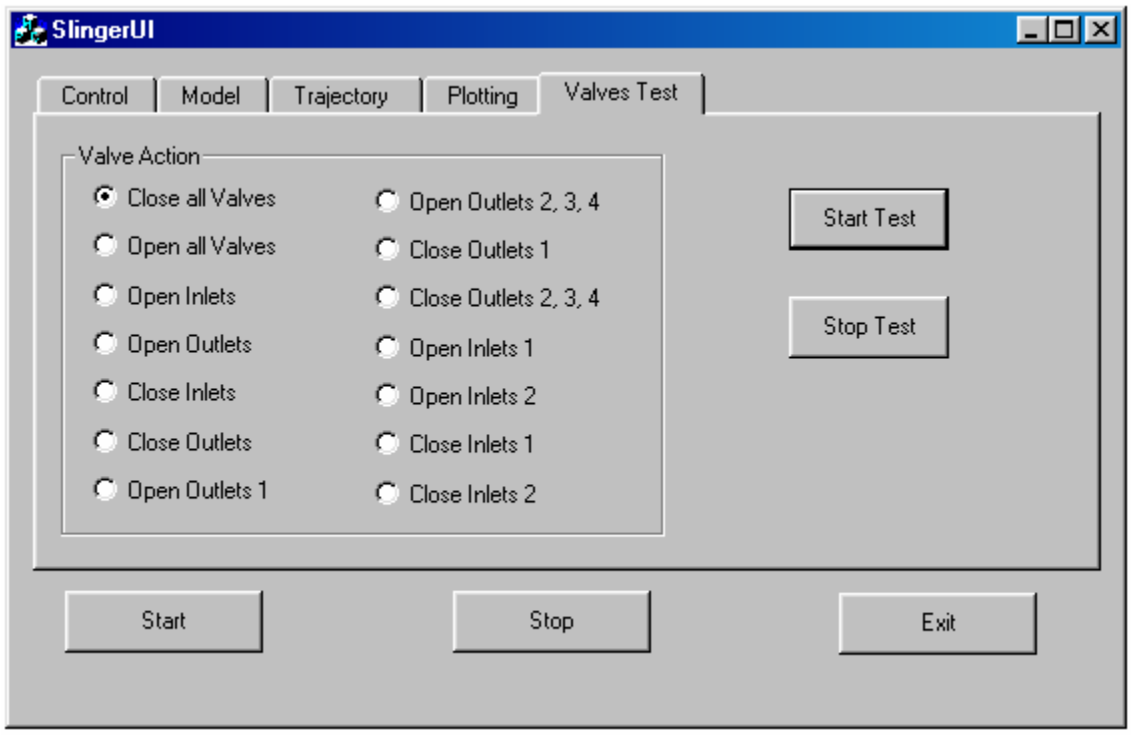

Figure 2.23: The Valves Test tab of the GUI

As we experienced a lot of problems making the valves island to work properly, a last tab is used to test the valves. Input and output valves can be tested, by choosing the desired valve and to start the test. An overview of the *valves test* tab is given in figure 2.23.

2.5 Conclusion

In this chapter, the hard- and software needed to construct the pendulum was described. By analyzing the joint characteristics, the muscles and actuators connection parameters were determined. To acquire the pressures in the muscles and the joint angle, and to control the valves, a data acquisition card is used. The control of the pendulum is done by a PC. To make the experimental setup user friendly a GUI was implemented.

Chapter 3

Control

3.1. Introduction

The main purpose of this work is to incorporate the exploitation of the natural dynamics by adapting joint stiffness in combination with trajectory tracking.
In section 3.2, the main focus is on the development of a tracking controller, which incorporates the actuator characteristics and dynamic model of the robot. The control strategy consists of a multilevel construction of several essential blocks, trying to cope with the non-linear structure using model-based feedforward techniques. This tracking controller will be incorporated in a simulation model and in the physical set-up.
Section 3.3 gives a mathematical formulation for compliance adaptation, in order to reduce energy consumption and control activity during the joint trajectory tracking.
A simulation model of a one-dimensional pendulum with one antagonistic muscle pair actuating the joint, is presented in section 3.4. This model is used to show the importance of appropriate stiffness selection in order to reduce control activity. A joint tracking controller is incorporated in a simulation model. Finally, some energy considerations concerning the proposed control strategy are given in section 3.5

3.2. Joint tracking controller

The joint tracking controller has to command the valves of the two muscles in order to track an imposed desired trajectory. The complete system incorporates several nonlinearities such as the non-linear behaviour of the pendulum configuration and the nonlinearities introduced by the antagonistic muscle set-up. The tracking controller is designed in a modular way, which means that the

controller can be easily adapted for an application with another mechanical configuration, but with an analogue antagonistic muscle actuator set-up. Therefore, the controller is multistage, of which each stage deals with the different nonlinearities separately. A schematic overview of the proposed control structure is given in figure 3.1. The controller consists of three parts: a feedback linearization module, a delta-p unit and a bang-bang pressure controller. The feedback linearization or computed torque module is a standard nonlinear control technique, which deals with the nonlinear behaviour of the mechanical pendulum configuration [1]. The delta-p unit translates calculated torques into desired muscle pressure levels, coping with the nonlinearities introduced by the muscle actuation system. Finally, the bang-bang pressure controller commands the valves in order to set the required pressures in the muscles.

This control structure will be implemented in a computer simulation of the pendulum, as well as in the control of the physical set-up.

As is said before, the pendulum consists of one modular part of 'Lucy', which means that the used tracking controller will have the same structure as described in [14]. For the sake of convenience, the same discussion on the control strategy will be given. Some of the modules were slightly changed: an integrator is added to the computed torque method, and of course the model dynamics and parameters are not the same. Special attention is also given to the estimation of these parameters.

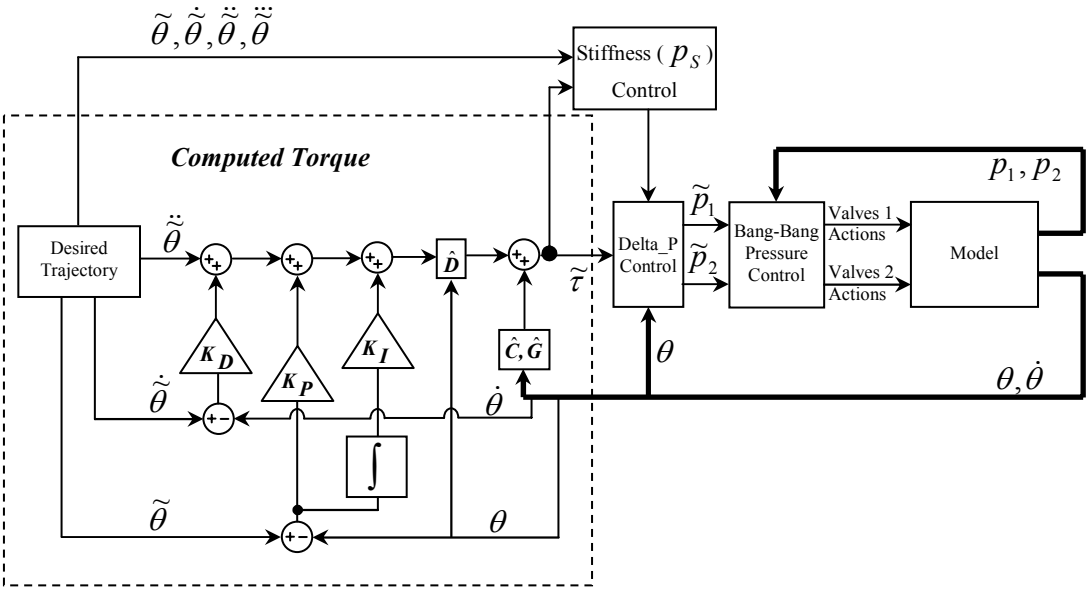

Figure 3.1: Schematic overview of the control structure

In the first module, the computed torque $\tilde{\tau}$ is calculated. The computed torque method consists in decomposing the controller into two parts. One part is model-based in that it makes use of the modelled dynamics of the particular system under control. The second part of the control is error-driven in that it forms error signals by differencing desired and actual variables and multiplies this by gains. It's also called the servo portion[1].

To find the model-based part, the rigid body dynamics can be written down:

$$\tau = \hat{D}(\theta)\ddot{\theta} + \hat{C}(\theta,\dot{\theta})\dot{\theta} + \hat{G}(\theta) \tag{3.1}$$

where $\hat{D}(\theta)$ is the inertia matrix, $\hat{C}(\theta,\dot{\theta})$ is the centrifugal and coriolis term, $\hat{G}(\theta)$ is the gravity term and θ the joints positions of the real system. In our case, the system is one-dimensional. Consequently, those matrices will consist of only one term. The symbol ^ denotes that the respective expressions are calculated with estimated parameter values. The main problem is to find an optimal model of the pendulum.
We can linearize this equation by choosing

$$\tau = \alpha\,\tau' + \beta \text{ , with } \alpha = \hat{D}(\theta) \text{ and } \beta = \hat{C}(\theta,\dot{\theta})\dot{\theta} + \hat{G}(\theta) \tag{3.2}$$

Filling this into the rigid body mechanics (3.1) gives:

$$\tau' = \ddot{\theta} \tag{3.3}$$

As we see, the resulting equation is that of unit-mass system. The design of the servo position is now very simple: gains are chosen as if we were controlling systems composed of single unit masses.

$$\tau' = \ddot{\tilde{\theta}} + K_D(\dot{\tilde{\theta}} - \dot{\theta}) + K_P(\tilde{\theta} - \theta) + K_I\int(\tilde{\theta} - \theta)dt \tag{3.4}$$

The symbol ~ represents required values. The gains K_I, K_P and K_D are manually tuned in order to influence controller performance. The following expression for the computed torque is thus obtained:

$$\tilde{\tau} = \hat{C}(\theta,\dot{\theta})\dot{\theta} + \hat{G}(\theta) + \hat{D}(\theta)\left[\ddot{\tilde{\theta}} + K_D(\dot{\tilde{\theta}} - \dot{\theta}) + K_P(\tilde{\theta} - \theta) + K_I\int(\tilde{\theta} - \theta)dt\right] \quad (3.5)$$

The required pressures values to be set in the muscles are then calculated by the delta-p control unit. These two gauge pressures of both muscles are generated as follows:

$$\tilde{p}_1 = \frac{p_S}{\hat{t}_1(\theta)} + \Delta\tilde{p} \quad (3.6a)$$

$$\tilde{p}_2 = \frac{p_S}{\hat{t}_2(\theta)} - \Delta\tilde{p} \quad (3.6b)$$

with p_S a parameter that is used to influence the sum of pressures and consequently the joint stiffness, $\Delta\tilde{p}$ influences the difference in pressure of the two muscles and consequently the generated torque. The functions $\hat{t}_1(\theta)$ and $\hat{t}_2(\theta)$ are calculated with estimated values of the muscle force functions and geometrical parameters of the pull rod and leverage mechanism of the actuation system. Expression (2.5) allows linking the required torque to the required pressure values in the muscles:

$$\tilde{\tau} = \tilde{p}_1\hat{t}_1(\theta) - \tilde{p}_2\hat{t}_2(\theta) = (\hat{t}_1(\theta) + \hat{t}_2(\theta))\Delta\tilde{p} \quad (3.7)$$

If the calculated pressure values $\tilde{p}_1$ and $\tilde{p}_2$ of equations (3.6) are set in the muscles, the generated torque depends only on $\Delta\tilde{p}$ and is independent of the joint stiffness parameter p_S, in case the modelling would be perfect. This means that joint stiffness is changed without affecting the joint angular position.

Feeding back the knee angle θ and introducing the torque $\tilde{\tau}$, expression (3.7) can be used to determine the required $\Delta\tilde{p}$:

$$\Delta\tilde{p} = \frac{\tilde{\tau}}{\hat{t}_1(\theta) + \hat{t}_2(\theta)} \tag{3.8}$$

The delta-p unit is actually a feedforward calculation from torque level to pressure level, using the cinematic model of the muscle actuation system. The calculated $\Delta\tilde{p}$ affects the torque required to track the desired trajectory, while p_S is introduced to determine the sum of the pressures, which influences the stiffness of the joint as was discussed in section 2.2.2.3. Increasing p_S lowers the compliance of the joint.

In the last control block the desired gauge pressures calculated by the delta-p unit are compared with the measured gauge pressure values after which appropriate valve actions are taken by a bang-bang pressure controller. We define the pressure error as $(p_{error} = \tilde{p} - p)$, with $\tilde{p}$ the desired pressure calculated by the delta-p unit and p the pressure measured in the muscle. The bang-bang pressure control scheme is given in figure 3.2.

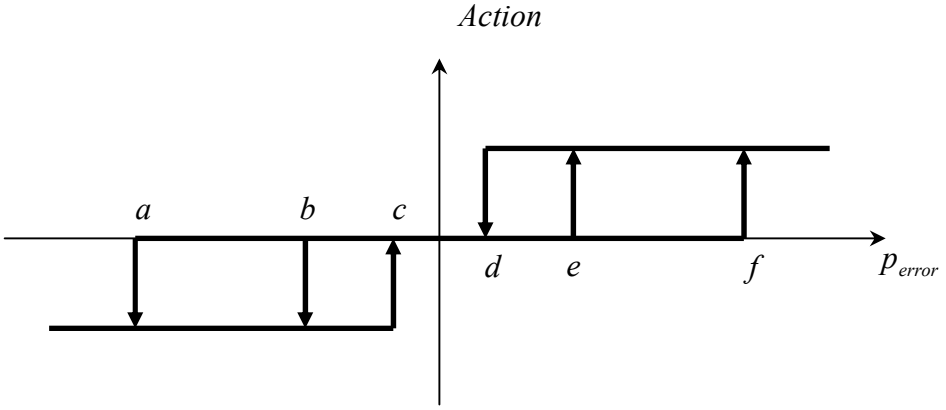

Figure 3.2: Bang-bang pressure control scheme

If the pressure difference stays between c and d, no valve action takes place (dead zone) and the muscle stays closed. In this situation the muscle is acting as a compliant passive element. If the pressure error is increasing and reaches level e, one inlet valve is opened in order to make the pressure rise to the desired

level. If one opened inlet valve is not enough and p_{error} is still increasing and becomes larger than f, a second inlet valve is opened. The inlet valves are closed again when the difference drops below level d. The same approach is used for negative values of p_{error}, but now exhaust valves will be opened. If p_{error} is beyond level a, 4 exhaust valves will be opened instead of 2.

3.3. Mathematical formulation for compliance adaptation

In section 2.2.2.3 a formulation of the compliance was given for closed muscles. As shown, a weighted sum of both pressures in the antagonistic muscle set-up determines the joint compliance, while pressure differences determine the generated torque and consequently also the joint position. This means that compliance can be set while controlling the position. This is interesting, because by setting the appropriate joint stiffness control activity can be reduced while tracking a desired trajectory.

In the previous paragraph, the parameter p_S, used to influence the sum of pressures and consequently the joint stiffness, was introduced. The question is now: what should be the value of p_S? In other words, what should be the joint stiffness, so that the natural motion "best" fits the desired trajectories? In this section a mathematical formulation developed by Verrelst [14], is given for estimating an appropriate value of p_S.

The starting-point for the estimation procedure is to fit the natural pressure slopes with the required ones. The desired pressures depend on the desired trajectory. The delta-p unit in combination with the computed torque module determinates the required pressures as explained in the previous section. Pressure changes with closed muscles are influenced by p_S.

The required pressure slopes are calculated by deriving equations (3.6) with respect to the trajectory $\tilde{\theta}$:

$$\frac{d\tilde{p}_1}{d\tilde{\theta}} = -\frac{p_S}{t_1^2}\frac{dt_1}{d\tilde{\theta}} + \frac{d\Delta\tilde{p}}{d\tilde{\theta}} \tag{3.9a}$$

$$\frac{d\tilde{p}_2}{d\tilde{\theta}} = -\frac{p_S}{t_2^2}\frac{dt_2}{d\tilde{\theta}} - \frac{d\Delta\tilde{p}}{d\tilde{\theta}} \tag{3.9b}$$

Taking into account equation (3.8), the derivatives can be expanded by:

$$\frac{d\Delta\tilde{p}}{d\theta} = \frac{1}{(t_1+t_2)^2}\left[(t_1+t_2)\tilde{K} - \left(\frac{dt_1}{d\tilde{\theta}} + \frac{dt_2}{d\tilde{\theta}}\right)\tilde{\tau}\right] \tag{3.10}$$

with $\tilde{K}$ (equation (2.12)) representing the stiffness associated with the desired trajectory and $\tilde{\tau}$ the torque calculated by the computed torque module.
On the other hand, combining equation (2.15), valid for closed muscles, with equations (3.6) yields:

$$\frac{d\tilde{p}_1}{d\tilde{\theta}} = -p_S\left(\frac{n}{t_1}\frac{V_{1_0}^n}{V_1^{n+1}}\frac{dV_1}{d\tilde{\theta}}\right) - (P_{atm} + \Delta\tilde{p})\left(n\frac{V_{1_0}^n}{V_1^{n+1}}\frac{dV_1}{d\tilde{\theta}}\right) \tag{3.11a}$$

$$\frac{d\tilde{p}_2}{d\tilde{\theta}} = -p_S\left(\frac{n}{t_2}\frac{V_{2_0}^n}{V_2^{n+1}}\frac{dV_2}{d\tilde{\theta}}\right) - (P_{atm} - \Delta\tilde{p})\left(n\frac{V_{2_0}^n}{V_2^{n+1}}\frac{dV_2}{d\tilde{\theta}}\right) \tag{3.11b}$$

The idea is to match for each muscle the required pressure slope with the slope associated with the natural dynamics, by selecting an appropriate p_S value. Once the desired trajectory is known, expressions (3.9) and (3.11) can be evaluated in every point θ_i. Subsequently a p_S value is searched in order to match as much as possible both pressure slopes. For each θ_i, equations (3.9a) and (3.11a) and equations (3.9b) and (3.11b) are thus respectively combined and each solved for a value $p_{S_j}^i$.

$$p_{S_1}^i = \left[\left(\frac{1}{t_1^2} \frac{dt_1}{d\tilde{\theta}} - \frac{1}{t_1} \frac{n}{V_1} \frac{dV_1}{d\tilde{\theta}} \right)^{-1} \left(\left(P_{atm} + \Delta\tilde{p} \right) \left(\frac{n}{V_1} \frac{dV_1}{d\tilde{\theta}} \right) + \frac{d\Delta\tilde{p}}{d\tilde{\theta}} \right) \right]_{\theta_i} \tag{3.12a}$$

$$p_{S_2}^i = \left[\left(\frac{1}{t_2^2} \frac{dt_2}{d\tilde{\theta}} - \frac{1}{t_2} \frac{n}{V_2} \frac{dV_2}{d\tilde{\theta}} \right)^{-1} \left(\left(P_{atm} - \Delta\tilde{p} \right) \left(\frac{n}{V_2} \frac{dV_2}{d\tilde{\theta}} \right) - \frac{d\Delta\tilde{p}}{d\tilde{\theta}} \right) \right]_{\theta_i} \tag{3.12b}$$

Note that the initial volume V_{j_0}, when closing a muscle is set equal to the actual volume V_j.

From here on, there are two options. We can use a constant p_S, as explained by Verrelst. The $p_{S_j}^i$ are calculated in each point θ_i, separated by equal time intervals along the desired trajectory, and a mean is then taken to select one p_S:

$$p_S = \frac{1}{2z} \sum_{i=1}^{z} \left[p_{S_1}^i + p_{S_2}^i \right] \tag{3.13}$$

with z the number of points chosen to evaluate equations (3.12)

This means that a constant p_S is used along the whole trajectory. Probably, a constant p_S will only be suitable for some simple trajectories. As we want a method for any trajectory, a variable p_S is needed. One solution is to use the same idea of comparing the pressure slopes for the complete trajectory at once, but for the calculation a differential formulation on p_S has to be solved. To avoid complicated calculations, it was chosen for evaluating the equations (3.12) at every sample time during the control of the pendulum. At every control sample time, the angle θ_i is acquired and both $p_{S_1}^i$ and $p_{S_2}^i$ are calculated. The mean for both muscles is then calculated with $p_S^i = \frac{p_{S_1}^i + p_{S_2}^i}{2}$, so that at every sample time a different p_S is set.

As we see in the equations (3.12a) and (3.12b) a correct estimation of the volume is needed. So the volumes of the end fittings and tubing's should be added. If this is not done, the equations (3.12a) and (3.12b) will not give the most suitable

p_S and an erroneous stiffness will be set. The influence of the end fittings and tubing volumes will be explained in more detail in the next chapter.

As mentioned in the previous chapter, special attention was given to the compliance calculation during the design of the GUI. On the *Control* tab the user can choose between three different options: he can set a constant p_S by giving it a certain value, or by calculating it with the method described above, or use a variable p_S, also calculated by the latter method.

3.4. The simulation model of the pendulum

3.4.1. Description of the pendulum set-up

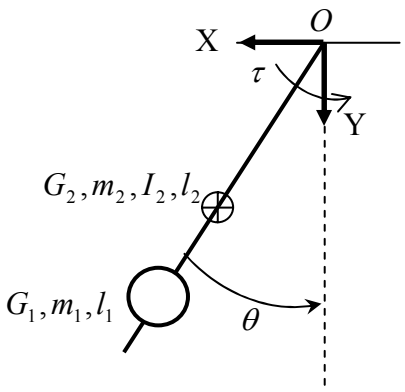

Figure 3.3: The pendulum model

The pendulum model consists of 2 parts: the link, and the mass. The mass is modelled as a point mass and is positioned at a distance l_1 of the rotation point. The length of the link is l_2, its mass m_2 and the moment of inertia about its centre of mass G_2 is I_1. The location of the centre of mass G_2 of the link is given by $OG_2 = \alpha l_2$, with $\alpha = 0.769$. The parameter values are given in table 3.

i	$l_i\,(m)$	$m_i\,(kg)$	$I_i\,(kgm^2)$
1	0.4	5.327	0.852
2	0.45	1.483	0.0362

Table 3.1: Inertial parameters of the pendulum model

An accurate estimation of those parameters is crucial, as well for the computer simulation as for the joint tracking controller. In general the model of the pendulum will not be perfect. Think for example of the friction model, this is not taken into account in our model. To illustrate the influence of the parameter errors on the joint tracking controller we can first look at the real pendulum dynamics:

$$\tau = D(\theta)\ddot{\theta} + C(\theta,\dot{\theta})\dot{\theta} + G(\theta) \tag{3.14}$$

Although, for our control law, we use equation (3.2) :

$$\tau = \alpha\,\tau' + \beta \text{ , with } \alpha = \hat{D}(\theta) \text{ and } \beta = \hat{C}(\theta,\dot{\theta})\dot{\theta} + \hat{G}(\theta)$$

where in this case $\hat{D}(\theta), \hat{G}(\theta)$ and $\hat{C}(\theta,\dot{\theta})$ are the estimated inertia, gravity and coriolis/centrifugal term.

Decoupling and linearizing will not therefore be perfectly accomplished when parameters are not known exactly. Starting from equation (3.5), the closed-loop equations for the system are given by:

$$\ddot{E} + K_D\dot{E} + K_P E + K_I \int E\,dt = \hat{D}^{-1}\left[\left(D-\hat{D}\right)\ddot{\theta} + \left(C-\hat{C}\right)\dot{\theta} + \left(G-\hat{G}\right)\right] \tag{3.15}$$

We clearly see that if the parameters are exactly estimated, the right hand disappears and no control error will be made. As mentioned before, this will not be the case in our physical setup. Therefore, some deviations on these model parameters were incorporated in the simulation.

3.4.2. The mechanical equations of the model

The equation of motion is given by (3.14):

$$\tau = D(\theta)\ddot{\theta} + C(\theta,\dot{\theta})\dot{\theta} + G(\theta)$$

Assuming the model as being frictionless, we can now calculate the elements of the inertia, coriolis and gravity terms (Appendix A):

$$D(\theta) = m_1 l_1^2 + m_2 \alpha^2 l_2^2 + I_2 \tag{3.16a}$$

$$C(\theta,\dot{\theta}) = 0 \tag{3.16b}$$

$$G(\theta) = -g\left(m_1 l_1 + m_2 \alpha\, l_2\right)\sin\left(\theta\right) \tag{3.16c}$$

3.4.3. The thermodynamical equations of the model

The equations describing the thermodynamic processes in the pneumatic system were already discussed by [14]. As we need these equations to understand how the computer simulation, explained in the next section, works, those equations will be repeated here.

The thermodynamic processes in the two muscles/valve systems are described by four first order differential equations. Two equations determine the pressure changes in both muscles of the pendulum and the remaining two describe conservation of mass in the respective muscle volume. In assumption that the pressurised air behaves like a perfect gas, the perfect gas law completes the set of equations required to run the simulation.

The first law of thermodynamics, while neglecting the fluid's kinetic and potential energy and assuming a polytropic process, can be written for each muscle as [14, Appendix B]:

$$\dot{p}_i = \frac{n}{V_i}\left(rT_{air}^{\sup}\dot{m}_{air_i}^{in} - rT_{air_i}\dot{m}_{air_i}^{ex} - \left(P_{atm} + p_i\right)\dot{V}_i\right) \tag{3.17}$$

with r the dry air gas constant. $T_{air}^{\sup}$ is the temperature of the supply air and T_{air_i} the temperature in muscle i. The total orifice flow through the opened inlet valves and exhaust valves of muscle i are given by $\dot{m}_{air_i}^{in}$ and $\dot{m}_{air_i}^{ex}$ respectively. The latter two can be calculated with the following equations, which represents a normalized approximation of a valve orifice flow defined by the International Standard ISO6358
[1989]:

$$\dot{m}_{air} = CP_u\rho_0\sqrt{\frac{293}{T_{air}^u}}\sqrt{1-\left(\frac{P_d/P_u - b}{1-b}\right)^2} \qquad if \qquad \frac{P_d}{P_u} \geq b \qquad (3.18a)$$

$$\dot{m}_{air} = CP_u\rho_0\sqrt{\frac{293}{T_{air}^u}} \qquad if \qquad \frac{P_d}{P_u} \leq b \qquad (3.18b)$$

with ρ_0 the air density at standard conditions. C and b are two flow constants characterising the valve system. The constant C is associated with the amount of air flowing through the valve orifice, while b represents the critical pressure ratio at which orifice air flows become maximal. P_u and P_d are the upstream and downstream absolute pressures, while T_{air}^u air is the upstream temperature. When choking occurs, equation (3.18b) is valid, otherwise equation (3.18a) is used. The muscles are controlled by a number of fast switching on/off valves. Once the actions (opening or closing) of the valves are known, all the air flows can be calculated in order to be substituted in (3.17). The temperature in the muscle is calculated with the perfect gas law:

$$T_{air_i} = \frac{P_i V_i}{m_{air_i} r} \qquad (3.19)$$

with $P_i = \left(p_i + P_{atm}\right)$ the absolute pressure in muscle i. The total air mass m_{air_i} is given by integration of the net mass flow entering muscle i:

$$\dot{m}_{air_i} = \dot{m}_{air_i}^{in} - \dot{m}_{air_i}^{ex} \qquad (3.20)$$

3.4.4. Complete simulation model

The structure of the complete simulation model is given in figure 3.4 and is based on the simulation model of 'Lucy'. The kernel of these simulations is based on three equation blocks, which integrates first order differential equations only. The differential equations are numerically integrated using a 4th order Runge-Kutta method with integration time step of 50 μs.

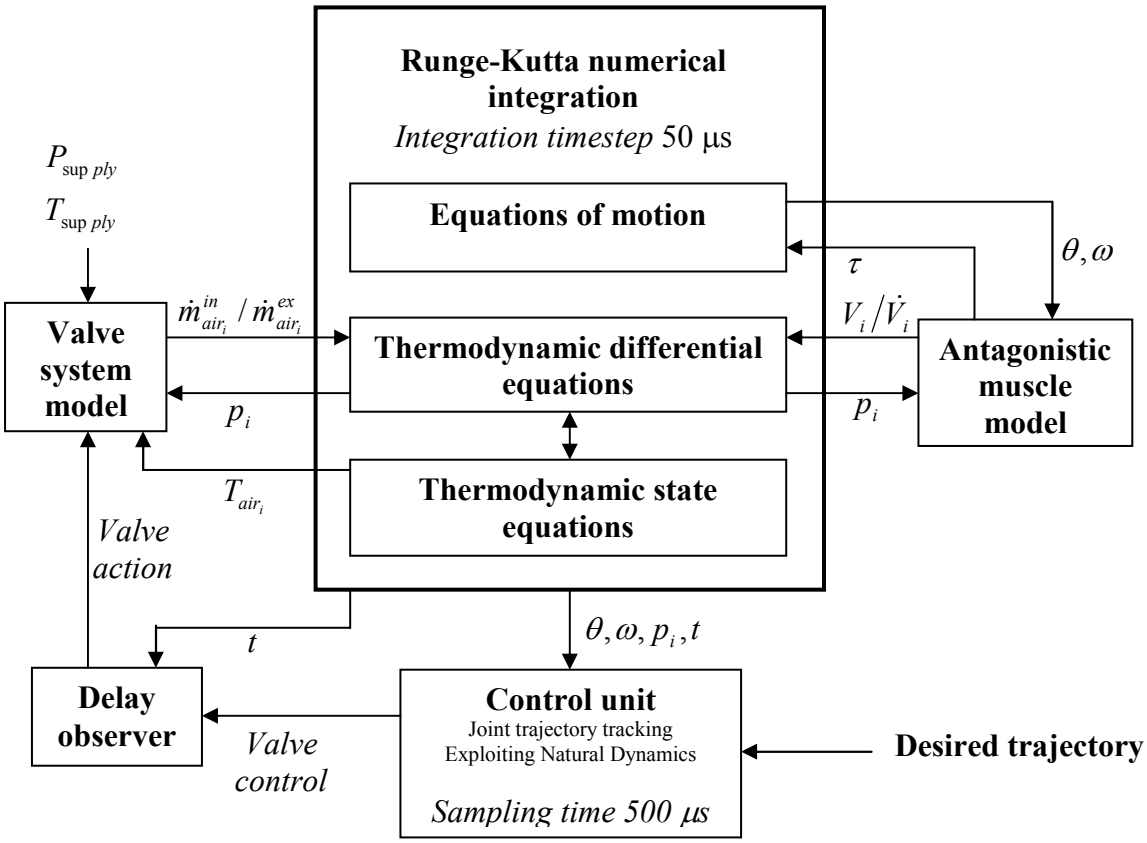

Figure 3.4: Structure of the complete simulation model

The first block contains the equations of motion given by (3.14). Since the equations of motion are second order, these equations have to be transformed into a set of first order equations. In order to do this, the angular velocity ω is introduced:

$$\omega = \dot{\theta} \tag{3.21}$$

In our case, the equation of motion can now be rewritten as two first order equations:

$$\begin{cases} \dot{\omega} = D(\theta)^{-1}\left[\tau - C(\theta,\omega) - G(\theta)\right] \\ \dot{\theta} = \omega \end{cases} \tag{3.22}$$

The thermodynamics of the joint is characterized by four first order differential equations on pressure (3.17) and air mass (3.20) (2 first order equations for each muscle). Finally the two thermodynamic state equations (3.19) complete the set.
The link between the equations of motion and the thermodynamic differential equations is given by the antagonistic muscle model. In this model the generated torque τ (3.7) of the joint is calculated with the pressure information of the thermodynamic block. To calculate this torque the polynomial forces (2.2) must be known. These are functions of the contraction (2.11), which can be calculated by knowing the angle information from the equations of motion. Additionally, to determine the pressure changes in the thermodynamic differential equation block, muscle volume and volume changes are needed. They are calculated with the polynomial volume functions (2.3). Consequently, angle and angular velocity are required from the equations of motion.
Starting from the desired trajectory and by taking the natural dynamics into account, the control unit determines the appropriate valve actions and sends valve control signals to the delay observer. The valves have an observed opening and closing time delay of about 1ms [13] This is incorporated in the delay observer. In the simulation a delay time of opening or closing the valve of 1 ms is used. The valve system model will then calculate the air mass flow rates for each muscle. Therefore, temperature and pressure in the muscles are required from the thermodynamic differential equations block.

Additionally, deviations can be introduced on the mass, centre of gravity and inertia parameters and on the force functions, in order to check the robustness of the controller, as was explained in the previous section.

3.5. Energy considerations

The main purpose of this thesis is to investigate the exploitation of the natural dynamics of the system in order to reduce energy consumption and control action. Therefore, it will be interesting to have an idea of the energy consumption and control action that takes place during the simulation or experiment.

As the valves are controlled by the control unit, the valve actions will give us an idea of the control action. The control signals to action the valves have two possible values: 1 for an open valve and 0 for a closed valve. To have an idea of the amount of control action, the control signals for the input as well as for the output valves are accumulated during the experiment or simulation. The time per period , during which the input/output valves are open is then calculated with:

$$Valve\ Action\,(ms/\ period) = \frac{sum(Valve\ Signals)}{f_{Sine-Wave}\,T_{acquisition}} * Sample\,Time * 1000 \qquad (3.23)$$

With $Sample\,Time$, the sample time at which data is acquired and not the controller sample time. In the case of the physical pendulum, the sample time at which data is acquired and the controller sample time are the same.

The thermodynamic conditions of the pressurized air also determine energy consumption. So apart from valve actions, it is interesting to consider actual air mass entering and leaving the total system.

The energy consumption depends not only on the air mass flows but is related to the thermodynamic conditions of the compressed air supply source. It is not straightforward to calculate the actual energy needed to power the pendulum, since this depends on how the pressurized air of the pneumatic supply source has been created. One way to give an idea of energy consumption is to calculate the exergy associated with the particular pneumatic air mass flow. Exergy is in fact the maxi-mum amount of energy, with respect to the surrounding environment, which can be transformed into useful work. For a compressor, the minimal work

needed to compress air from pressure level p_1 to p_2 is done at isothermal conditions and can be calculated as follows [9]:

$$\dot{W}_{isotherm} = \dot{m}_1 r T_2 \ln \frac{p_1}{p_2} \tag{3.24}$$

hereby assuming the air to behave as a perfect gas. The symbol $\dot{m}_1$ represents the total air mass flowing through the compressor at pressure level p_1, r is the dry air gas constant and T_2 is the temperature the air at pressure level p_2 expressed in Kelvin.

Using this equation we can calculate the exergy of the supply source as well as the exergy of the air leaving the muscles. The exergy of the supply source for muscle i is given by:

$$W^{in}_{isotherm,i} = \int \left(\dot{m}^{in}_{air_i} r T_{atm} \ln \frac{p_{supply}}{p_{atm}} \right) dt \tag{3.25a}$$

, while the output exergy can be calculated with:

$$W^{out}_{isotherm,i} = \int \left(\dot{m}^{out}_{air_i} r T_{air_i} \ln \frac{p_i}{p_{atm}} \right) dt \tag{3.25b}$$

During the simulation, the absolute supply level is set at 7 bar, the atmospheric absolute pressure at 1 bar and the atmospheric temperature is 293 K.

3.6. Conclusion

In this chapter a control architecture structure for the pendulum was discussed. The structure covers the exploitation of the natural dynamics in combination with joint trajectory tracking. The joint trajectory tracking controller uses a computed torque method to cope with the nonlinear behavior of the pendulum

configuration. The calculated torques are then transformed into desired muscle pressure levels by a delta-p unit, coping with the nonlinearities introduced by the muscle actuation system. Finally, a bang-bang pressure controller commands the valves in order to set the required pressures in the muscles. The exploitation of the natural dynamics is important, as it will decrease energy consumption and control action. In this context, two slightly different mathematical formulations were given to predict an adequate stiffness setting. First, a suitable constant stiffness was discussed. In the second formulation, the stiffness is changed online, which makes it more suitable for complicated trajectories.

A simulation model, which incorporates this control architecture as well as the modelling of the pendulum dynamics and the thermodynamic processes, which take place in the muscles, were described. This simulation model will be used to investigate exploitation of the natural dynamics and particularly to test the mathematical formulation described for that purpose. Finally, some energy considerations were made, in order to have an idea about the amount of energy consumption and valves action during the simulation or experiment.

Chapter 4

Results and discussion

4.1. Introduction

In the previous chapters, the experimental setup and simulation model as well as a control architecture, which combines the exploitation of the natural dynamics with a trajectory tracking controller, were described. To evaluate whether the proposed controller can meet tracking requirements and deal with the natural dynamics of the system, it was incorporated into the computer simulation and the physical pendulum. This chapter will give results on this theme for both simulation and practical set-up.

Results on the simulation model will be given in section 4.2. First of all the trajectory tracking control will be evaluated. The influence of erroneous model parameter estimations will be shown. Secondly, the influence of the joint compliance on the energy consumption and valve actions will be discussed. In this context, special attention is given to the evaluation of the mathematical formulations given in the previous chapter for estimating the appropriate joint stiffness.

In section 4.3, tracking experiments on the physical set-up will be discussed. Successively, the possibility to decrease control activity and energy consumption by setting a suitable stiffness, will be shown on the physical pendulum.

4.2. The simulation model

4.2.1. Evaluation of the joint trajectory tracking controller

4.2.1.1. General considerations

As mentioned in chapter 3, the control architecture consists of 3 main blocks: a feedback linearization module, a delta-p unit and a bang-bang pressure controller. The computed torque incorporates a model-based module and a servo control. The model-based part requires a good estimation of the model parameters, as was explained before. In order to investigate the influence of a wrong estimation of the model parameters, deviations on the mass, inertia, centre of gravities and force function were introduced into the simulation. A simulation with 0 % deviation, which means that the parameter estimations are exact, will be compared with a simulation with 10 % deviation on the inertia, 7.5 % on the centre of gravity and 5% on the mass and the force function. The servo portion of the computer torque module requires a correct tuning of the gains. This was done intuitively, but in such a way that stability is still ensured and control actions are minimized without affecting the tracking accuracy.

	p_{error} (mbar)	Valve action
a	-120	Open all exhaust valves
b	-60	Open one exhaust valve
c	-50	Close all exhaust valves
d	50	Close all inlet valves
e	60	Open one inlet valve
f	120	Open all inlet valves

Table 4.1: Pressure reaction levels of the bang-bang pressure controller, used in simulation

The bang-bang controller compares the required pressure to be set into the muscle with the measured gauge pressures and takes the appropriate valve actions depending on the various reaction levels. These levels were also manually tuned in order to minimize energy consumption by taking into account the trajectory tracking accuracy. The values of the pressure reaction levels are given in table 4.1

The controller sampling time is set to 2 ms and a valve delay time of 1 ms is introduced. The valve delay time corresponds with the real data, recorded by Verrelst. As was mentioned in chapter 2, a controller sampling time of 2 ms is used for the control of the physical pendulum.

Next, the trajectory tracking control shall be evaluated by imposing a desired sine-wave trajectory with a frequency of 2 Hz and an amplitude of 5°. The stiffness parameter p_S is set to 20 Nm. This is chosen as an example to validate the trajectory tracking, without taking into account the natural dynamics of the system

4.2.1.2. Results and discussion

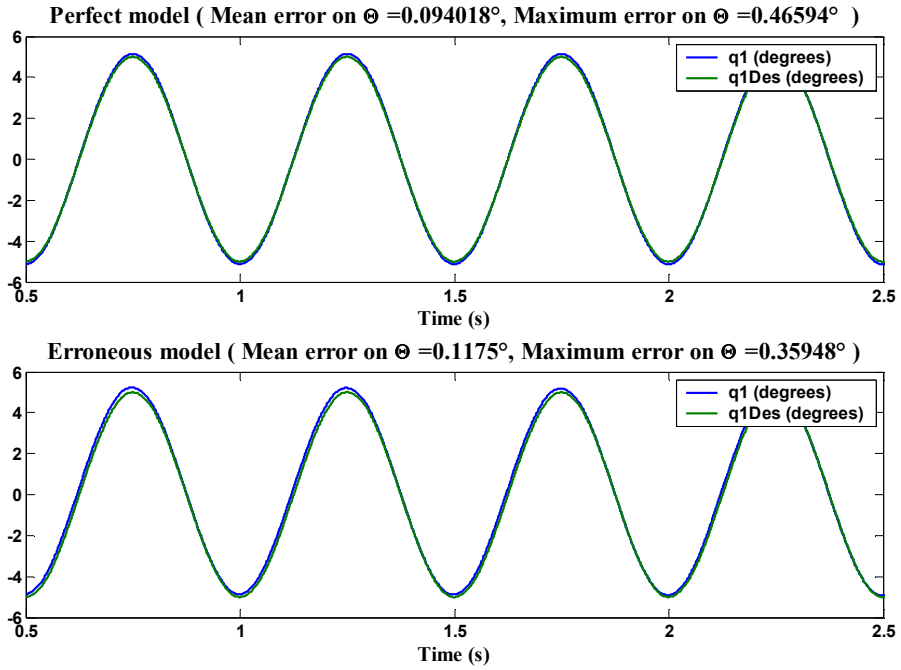

Figure 4.1: The joint angle θ for perfect and erroneous parameter estimations of the model

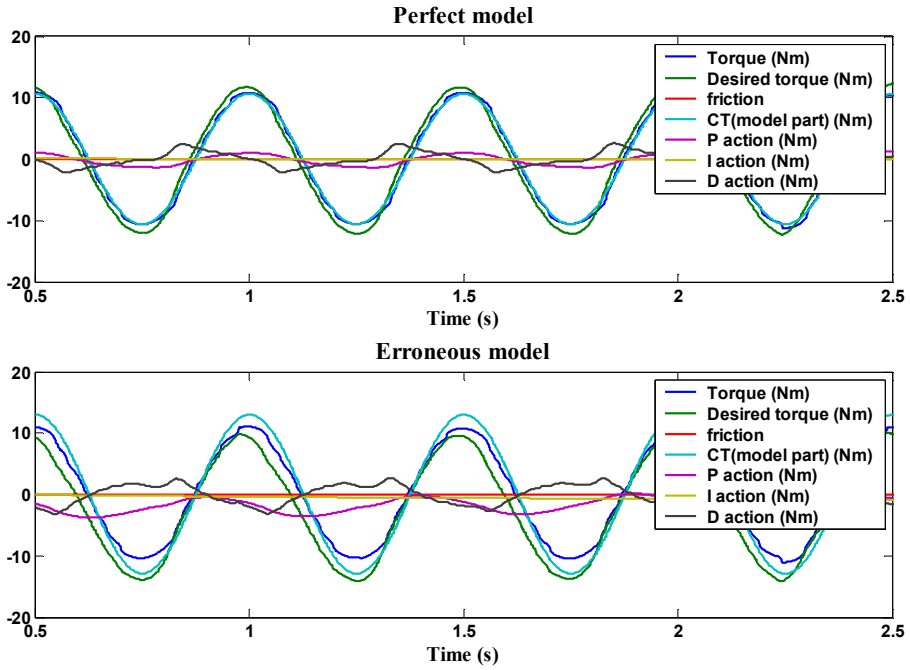

Figure 4.2: Torques of the joint for perfect and erroneous parameter estimations of the model

Figure 4.1 depicts the graphs of the angle θ for the perfect and erroneous model. The first period was omitted because some settling time is needed and is not interesting for the purpose of this section. As we see, the tracking controller unit can still cope with the introduced errors. In fact the tracking errors are very small. The difference between both simulations, and thus the influence of erroneous parameter estimation, is better seen on figure 4.2., were the required torques, calculated by the inverse dynamic control block, and the actual applied torques are depicted. The model-based part and the servo portions are also plotted.

In the perfect model, a little difference is observed between required and applied torque, due to a minimum pressure error required for the bang-bang controller to activate. The desired torque is almost equal to the model part of the computed torque. This is what we expected, because the model part was calculated with exact parameters. The servo portion deals with the difference in required and measured angle position and velocity. The erroneous model shows the influence of the erroneous estimation of the model parameters. First of all, there is a bigger difference between the applied and required torque because of the influence of

the force function errors. The model-based part of the computed torque differs substantially of the calculated torque, due to the introduction of deviations on the mass and inertia. The servo portion has to take more action, as the model-based part is using wrong parameters.

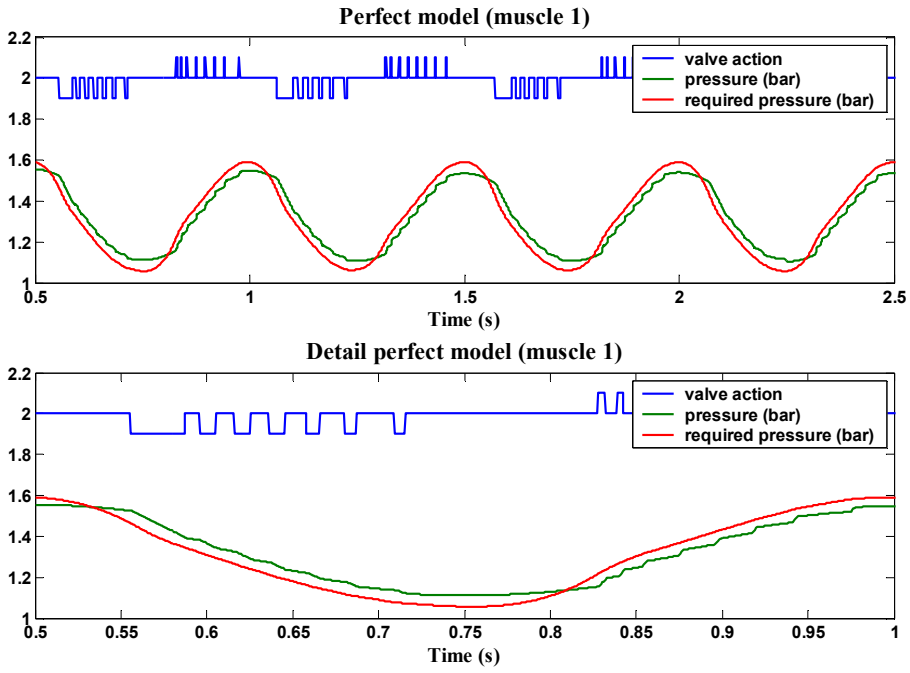

Figure 4.3: Muscle 1 pressure with valve action for perfect model.

Figure 4.3. depicts required and actual gauge pressures and valve actions taken by the bang-bang controller for muscle 1. A closed valve is represented by a horizontal line at the 2 bar pressure level. An open inlet valve is represented by a small peak upwards, while an open outlet valve is represented by a downwards peak. Larger peaks means that 2 inlets or 4 outlets are opened. From figure 4.3. we can conclude that the bang-bang controller is able to track the desired pressure quite accurately. No action taken by the valves, means that the pressure error p_{error} is situated in the dead zone of the bang-bang controller. This is the case between 0.708 s and 0.826 s. During this period muscle 1 is closed, and the natural dynamics of the system is exploited. It's now clear that the dead zone of the bang-bang controller will be very important to decrease the energy consumption and should be exploited as much as possible. This will be discussed in the following section.

4.2.2. Exploitation of the natural dynamics

4.2.2.1. Experiments

If we set some pressure values in both muscles of the antagonistic setup, close them and then release the pendulum from a position different of the equilibrium, the pendulum starts oscillating with a certain frequency. If this frequency corresponds with the desired trajectory, no valve action needs to be taken. This means that if stiffness is set in such a way that the natural dynamics of the system suits the desired trajectory, energy consumption will be minimized during tracking. The first simulations were done in this context. A constant p_S, the parameter to influence the sum of the pressures and consequently the joint stiffness, was set. This will be done for two different values of p_S, in order to show the importance of setting a correct stiffness for minimizing the energy consumption. The desired trajectory again is a sine-wave with a frequency of 2 Hz and an amplitude of 5 °.

In a second series of simulations, the mathematical formulation proposed by Verrelst and described in chapter 3 will be evaluated for different sinusoidal trajectories. Still, a constant p_S will be used.

Finally, the possibility to track a random trajectory with exploitation of the natural dynamics, will be investigated in the third series of simulations. The stiffness is changed online in order to set the most suitable stiffness at every control sample time.

No parameter deviations are introduced in the simulations. The controller sampling time and the valve delay time are still 2 ms, respectively 1 ms.

4.2.2.2. Results and discussions

Simulation 1: the importance of setting a suitable stiffness

We can illustrate the influence of the stiffness by considering the unactuated oscillation with closed muscles of the pendulum as was explained in the previous section and compare it with the desired trajectory. In figure 4.4, one period of the unactuated oscillation is shown for 2 different values of p_S, as well as the 2 Hz sine wave that has to be tracked.

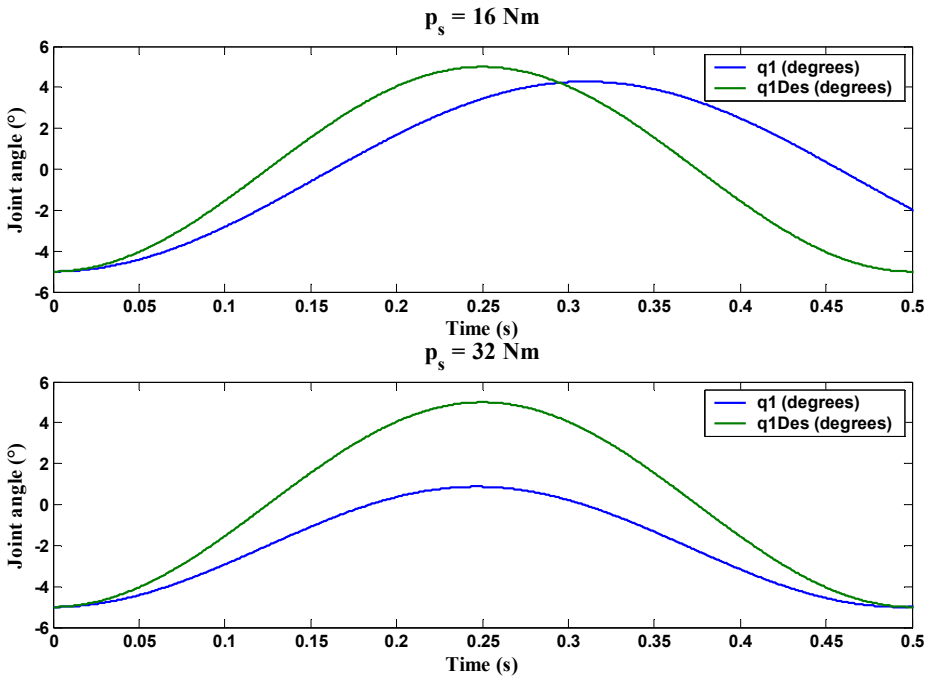

Figure 4.4: Actual and desired joint angle with closed muscles for $p_S = 16\ Nm$ and $p_S = 32\ Nm$

For both stiffness', the oscillation does not fit the desired trajectory, but for $p_S = 32\,Nm$, we can see that the base frequency is near to 2 Hz. We can expect that for $p_S = 32\,Nm$, the valve actions and energy consumption will be less than in the case of $p_S = 16\,Nm$, as the natural dynamics fits best the imposed trajectory. To investigate this assumption, a simulation of an actuated oscillation was done for $p_S = 16\,Nm$ and $p_S = 32\,Nm$. Figure 4.5. depicts the joint position

and angle velocity of the two simulations for one period. There is no significant difference between the two simulations concerning the joint angle and angle velocity. The tracking is slightly better for the case where $p_S = 32\ Nm$.

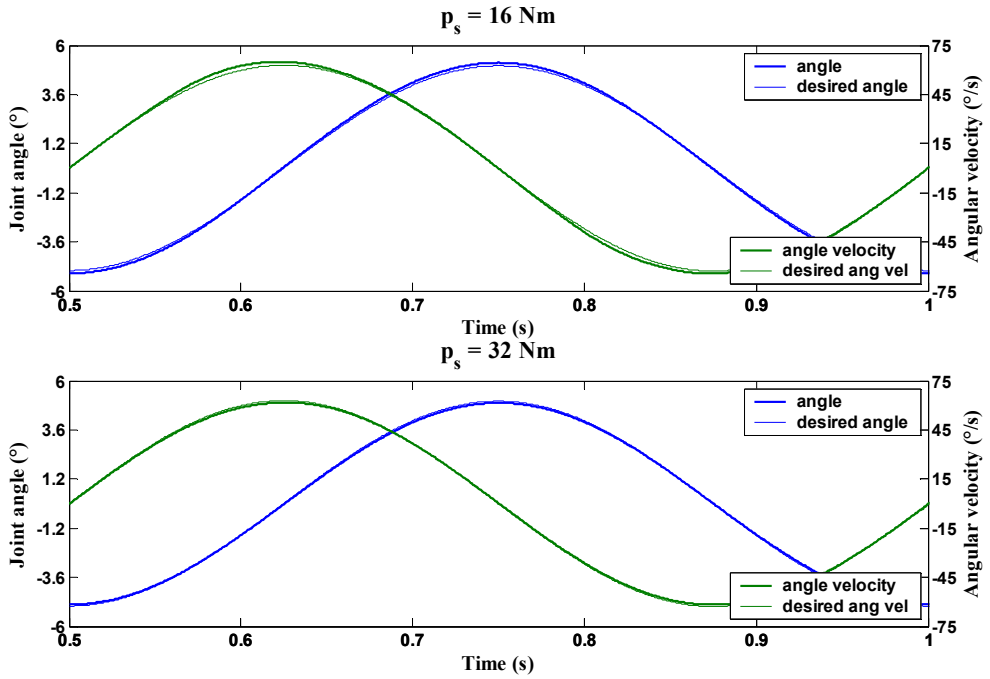

Figure 4.5: Actual and desired joint angle and angular velocity for $p_S = 16\ Nm$ and $p_S = 32\ Nm$

In figure 4.6 and 4.7 the gauge pressures and the valve actions are depicted. To get a clearer view on the valve actions, 2 periods are shown on the right of each figure. For the same reason as before, the first period is not shown. In figure 4.7 the mean pressure is twice as high as in figure 4.6, this because of the difference in value of p_S. A very clear difference can be observed between the two simulations. Looking at the valve action, we can immediately conclude that the case where $p_S = 32\ Nm$, is the most appropriate one to track a sine wave with a frequency of 2 Hz. That is what we already suggested before. For example, between 4.29 and 4.91 seconds no action

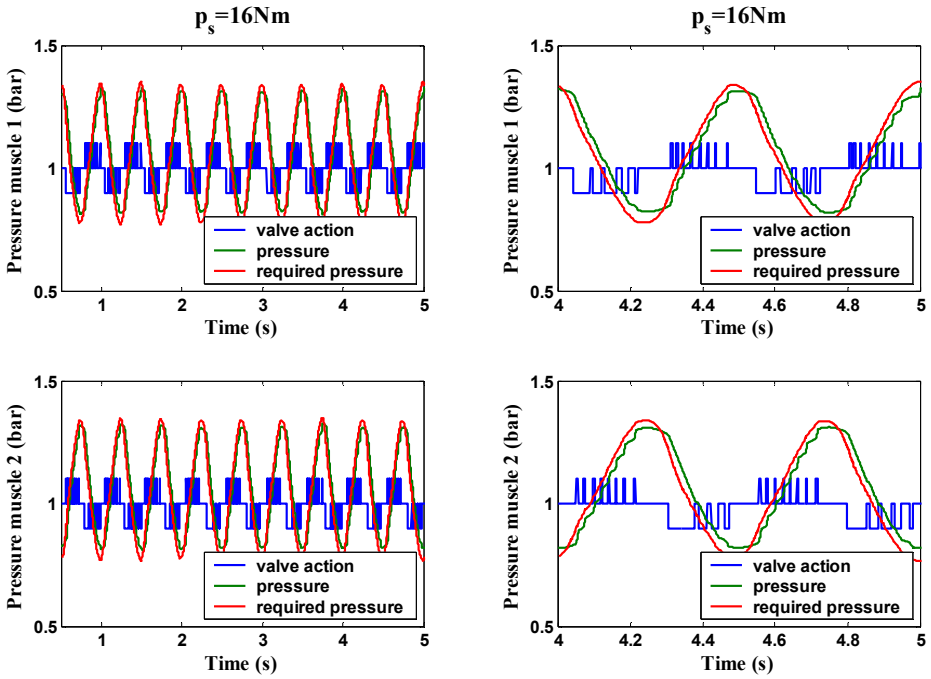

Figure 4.6: Actual and required pressure in muscle 1 and 2 for $p_S = 16\ Nm$

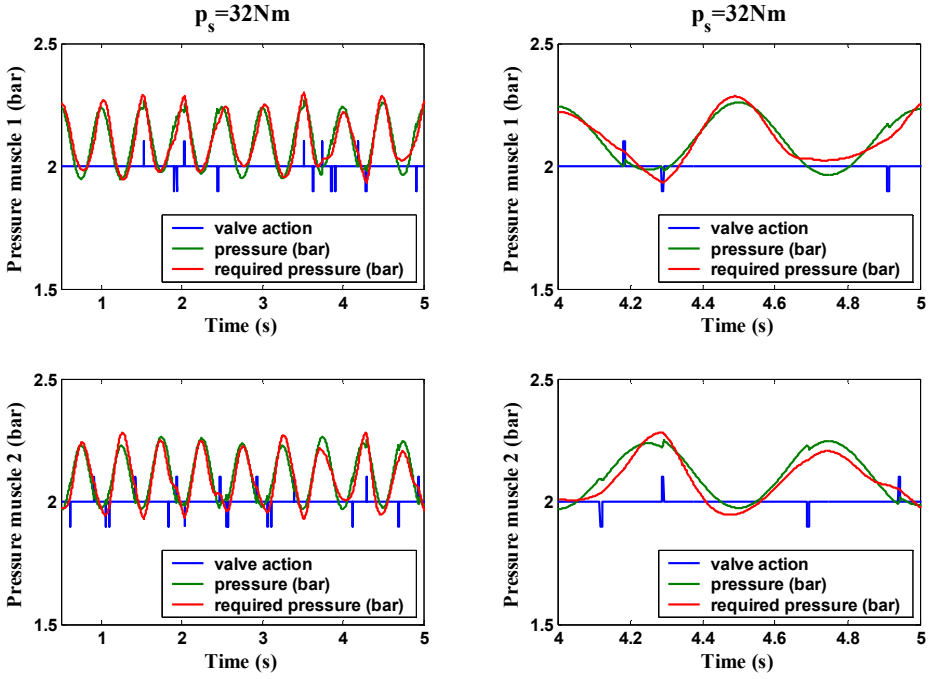

Figure 4.7: Actual and required pressure in muscle 1 and 2 for $p_S = 32\ Nm$

is taken by the valves of muscle 1 (or between 2.45 and 3.51s). The reason for this is that the pressure slope induced by the natural dynamics of the system, fits the pressure slope required to track the desired trajectory. We can also

understand why the pressure levels of the bang-bang controller are so important during the exploitation of the natural dynamics. The pressure error of muscle 1 near to 4.75 seconds has a maximum value of 59 mbar, which means that p_{error} is still situated in the dead zone. A smaller dead zone would have required the bang-bang controller to take action. A larger dead zone will increase the exploitation of the natural dynamics, but a larger deviation on the trajectory tracking will be observed. A compromise has to be made between control action and tracking error.

Table 4.2 gives a summary of the air mass flow, the exergy and the valve action for both simulations over one period. The valve actions are defined as in (3.23)

	$p_S = 16\ Nm$			$p_S = 32\ Nm$		
	Muscle 1	Muscle 2	Total	Muscle 1	Muscle 2	Total
Airflow input	120.1 mg	107.9 mg	228.0 mg	21.7 mg	13.9 mg	35.6 mg
Airflow output	111.4 mg	116.6 mg	228.0 mg	14.1 mg	22.1 mg	36.2 mg
Exergy inlet	19.7J	17.7 J	37.4 J	3.6 J	2.3 J	5.9 J
Exergy outlet	6.8 J	7.0 J	13.8 J	1.4 J	2.1 J	3.5 J
Inlet valve action	39.8 ms	36.0 ms	75.8 ms	7.7 ms	4.9 ms	12.6 ms
Outlet valve action	134.4 ms	141.8 ms	276.2 ms	10.5 ms	16.7 ms	27.2 ms

Table 4.2: Air mass flow, exergy and valve action during one period of a sine wave trajectory with frequency of 2 Hz for $p_S = 16\ Nm$ and $p_S = 32\ Nm$

The most interesting value is the exergy inlet, because this will give an indication of the energy consumption of the system. As we can see the total input exergy in the case of $p_S = 32\ Nm$ equals 5.9 J, which is much lower than 37.4 J in the case of $p_S = 16\ Nm$. Therefore, from this experiment we can conclude that a suitable stiffness affects in a positive way the energy consumption and control action during the trajectory tracking.

Simulation 2: evaluation of the mathematical formulation

The main goal is to see whether the mathematical formulation given by Verrelst is usable. Therefore, in this simulation, joint sine wave trajectories with different frequencies are imposed.

Table 4.3 gives an overview of the different sine wave trajectories for which the mathematical formulation was evaluated. In the second column the calculated values of p_S, are given. The values in the third column give the optimal p_S, for the corresponding trajectory. For each trajectory, the latter values were obtained by varying p_S and evaluate where the energy consumption and valve actions are minimized.

Sine wave frequency (Hz)	$p_S^{Calculated}\,(Nm)$	$p_S^{simulation}\,(Nm)$
1.5	12.6	12.5
1.75	21.4	21
2	31.7	31
2.25	43.2	42.5

Table 4.3: Calculated and simulated optimal values of p_S for different sine waves trajectories

Figure 4.8 depicts the energy consumption and valve actions per period for the different sine waves in function of p_S. For each trajectory, there is a p_S where energy consumption and valve action is minimum. This is the most optimal p_S. By comparing the calculated and the optimal p_S, we can conclude that the mathematical formulation is indeed suitable for setting the stiffness. The optimal p_S is increasing as the frequency is increasing. This was expected because p_S is influencing the stiffness and a higher oscillation frequency requires a higher stiffness.

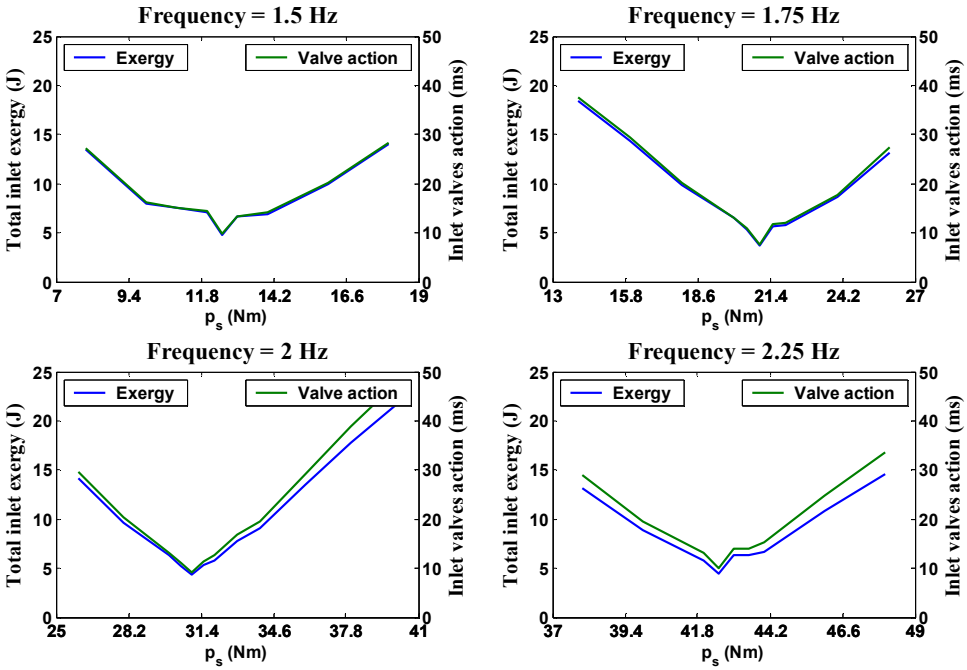

Figure 4.8: Energy consumption and valve action in function of p_S, for different trajectories

In the previous discussion only sine wave trajectories were imposed. For these trajectories the passive behaviour fits the imposed trajectory if p_S is set right. In this case a constant p_S value is justified.

We have to remember that the goal of this thesis is to investigate the possibility to exploit natural dynamics for implementing it later into the biped 'Lucy'. In general, the trajectories for such a biped are not just sine waves with only one frequency component. For such a situation, a constant p_S will not be suitable as shown in figure 4.9. In this figure, a sine wave with a linear increasing frequency from 1.5 Hz to 2 Hz is imposed. Only the pressure course for one muscle is shown here. The trajectory can still be tracked but we can clearly see that the natural dynamics are only exploited in the time interval [2,2s – 3s] , or in other words, for a certain frequency range of the imposed trajectory. At a frequency higher than 1.92 Hz even 4 exhaust valves are opened, in order to increase the flow rate and consequently track the required pressure course. Note also that the mean pressure inside the muscle remains constant during the whole simulation, due to a constant $p_S = 21Nm$.

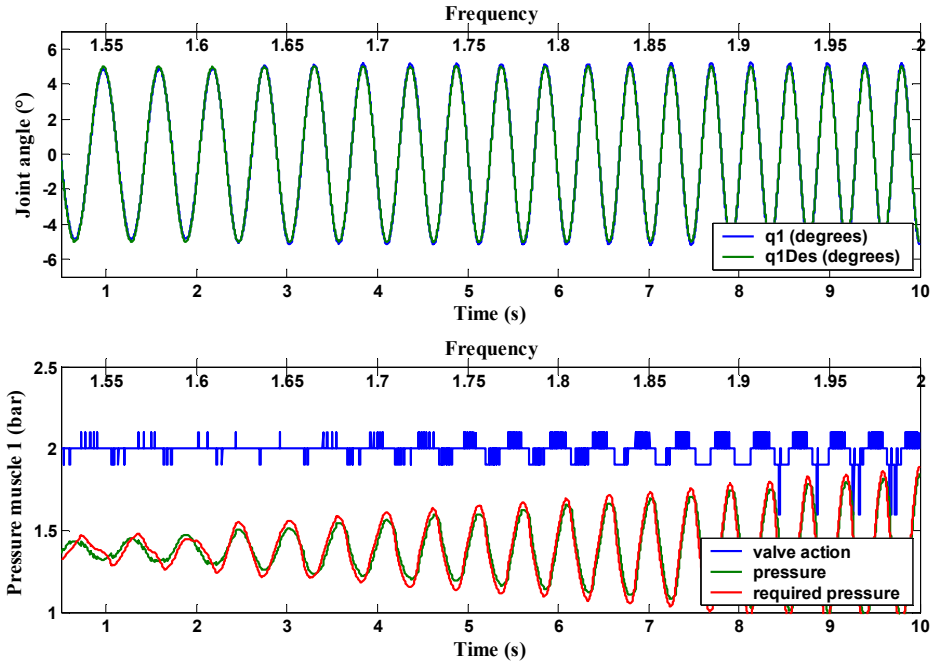

Figure 4.9: Joint angle, pressure and frequency for a trajectory with linear varying frequency

The conclusion of this simulation is that a varying p_S will be more suitable for trajectories different from a pure sine wave. This will be the discussion of the next simulation.

Simulation 3: changing the stiffness online

The purpose of this simulation is to evaluate the method of using a varying p_S, or stiffness, as described in chapter 3. This was done by imposing the same trajectory as in figure 4.9.

First, some comments have to be given on the equations that were used during this simulation. In chapter 3 a complete description of the mathematical formulation was given. Using these equations led to unsatisfying results: the stiffness $\widetilde{K}$ associated with the desired trajectory, became infinitive in some points.

The explanation for this phenomenon can be found by starting from the dynamically required stiffness, derived from the equation of motion:

$$\begin{aligned}\widetilde{K} &= \frac{d\widetilde{T}}{d\widetilde{\theta}} = \frac{d}{d\widetilde{\theta}}\left(d_{11}\frac{d^2\widetilde{\theta}}{dt^2} + g_{11}sin(\widetilde{\theta})\right) \\ &= d_{11}\frac{d^3\widetilde{\theta}}{dt^3}\frac{dt}{d\widetilde{\theta}} + g_{11}cos(\widetilde{\theta}) = d_{11}\left(\frac{d^3\widetilde{\theta}}{dt^3}\Big/\frac{d\widetilde{\theta}}{dt}\right) + g_{11}cos(\widetilde{\theta})\end{aligned} \qquad (4.1)$$

with:

$$\begin{cases} \widetilde{\theta} = A\,cos(\omega' t) & (4.2a)\\ \omega' = \omega_0 + \omega t & (4.2b)\\ \omega = \dfrac{\omega_{\max} - \omega_{\min}}{t_{simulation} - 1} & (4.2c)\end{cases}$$

The derivatives of the desired trajectory $\widetilde{\theta}$ are given by:

$$\frac{d\widetilde{\theta}}{dt} = -A\,sin\left(\omega_0.t + \omega.t^2\right)\left(\omega_0 + 2\omega.t\right) \qquad (4.3a)$$

$$\frac{d^2\widetilde{\theta}}{dt^2} = -A\,cos\left(\omega_0.t + \omega.t^2\right)\left(\omega_0 + 2\omega.t\right)^2 - 2\omega A\,sin\left(\omega_0.t + \omega.t^2\right) \qquad (4.3b)$$

$$\begin{aligned}\frac{d^3\widetilde{\theta}}{dt^3} &= A\,sin\left(\omega_0.t + \omega.t^2\right)\left(\omega_0 + 2\omega.t\right)^3 - 4\omega A\,cos\left(\omega_0.t + \omega.t^2\right)\left(\omega_0 + 2\omega.t\right) \\ &\quad -2\omega A cos\left(\omega_0.t + \omega.t^2\right)\left(\omega_0 + 2\omega.t\right)\end{aligned} \qquad (4.3c)$$

Thus we have for $\widetilde{K}$:

$$\widetilde{K} = d_{11}\left(\left(\omega_0 + 2\omega.t\right)^2 - 6\omega\,cotg\left(\omega_0.t + \omega.t^2\right)\right) + g_{11}cos(\widetilde{\theta}) \qquad (4.4)$$

We see that a cotg() functions arises for this specific trajectory. The course of $\widetilde{K}$ is depicted in the first plot in figure 4.10. In the second plot, the cotg( ) term is given. The latter explains why $\widetilde{K}$ is being infinitive. The cotg( ) term can be

seen as a noise signal disturbing $\widetilde{K}$ and is therefore neglected. The resulting course of $\widetilde{K}$ is given in the third plot.

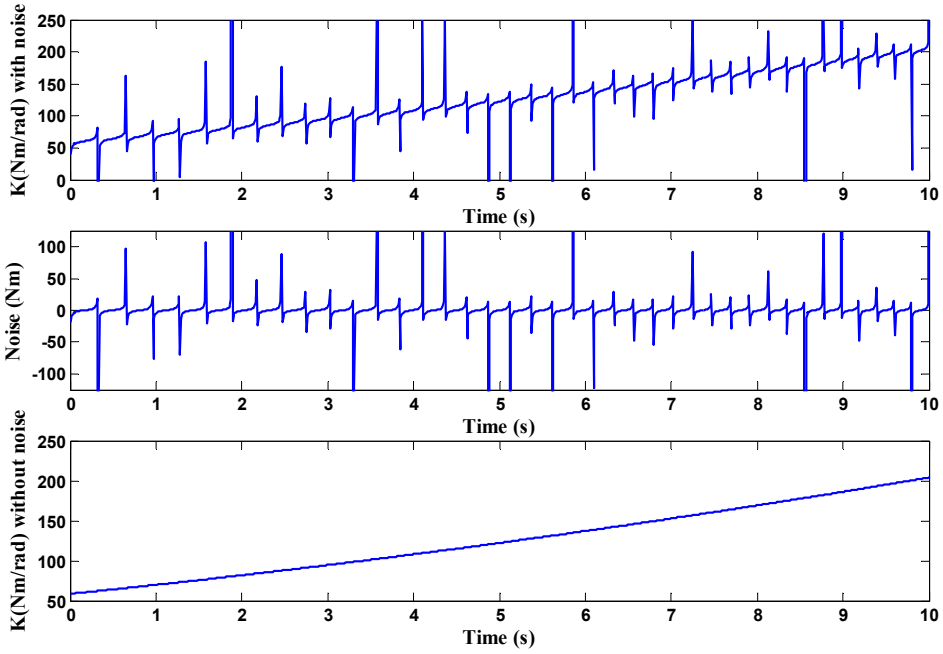

Figure 4.10: Stiffness $\widetilde{K}$ and noise due to cotg( ) term for the specific trajectory

$\widetilde{K}$ is now given by:

$$\widetilde{K} = d_{11}(\omega_0 + 2\omega.t)^2 + g_{11}cos(\widetilde{\theta}) \tag{4.5}$$

In the graph at the bottom of figure 4.10, we can observe that the required stiffness is increasing as the frequency increases. This is what we expected, because if the frequency of the imposed trajectory increases, a higher stiffness of the antagonistic setup with closed muscles will be needed in order to exploit natural dynamics.

Using this equation, running the simulation for an imposed trajectory with frequency varying between 1.5 Hz and 2 Hz and using a varying p_S, gives us the pressure course as depicted in figure 4.11. To compare this to the situation where a constant p_S was used, the pressure course from figure 4.9 was redrawn in figure 4.12. Comparing figure 4.11 and 4.12, we can conclude that valve

action is extremely decreased. The natural dynamics are now being exploited during the whole simulation, this by making p_S variable.

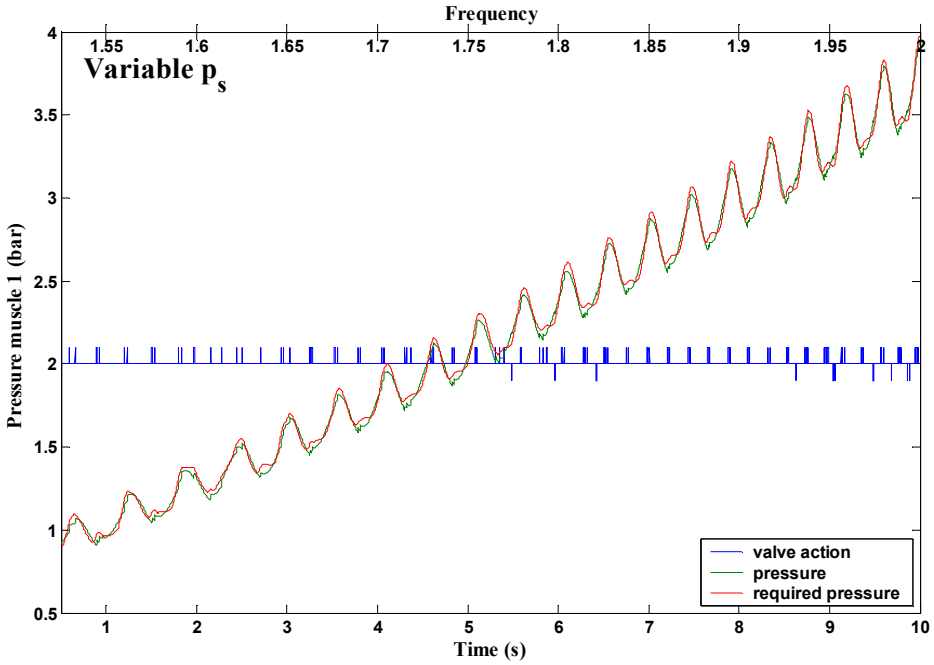

Figure 4.11: Actual and required pressure and valve action for a trajectory with linear varying frequency and p_S online changed.

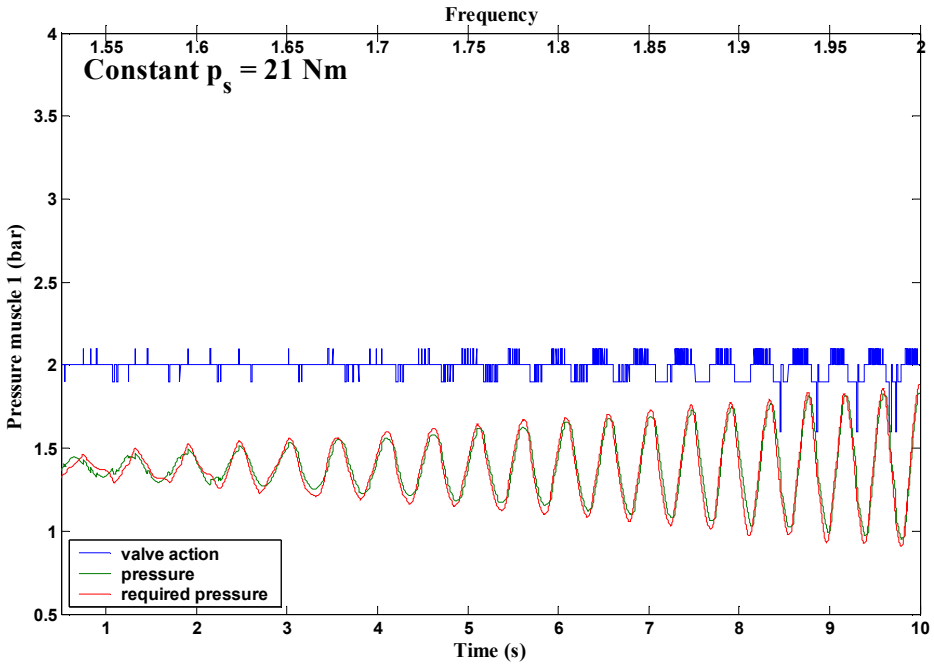

Figure 4.12: Actual and required pressure and valve action for a trajectory with linear varying frequency and a constant p_S.

Because the required oscillation frequency is increasing, energy has to be injected into the system. This explains why in figure 4.11 more inlet valve actions are taken during the whole trajectory. Once, the frequency remains constant, the inlet valve actions will decrease, since no additional energy has to be injected.

Note that the pressure is increasing as the frequency of the imposed trajectory increases. As mentioned before, the required stiffness raises as the frequency raises, which means that the sum of pressures in the muscles has to increase. This also means that p_S increases, as it represents a parameter to influence the sum of the pressures. The evolution of p_S along the trajectory is shown in figure 4.13.

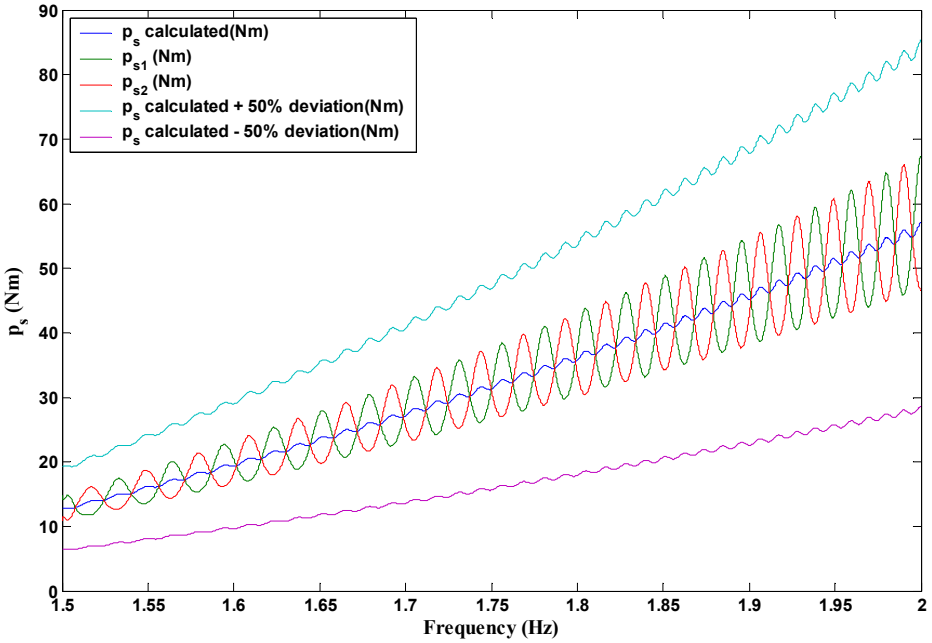

Figure 4.13: p_S in function of the frequency of the imposed trajectory.

Deviations on p_S were introduced to investigate the effect on the valve control when the online calculation of p_S is not giving the correct value. This can be interesting to know, since we can already expect that the online calculation of the optimal p_S for the simulation will not necessarily give the optimal p_S for the physical pendulum. The influence on the valve actions is given in figure 4.14. On the left we can see the valve actions during the whole simulation and on the

right a detailed view is given. We can draw the same conclusion as before: a wrong variable value of p_S will increase the valve actions. Therefore, it will be important to have a good model of the pendulum setup, such that the method with variable stiffness can be used during experiments.

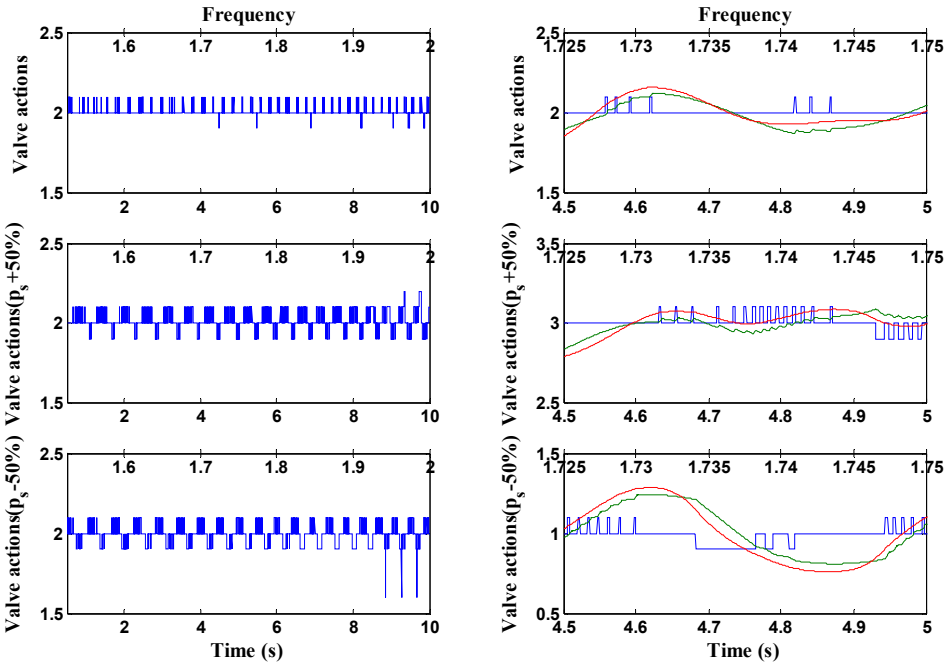

Figure 4.14: Effect on the valve actions due to deviation on the online changing parameter p_S

With this simulation, the importance of using a variable p_S for tracking trajectories with not only one frequency component, has been showed. Using a variable p_S, will result in a variable mean of the pressure in each muscle separately. Therefore, the antagonistic setup should be designed in such a way that p_S stays between a certain range, in order to limit the gauge pressure in the muscles between 0 bar and 3.5 bar. Or, in the case of the biped 'Lucy', the generated trajectories should take into account those limits if natural dynamics should be exploited.

4.3. The physical pendulum

4.3.1. Evaluation of the joint trajectory tracking controller

In the previous section the joint trajectory tracking controller was evaluated by means of computer simulations. The physical pendulum was built in order to perform some tracking experiments, and to adapt the simulation model according to the experimental data. In this section the performance will be discussed and an overview will be given of which parameters differs from the simulation model. A correct estimation of these parameters was not done, but the importance should not be neglected.

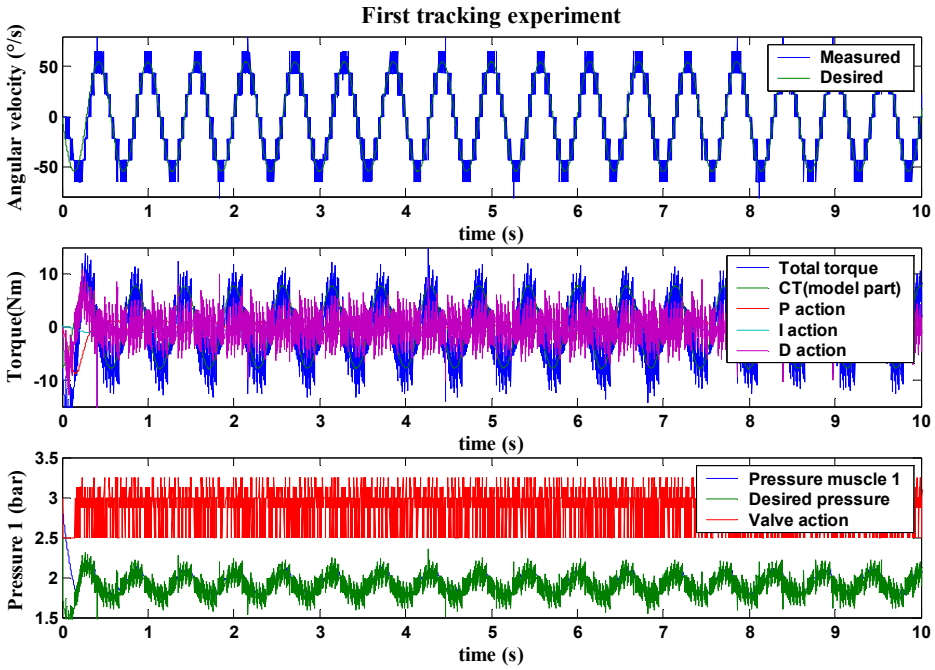

Figure 4.15: Angular velocity, computed torque and absolute pressure for first tracking experiment

In order to investigate if exploitation of the natural dynamics is possible, a good working trajectory tracking controller has to be implemented. In a practical setup, some additional problems arise, e.g. noise on the pressure sensor signal or small errors in the joint angle information. An even more important problem is the measuring of the angular velocity. The angular velocity is required by the computed torque module, and in order to have a stable controller, this parameter

has to be well known and as much as possible free of noise. As we cannot directly measure the angular velocity, it should be calculated numerically, starting from the joint angle acquired with the incremental encoder. Therefore, a first order numerical method was used. Figure 4.15 shows the angular velocity, the computed torque performance and the absolute pressure in muscle 1 for the first tracking experiment. A sine wave with a frequency of 1.75 Hz was imposed and a constant $p_S = 14\ Nm$ was used. As we can see, a lot of noise appears on the angular velocity signal. This will have an impact on the tracking controller as the servo portion will have to cope with this noise. We clearly see that the D-action is trying to eliminate this noise. The delta-p unit transforms the noisy computed torque to pressure levels, which means that a lot of valve action will be taken by the bang-bang controller as shown at the bottom of figure 4.15. The valves are switching a lot, and most of the time the 4 outlet or 2 inlet valves are opened in order to track the pressure course. With regard to energy consumption, this is unacceptable.

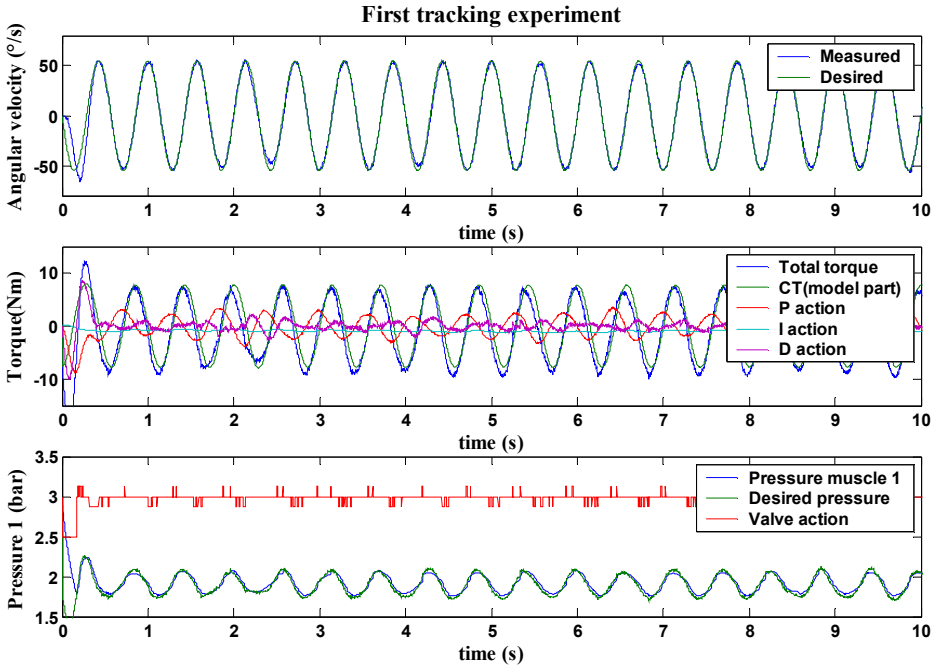

Figure 4.16: Angular velocity, computed torque and absolute pressure for a tracking experiment by using a filter on the angular velocity.

To avoid such problems, a first order digital filter was used on the angular velocity. A bilinear transformation was done in order to convert an analog to a

digital filter. The bilinear transformation is a mathematical mapping of variables. In digital filtering, it is a standard method of mapping the s or analog plane into the z or digital plane. It transforms analog filters, designed using classical filter design techniques, into their discrete equivalents [19]. The first order analog filter used on the physical pendulum is given by:

$$H_a(s) = \frac{1}{\frac{s}{\omega_a} + 1} \tag{4.6}$$

Pre-warping the filter design gives:

$$\omega_a = \frac{2}{T_S} \tan\left(\frac{\omega_d^{cut-off} T_S}{2} \right) \tag{4.7}$$

with T_s, the sample time and $\omega_d^{cut-off}$ the cut-off pulsation of the desired digital filter, given by:

$$\begin{cases} \omega_d^{cut-off} = 2\pi f_{cut-off} & \text{(4.7a)} \\ f_{cut-off} = 10\,Hz & \text{(4.7b)} \\ T_S = 2ms & \text{(4.7c)} \end{cases}$$

The bilinear transformation is given by:

$$H_d(z) = H_a\left(\frac{2}{T_S} \left(\frac{z-1}{z+1} \right) \right) \tag{4.8}$$

which results in the digital filter:

$$H_d(z) = \frac{b_1 z + b_0}{a_1 z + a_0} \tag{4.9}$$

With

$$\begin{cases} a_0 = \left(1 - \frac{2}{T_S \omega_a}\right) \Big/ \left(1 + \frac{2}{T_S \omega_a}\right), a_1 = 1 & \text{(4.9a)} \\ b_0 = b_1 = 1 \Big/ \left(1 + \frac{2}{T_S \omega_a}\right) & \text{(4.9b)} \end{cases}$$

The introduction of a filter greatly improved the performance of the joint trajectory controller. Figure 4.16 shows the angular velocity, computed torque and the absolute pressure when a filter is used. Very remarkable is the effect of the filter on the valve actions and is a first step in the correct direction concerning energy consumption. The gains used by the servo portion of the computed torque, were manually tuned in such a way that stability is still ensured and control actions are minimized without affecting the tracking accuracy. As was explained, in chapter 3 it is important to have a good estimation of the model parameters, in order to reduce the servo portion to a minimum. No friction model was used during the experiment. Also the existing of small air leaks in the muscles and tube connections were not taken into account. In the future, a fine-tuning of the model should be made.

The joint angle is given in figure 4.17. We can see that the control unit is suitable to track this trajectory. During the first period, tracking is not so accurate. An explanation can be found in the pressure course also depicted in figure 4.15. In the beginning, the pendulum is at rest at an angle of 5 °. The muscles are inflated and a certain pressure is set into the muscle. Once the experiment starts, a pressure much lower than the actual pressure is needed. All the outlet valves are opened in order to track the pressure course, but this is not enough. The pressure gradient over the valves is insufficient, so that the time constant of deflation is too large in comparison to the requirements associated with the imposed pressure course. This can cause the pendulum to become unstable. A reason for this unwanted phenomena, is the use of an exhaust silencer, as it obstructs the dynamic performance of the muscle deflation. The

pressure rise in the silencer lowers the exhaust airflow. During the construction, this silencer was made as large as possible to avoid such situations.

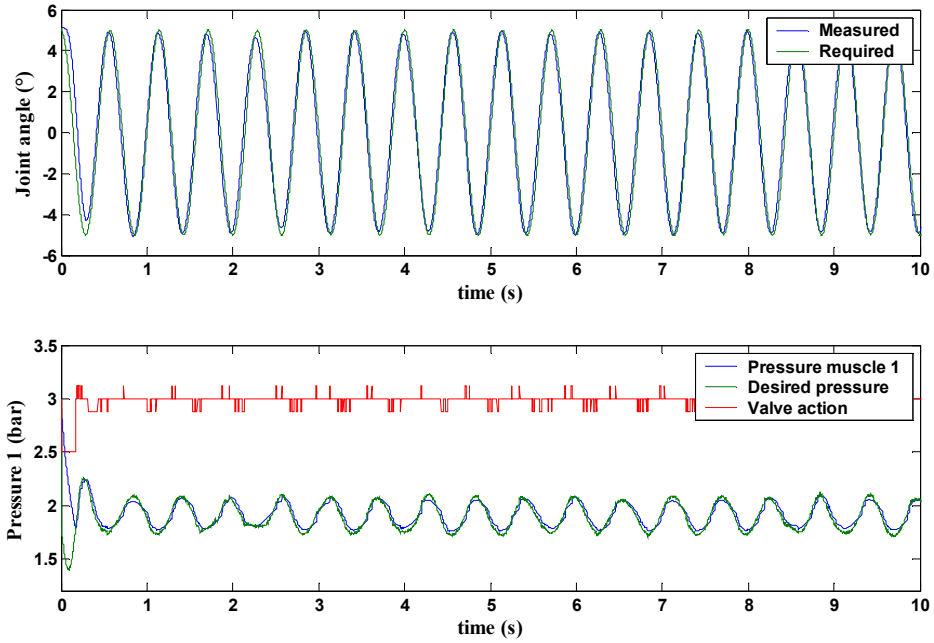

Figure 4.17: Measured and desired joint angle θ and pressure course for muscle 1

Other solutions for this problem are increasing the outlet valves, or setting the initial muscle pressure at a lower level. The first option is important if high oscillation frequencies are needed, since high pressure gradients over the valves will then be required.

The reason why the initial pressure is set at such a high level requires an explanation. In the beginning, the idea was to start at an initial angle of zero degrees and to use a sine function for the imposed trajectory. Because of a discontinuity in the angular velocity ($\dot{\theta}(t=0_{-})=0$, $\dot{\theta}(t=0_{+})=A\omega$), instability occurred. Therefore, we opted to start at an initial angle equal to the amplitude of the imposed trajectory. The trajectory used to bring the pendulum in its initial position as depicted in figure 4.18. By using this trajectory, the discontinuity of the angular velocity is eliminated. When the initial angle is reached, a certain settling time is needed for the pendulum to stay at rest. The settling time can seriously be decreased by increasing the stiffness of the joint. This means that

p_S has to be increased during the tracking of the initial trajectory, and as a consequence the initial pressure will be at a higher level.

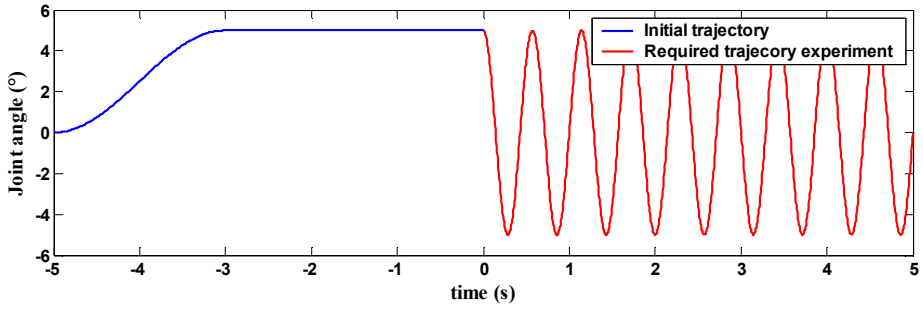

Figure 4.18: Initial trajectory and imposed trajectory during experiments

During the experiments an increasing deviation on the joint angle was observed as the time increased due to some miscounts of the encoder signal. This was not a problem in the context of this thesis, because the acquisition time during the experiments was relatively short. But in the future, the third signal of the incremental encoder should also be incorporated, in order to reset the encoder counter when the pendulum passes trough his reference angle.

Based on this section, we can conclude that the proposed control architecture is able to track sine wave trajectories. In order to reduce energy consumption, the exploitation of the natural dynamics is required. This is shown in the next section.

4.3.2. Exploitation of the natural dynamics

4.3.2.1. General considerations

We want to investigate the exploitation of the natural dynamics of the system in order to reduce energy consumption. A method to estimate the energy consumption was given in chapter 3. Of course, this will not give us the correct value, but it is interesting to have an idea of the energy consumption and control action taking place during the experiment. If a correct estimation is needed,

measurement of the airflow, air temperature and muscle volume will be needed. In our case, we only want to investigate whether the PPAM can be used to exploit the natural dynamics of the system and therefore the formulation from chapter 3 will do. The calculation of the energy is only started after two seconds of acquisition, when the pendulum is in regime.

As mentioned before, the dead zone of the bang-bang controller has an important influence on energy consumption. Changing the pressure levels of the bang-bang controller will increase or decrease valve actions. In order to investigate only the influence of the stiffness on the energy consumption and valve actions, these pressure levels were set to constant values given by table 4.4. These values were manually tuned, so that control effort is minimized by taking into account the trajectory tracking accuracy

	$P < 2.5\,bar$	$P \geq 2.5\,bar$	Valve action
	p_{error} (mbar)	p_{error} (mbar)	
a	-120	-120	Open all exhaust valves
b	-60	-30	Open one exhaust valve
c	-40	-25	Close all exhaust valves
d	40	25	Close all inlet valves
e	60	30	Open one inlet valve
f	120	120	Open all inlet valves

Table 4.4: Pressure levels of the bang-bang controller for the physical pendulum

4.3.2.2. Results and discussion

In the context of the exploitation of the natural dynamics, one experiment was done on the physical pendulum. The main goal is to find out if energy consumption and control action can be minimized by setting the appropriate stiffness and to determine the value of the optimal stiffness. Therefore, the stiffness parameter p_S was varied, and for different trajectories, energy consumption and valve action were calculated. The same experiment was done

in the computer simulation model, of which results were already shown in figure 4.8. Remember that in the simulation model, the optimal p_S and the p_S found with the mathematical formulation given by Verrelst were compared. We concluded that the method of the pressure slopes was suitable for sine trajectories with one frequency component, as the two values were almost the same.

In the case of the physical pendulum, energy consumption and valve action, defined by (3.23), for one period of different trajectories are given in figure 4.19.

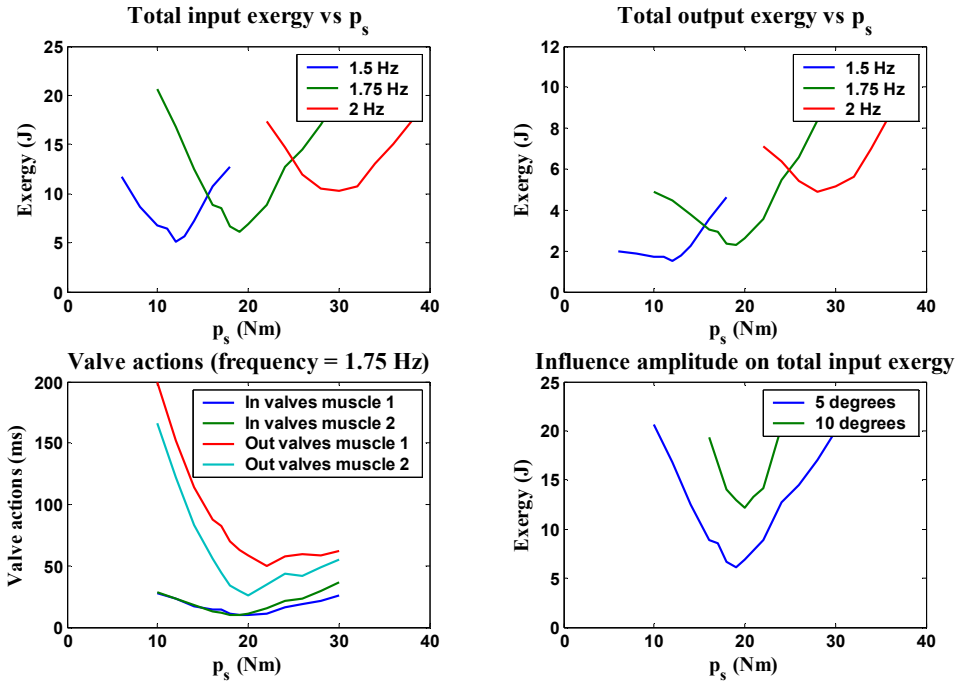

Figure 4.19: Energy consumption and valve action for one period of different trajectories in function of the stiffness parameter p_S

We can clearly identify optimal values for p_S, where energy consumption and valve actions are minimized. This is also illustrated by figure 4.20,where the valve actions, required to track a trajectory with a frequency of 1.75 Hz and an amplitude of 5 degrees is depicted. In this figure two different values of p_S were set, a wrong and the optimal value. If we look between 1.32s and 1.7s, no valve action is taken for $p_S = 19Nm$, because the natural pressure course fits the required one. Comparing with $p_S = 30Nm$, we can conclude that it is important

to set the right stiffness in order to exploit the natural dynamics of the pendulum. This was already concluded in simulation, but now it is confirmed in practice.

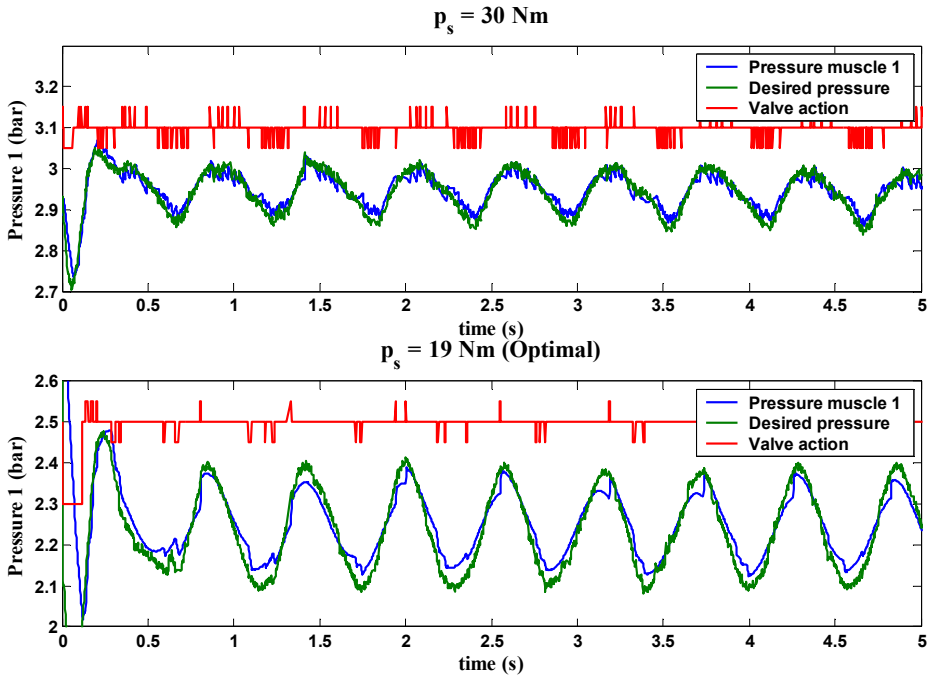

Figure 4.20: Influence of the stiffness parameter p_S on the valve action and the absolute pressure in the muscle

Another way to illustrate how p_S influences the natural dynamics, is the unactuated oscillation of the pendulum for the two different stiffness parameters. This is given in figure 4.21. After 10 seconds of control, the muscles are closed. If the stiffness is suitable, when $p_S = 19Nm$, the base frequency of the uncontrolled oscillation approximates 1.75 Hz during the two first periods. While when $p_S = 30Nm$, the base frequency is situated around 2 Hz, since the stiffness of the joint is higher. When $p_S = 10Nm$ the base frequency is about 1.4 Hz, since the stiffness of the joint is lower. We only consider the two first periods, because due to friction and leakage of the pneumatic system, the uncontrolled oscillation will damp and frequency will change.

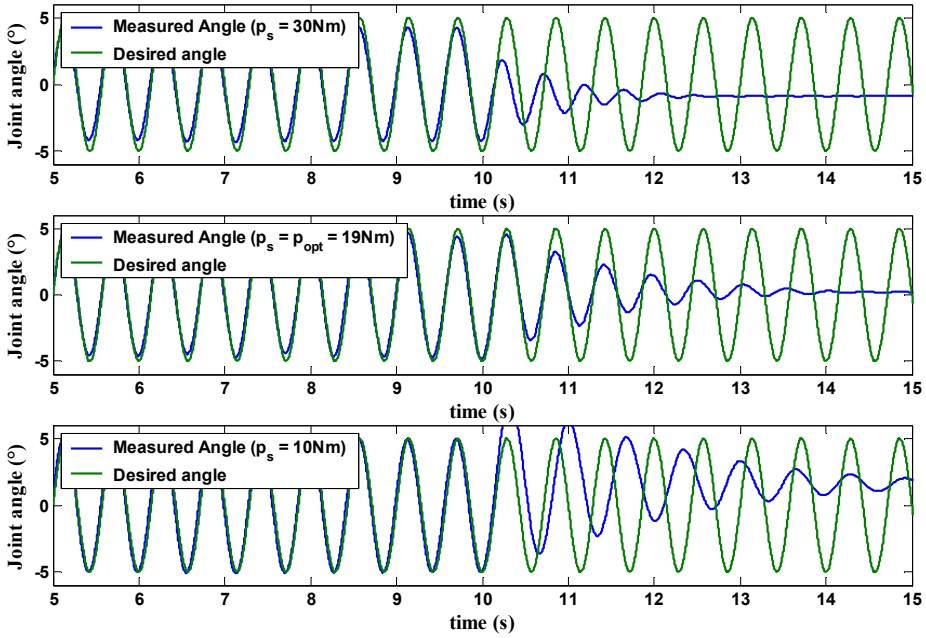

Figure 4.21: The uncontrolled oscillation of the pendulum for three different stiffness parameters p_S after a controlled period of 10 seconds

As was mentioned before and shown in figure 4.20, setting a different stiffness changes the mean pressure. This means that the stiffness is bounded between two values, since the absolute pressure in the muscle is limited between 1 and 4.5 bar. Varying the stiffness till those limits were reached, showed that the range of p_S for this pendulum is bounded between 6 and 40 Nm

In figure 4.19, the influence of the amplitude on the input exergy is shown. The amplitude has little influence on the optimal stiffness, like was expected, but energy consumption seems to be higher. Due to the nonlinear torque to angle relation, the shape of the passive trajectory deviates from a pure sine-wave. The deviation from the sine-wave increases for larger amplitudes. Consequently, more valve switching is needed for larger movements. This clearly shows the importance of designing a joint with a linear torque characteristic when muscles are closed, when sine-wave trajectories with one frequency component are imposed.

In order to see whether the method of the pressure slopes can be used on the practical setup, a resume of the optimal p_S values of the experimental setup is given in table 4.5 and compared with the calculated and simulation values.

Sine wave frequency (Hz)	$p_{S,optimal}^{Experimental}(Nm)$	$p_S^{Calculated}(Nm)$	$p_{S,optimal}^{simulation}(Nm)$
1.5	12	12.6	12.5
1.75	19	21.4	21
2	29-30	31.7	31

Table 4.5: Experimental, calculated and simulated optimal values of p_S for different sine-wave trajectories

The experimental values are near to the calculated and simulated values. From this we can conclude that the method of the pressure slope could be used, but only as an approximation of the optimal stiffness. The stiffness will not be set at his optimal value, but still energy consumption and valve action will be decreased and natural dynamics will be exploited.

The error that is made by using this method, can be decreased by a better parameter estimation, e.g. leaks in the tubing and muscle and friction. The most important parameters to be estimated, are the volume of the muscle and the polytropic exponent. The volume is calculated using the estimated polynomial fitting described in section 2.2.1., which does not take into account the volumes of the end fittings and tubing's. Besides this, the estimated polynomial fitting was done on a theoretical model of the muscle. For the mathematical description of the enclosed volume, the pleated polyester membrane is approximated by considering at each parallel section a circular membrane pattern instead of the pleated structure. No experimental data on the volume has ever been acquired. The polytropic exponent is introduced to describe deviations from the isentropic expansion/compression taking place when muscles are closed and the pendulum is oscillating. The value of the exponent should be experimentally estimated and may depend on the specific process. The estimation of these parameters was not done during this thesis, but is very importance if a varying stiffness has to be

used in combination with trajectory tracking. But still, promising results were produced.

4.4. Conclusion

In this chapter the trajectory tracking control structure as described in chapter 3 was evaluated on a computer simulation model and a physical pendulum. The simulation model showed that the proposed control architecture copes with the nonlinearities introduced by the actuator characteristics and dynamic model of the pendulum. The importance of a correct estimation of the model parameters was demonstrated by introducing deviations on the inertia, the mass, the centre of gravity and on the force function. The implementation of the control unit into the physical pendulum required the introduction of a filter to reduce the noise on the calculated angular velocity. A tracking experiment illustrates that the control unit is able to follow a sine-wave. The main differences with the simulation model were also discussed.

In the context of the exploitation of the natural dynamics, 3 experiments were performed on the computer simulation model and one on the physical pendulum. In the first experiment, the simulation results showed the importance of setting the right joint stiffness in order to reduce control effort and energy consumption. In the second experiment, the mathematical formulation, described in section 3.3, was evaluated. Therefore, the constant stiffness obtained by this method was compared with the optimal stiffness found by tuning the stiffness manually. We concluded that the mathematical formulation can indeed be used to estimate the optimal stiffness, when a sine-wave with one frequency component is imposed. In order to exploit the natural dynamics for trajectories with more than one frequency component, the stiffness was changed online in experiment 3. A sine-wave trajectory with linear varying frequency was imposed. By using the method of varying stiffness, the control unit was able to track the desired trajectory in combination with the exploitation of the natural dynamics.

The experiment on the physical pendulum was performed to find out if energy consumption and control action can practically be minimized by setting the appropriate stiffness and to determine the value of the optimal stiffness. For

different trajectories, the optimal stiffness was found. By comparing the experimental values of the stiffness parameter with those found in the simulation, we were able to conclude that the method of the pressure slopes can be used to approximate the optimal stiffness. A better parameter estimation of the pendulum's model and the bang-bang controller's pressure level will decrease the error made on the estimation of the stiffness.

Once these parameters are correctly estimated, we should be able to vary the stiffness along the trajectory. Therefore, adapting the pendulum model to all experimental data and tuning the bang-bang controller is the next step to take in order to completely exploit the natural dynamics.

Chapter 5

General conclusions and future perspectives

This thesis reports on the design, construction and control of a one-dimensional pendulum actuated by a pair of pleated pneumatic artificial muscles (PPAM). Pneumatic artificial muscles have very interesting characteristics towards exploitation of natural dynamics of the system. Due to the compressibility of air and the dropping force to contraction characteristic, a joint actuated by two antagonistically positioned muscles has a compliant behaviour, which can be adapted while controlling position. The main purpose is to use this adaptable joint compliance to combine exploitation of natural dynamics combined with joint trajectory control, in order to reduce control effort and energy consumption significantly. The joint trajectory controller tracks the imposed trajectory, while changing the joint stiffness, as such that the natural trajectory corresponds as much as possible to the reference trajectories. The investigation on this theme is done on both a computer simulation model and a physical pendulum. The latter, together with its soft- and hardware, had to be designed and constructed. A lot of time was spent on testing and debugging the different components.

Chapter 2 discusses both mechanical and electronic design required for a well working physical setup. The mechanical design focuses on the actuator connection, as it defines the joint characteristics of the antagonistic muscle setup and consequently the compliance. Therefore a formal description of the joint kinematics is given and it is shown that the joint position is influenced by differences in both muscle pressures; while the compliance of the joint, with closed muscles, is set by a weighted sum of pressures. The basic frame, supporting structure and pneumatic circuit are assembled to form one modular part of 'Lucy'. In order to control the pressure in a muscle, fast switching on/off valves are used. The electronics required to action these valves together with the pressure sensors and the incremental encoder are tested and described. A data

acquisition card serves as a data transfer agent between the experimental setup and a computer, on which the complete control of the pendulum is implemented.

The control architecture used to combine joint trajectory tracking with exploitation of the natural dynamics, is explained in chapter 3. The joint trajectory tracking controller consists of a multilevel construction of several essential blocks, which try to cope with the system's nonlinearities at separate levels. A model-based feedforward controller calculates the required torques to track the desired joint trajectories. These calculated torques are then transformed into desired muscle pressure levels by a delta-p unit, coping with the nonlinearities introduced by the muscle actuation system. Finally, a bang-bang pressure controller with dead-zone commands the valves in order to set the required pressures in the muscles. A mathematical formulation is given in order to incorporate the natural dynamics in the control unit. The starting point for finding an appropriate constant stiffness, is to fit the natural pressure slopes, this is when both muscles are closed, with the required ones. The better these two fit, the less action will be taken by the bang-bang controller. Consequently, energy consumption and control effort are decreased. Based on this formulation, an additional method is given to change the stiffness online. In order to evaluate the tracking controller and the pressure slope method, a simulator, based on the one used for 'Lucy', is developed.

Chapter 4 gives an overview of the results that are obtained with the computer simulation model and the practical setup. For both, tracking experiments are performed in order to evaluate the robustness of the trajectory tracking controller. From these experiments, the conclusion can be drawn that the proposed control structure is indeed suitable to track imposed trajectories. Great importance is attached to the incorporation of the natural dynamics of the system. First of all, the simulation model is used to show the influence of setting a constant suitable stiffness on the energy consumption and control effort when a sine-wave with only one frequency component is imposed. The optimal stiffness values are found for different frequencies of the imposed sine-wave. These values are then compared to the constant values obtained with the method of pressure slopes. Based on these results, we can consider that the method can be used for setting the suitable stiffness. We can draw the same conclusion for the method of changing the stiffness online. This is interesting for further research on 'Lucy',

since the required trajectories are not pure sine-waves and thus an online varying stiffness will be needed in order to exploit natural dynamics of the complete robot. Experiments on the physical pendulum are performed, in order to find the optimal stiffness for imposed sine-wave trajectories with one frequency component. These optimal values are compared with the simulation values. The results are very promising, as both values are situated near to each other. This means that a method is found to control the stiffness of the physical pendulum in order to exploit the natural dynamics in combination with trajectory tracking.

Two main steps should be taken to improve the performance the stiffness control:

- A correct estimation of the pendulum's parameters. The muscle volumes, the polytropic exponent and the friction are the most important parameters to be estimated.
- Fine tuning of the pressure levels of the bang-bang controller. The dead zone should be exploited as much as possible, without losing tracking accuracy.

Before using this technique on 'Lucy', a study should be done on a double pendulum, in order to investigate the coupling effects, which can lead to chaotic behaviour of the system. Finally, the same investigation should be done on an inverted pendulum.

To conclude, in this master thesis the first steps in the direction of exploitation of natural dynamics by using PPAM's were made.

Appendix A

Dynamic model of the pendulum

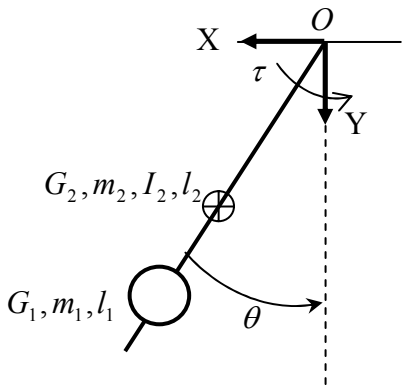

Figure A.1: Schematic overview of the studied model

In this section the equation of motion for the model depicted in figure A.1 is derived. A Newton-Lagrange formulation of the equation of motion is used for this purpose. The model has only one DOF θ:

$$\frac{d}{dt}\left\{\frac{\partial K}{\partial \dot{\theta}}\right\} - \frac{\partial K}{\partial \theta} + \frac{\partial U}{\partial \theta} = Q_\theta \tag{A.1}$$

K is the total kinetic energy and U the potential energy. Q_θ is the generalized force associated with the pendulum.

The kinematic expressions for the positions and velocities of the centers of mass for the different links are given by:

$$\overline{OG_1} = l_1\left(\sin\theta, \cos\theta\right)^T \tag{A.2}$$

$$\overline{OG_2} = \alpha\, l_2\left(\sin\theta, \cos\theta\right)^T \tag{A.3}$$

$$\bar{v}_{G_1} = l_1\left(\cos\theta, -\sin\theta\right)^T \dot{\theta} \tag{A.4}$$

$$\bar{v}_{G_2} = \alpha\, l_2\left(\cos\theta, -\sin\theta\right)^T \dot{\theta} \tag{A.5}$$

The total potential energy of the pendulum is equal to:

$$U = m_1 g Y_{G_1} + m_2 g Y_{G_2} \tag{A.6}$$

Which results in:

$$U = g\left(m_1 l_1 + \alpha\, m_2 l_2\right)\cos\theta \tag{A.7}$$

The partial derivative becomes:

$$\frac{\partial U}{\partial \theta} = -g\left(m_1 l_1 + \alpha\, m_2 l_2\right)\sin\theta \tag{A.8}$$

The kinetic energy K_i of part i is given by:

$$K_i = \frac{1}{2} m_i v_{G_i}^2 + \frac{1}{2} I_i \omega_i^2 \tag{A.9}$$

with ω_i the angular velocity for part i. For the two parts this becomes:

$$\begin{aligned} K_1 &= \frac{1}{2} m_1 {l_1}^2 \dot{\theta}^2 \\ K_2 &= \frac{1}{2}\left(m_2 \alpha^2 {l_2}^2 + I_2\right)\dot{\theta}^2 \end{aligned} \tag{A.10}$$

The total kinetic energy is the sum of these two terms:

$$K = \frac{1}{2}\left(m_1 {l_1}^2 + m_2 \alpha^2 {l_2}^2 + I_2\right)\dot{\theta}^2 \tag{A.11}$$

Now the different derivatives of the kinetic energy can be calculated:

$$\frac{d}{dt}\left\{\frac{\partial K}{\partial \dot{\theta}}\right\} = \left(m_1 {l_1}^2 + m_2 \alpha^2 {l_2}^2 + I_2\right)\ddot{\theta} \tag{A.12}$$

$$\frac{\partial K}{\partial \theta} = 0 \tag{A.13}$$

The torque τ applied in the pivot point represents the generalized force. So the equation of motion for this model can be summarized as followed:

$$\tau = D(\theta)\ddot{\theta} + C(\theta,\dot{\theta})\dot{\theta} + G(\theta) \tag{A.14}$$

With:

$$\begin{aligned} D(\theta) &= m_1 l_1^2 + m_2 \alpha^2 l_2^2 + I_2 \\ C(\theta,\dot{\theta}) &= 0 \\ G(\theta) &= -g\left(m_1 l_1 + m_2 \alpha\, l_2\right)\sin\left(\theta\right) \end{aligned} \tag{A.15}$$

Appendix B

Safety Board

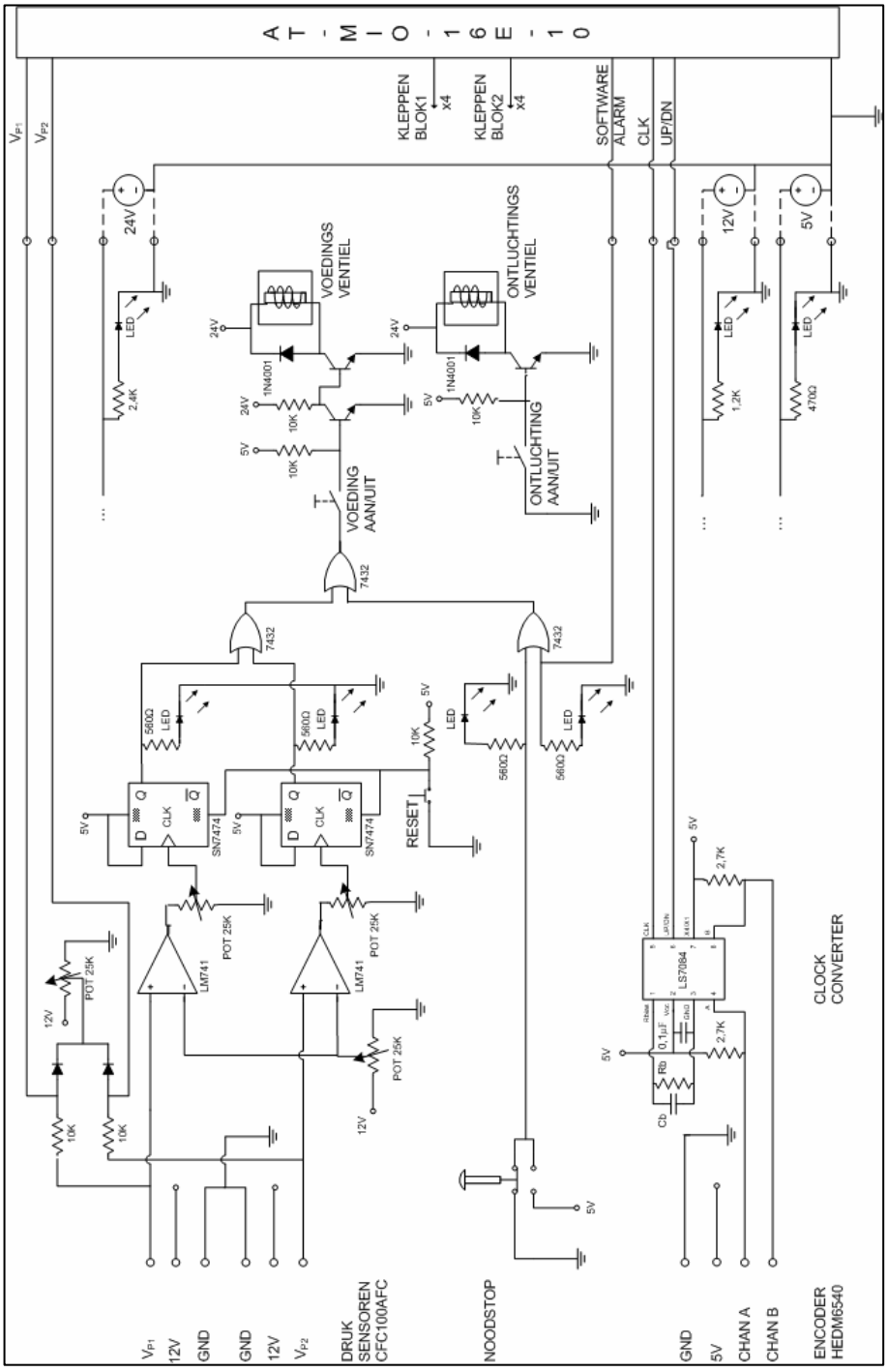

Figure B.1: Electronic scheme of the safety, supply and transformation board

Bibliography

1. Robotics

[1] Craig, J. J. [1986]. *Introduction to Robotics: Mechanics & Control*, Addison-Wesley Publishing Company

[2] Daerden, F. [1999]. *Conception and Realization of Pleated Pneumatic Artificial Muscles and their Use as Compliant Actuation Elements*, PhD thesis, Vrije Universiteit Brussel.

[3] Garcia, M., Chatterjee, A., Ruina, A. and Coleman, M. [1998]. The simplest walking model: Stability, complexity, and scaling, *ASME Journal of Biomechanical Engineering* 120: 281-288.

[4] Hurst, W., Chestnutt, J., E. and Rizzi, A., A. [2004]. An actuator with Mechanically Adjustable Series Compliance, technical report CMU-RI-TR-04-24, Robotics Institute, Carnegie Mellon University.

[5] McGeer, T. [1990]. Passive dynamic walking, *International Journal of Robotics Research (Special Issue on Legged Locomotion)* 9(2): 62-82.

[6] Pratt, J. E. and Pratt,G. [1998]. Exploiting natural dynamics in the control of a planar bipedal walking robot, *Proceedings of the 36th Annual Allerton Conference on Communication, Control, and Computing*, Monticello, Illinois.

[7] Pratt, J. E. [2000]. *Exploiting Inherent Robustness and Natural Dynamics in the Control of Bipedal Walking Robots*, PhD Thesis, Massachusetts Institute of Technology (MIT), Massachusetts, USA.

[8] Pratt, G., Williamson, M., Dillworth, P., Pratt, J. andWright, A. [1995]. Stiffness isn't everything, *Proceedings of the Fourth International Symposium on Experimental Robotics*, Stanford, California, USA, pp. 253-262.

[9] Rogers, G. and Mayhew,Y. [1992]. Engineering Thermodynamics, Work and Heat Transfer, John Wiley & Sons, New York, USA

[10] Tonietti G., Schiavi R. and Bicchi A. [2004]. Design and Control of a Variable Stiffness Actuator for Safe and Fast Physical Human/Robot Interaction*, Proceedings of the 2004 International Conference on Robotics and Automation,* Interdepartmental Research Center "E. Piaggio" Faculty of Engineering, University of Pisa, Italy

[11] Vanderborght, B. [2003] *Quasi-statische controle van een stappende robot aangedreven door actuatoren met regelbare stijheid*, Master Thesis, Vrije Universiteit Brussel (VUB).

[12] van der Linde, R. [2001]. *Bipedal Walking with Active Springs, Gait Synthesis and Prototype Design*, PhD thesis, Technische Universiteit Delft.

[13] Van Ham, R., Daerden, F., Verrelst, B., Lefeber, D. and Vandenhoudt, J. [2002]. Control of pneumatic artificial muscles with enhanced speed up circuitry., *Proceedings of the 5th International Conference on Climbing and Walking Robots and the Support Technologies for Mobile Machines*, Paris, France, pp. 195-202.

[14] Verrelst, B. [2005]. *A Dynamic Walking Biped Actuated By Pleated Pneumatic Artificial Muscles: Basic concepts and control issues*, Phd Thesis, Vrije Universiteit Brussel (VUB).

[15] Wisse, M. [2004]. *Essentials of Dynamic Walking : Analysis and Design of Two-Legged Robots*, PhD thesis, Technische Universiteit Delft.

[16] http://mms.tudelft.nl/dbl

[17] http://world.honda.com/ASIMO/

[18] http://www.sony.net/SonyInfo/QRIO/

2. Programming

http://www.codeguru.com

Visual studio 6.0 MSDN

[19] http://www.mathworks.com

3. Data acquisition card.

AT E Series User Manual, Multifunction I/O Devices for the PC AT, National Instruments, 2002.

[20] *NI-DAQ Function Reference Manual for PC Compatibles Version 6.6*, National Instruments, 1999.

http://www.ni.com